CORRUGATED CORE SANDWICH STEEL PANEL

Quantifying performance improvement between empty and filled sandwich panels using J-Integral based local approach

Saurabh Gunecha

Technische Universiteit Delft

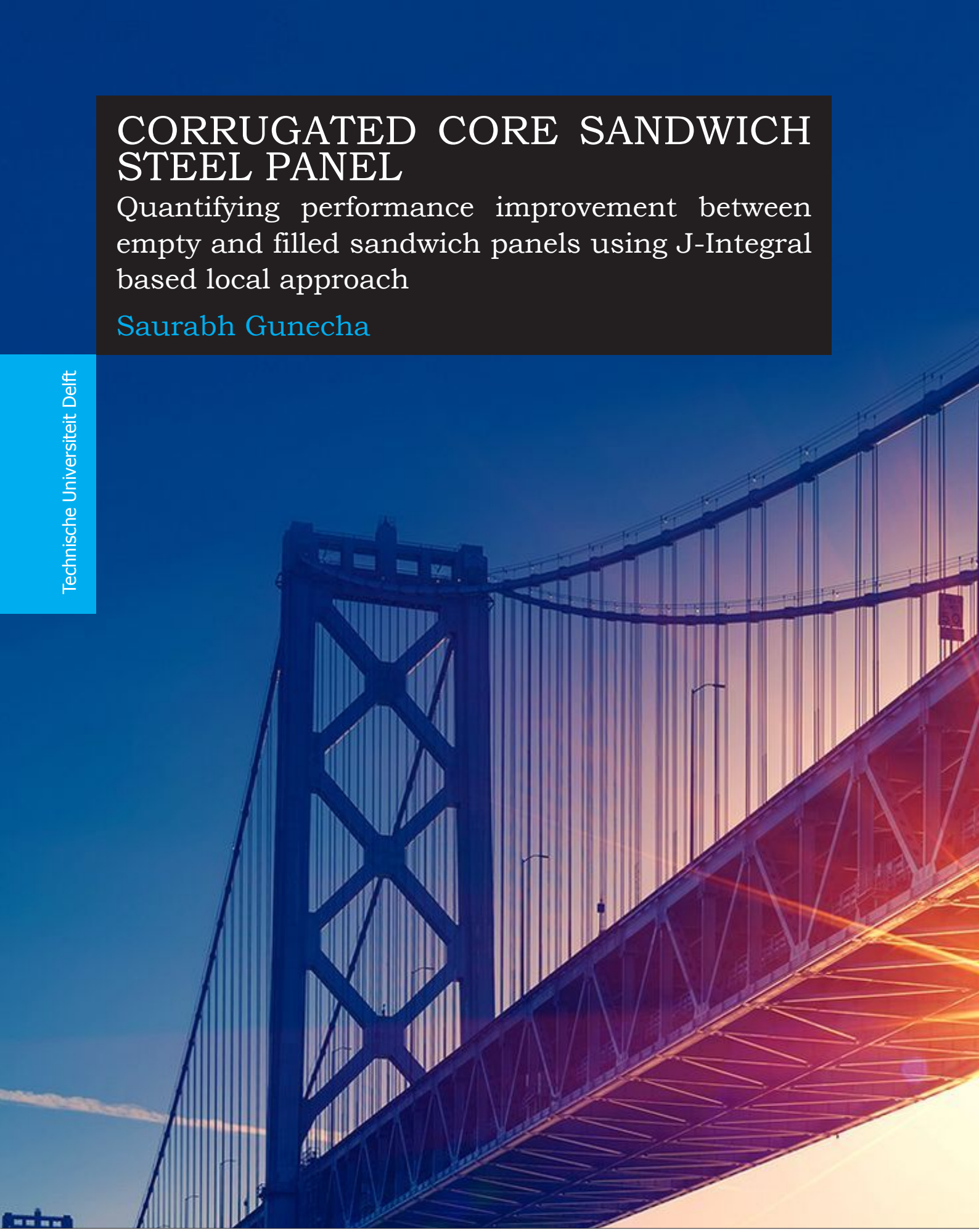

TU Delft Delft University of Technology

Challenge the future

CORRUGATED CORE SANDWICH STEEL PANEL

Quantifying performance improvement between empty and filled sandwich panels using J-Integral based local approach

by

Saurabh Gunecha

in partial fulfillment of the requirements for the degree of

Master of Science
in Structural Engineering

at the Delft University of Technology,
to be defended publicly on May 28, 2019 at 1500 hours

Student number:	4631935	
Project duration:	May 5, 2018 – May 28, 2019	
Supervisor:	Weijian Wu	TU Delft
Thesis committee:	Prof. dr. M. Veljkovic (Chair)	TU Delft
	Dr. HaoHui Xin	TU Delft
	Ir. Jos van Boheemen	Provincie Noord Holland
	Prof. dr. ir. M.A.N. Hendriks	TU Delft
	Weijian Wu	TU Delft

TU Delft Provincie Noord-Holland

Abstract

Orthotropic bridges are being built for more than half a century. These bridges are prone to high cycle fatigue due to traffic loading. Early onset of fatigue cracking is a serious issue in both old and recently built bridges. To prevent this a number of different cross section have been suggested. *Sandwich Panel* is one of the suggested alternative that has become more feasible to produce due to advancement in Hybrid Laser Arc Welding (HLAW) technology. One type of sandwich panel with corrugated core was investigated in this thesis. Ease of manufacturing, stronger welds, reduced complexity of welding and improved transverse shear stiffness are some advantages of sandwich panel over conventional orthotropic decks.

The aim of this thesis is to apply J-Integral based local approach for fatigue assessment of sandwich panels subjected to lateral loads. J-Integral represents a way to calculate the strain energy release rate and is a measure of crack tip elastic-plastic field. It has already been used successfully to quantify fatigue performance of web core sandwich panels and is therefore used in this thesis. A second aim of this thesis is to justify the use of foam filling in sandwich panels by comparing fatigue performance of empty and foam filled sandwich panels. For validation, bending behaviour of panel was first investigated using Finite Element Analysis (FEA). The model developed for dual stake laser welded panel accurately estimated response parameters (compared to experimental results of Tan et al. [33]) like maximum deflection (2.2% difference), critical stresses in transverse direction (9% difference) for top and bottom face plates etc. For verification of *Contour Integral* technique of Abaqus/CAE, J-Integral at notch tip of ASTM CT specimen was calculated. Compared with empirical solution the FE estimate showed 16% difference with FE estimate being more conservative.

Seven different types of foam were considered as filling in sandwich panels. The foams were of polymeric type - H45, H60, H80, H100, H130, H180, H200, and H250 (Unit weight of foams - 48 to 250 kg/m^3 and Young's Modulus - 45 to 250 MPa). Based on two stage 3D FEA on empty and foam filled sandwich panels, it was observed that J-Integral value at critical tensile notch decreased consistently as stronger foam fillings were used in the panel (83.8% reduction observed between empty panel and H250 foam filled panel). Cycles to failure for panels were calculated using regression equation derived from existing research on web-core sandwich panel. Between empty and H100 foam filled panel an increase of 171 times was observed in cycles to failure. This increase justifies the use of foam filling.

Keywords: Sandwich Panel, Corrugated core, J-Integral, Local Approach, Fatigue, Foam filling

Saurabh Gunecha
Delft, May 2019

Acknowledgements

I would like to acknowledge the people whose support have helped me during this thesis:

Prof. Milan Veljkovic, who introduced me to the topic, gave initial support and guided me in the right direction. Ir. Jos van Boheemen, for providing me with an opportunity to carry out this work in collaboration with Provincie Noord Holland. Your constant support, encouragement and lively discussions on different aspects of this thesis have made an invaluable contribution to this work.

Weijian Wu and Haohui Xin, for giving me time to discuss the thesis progress and for suggestions on improving the quality of FE models. Prof. dr. ir. M.A.N. Hendriks, for his valuable comments on the FE Models and thesis drafts. All the colleagues at Provincie Noord Holland, for providing a warm and welcoming atmosphere.

All the friends I have made through U-Base who helped me better navigate the TU life.

My family, for supporting me through thick and thin.

Many thanks to all the above people without whom this thesis would not be possible.

Contents

List of Figures

List of Tables

List of Abbreviations

CCSSP	Corrugated Core Sandwich Steel Panel
FEA	Finite Element Analysis
FEM	Finite Element Method
OSD	Orthotropic Steel Deck
HAZ	Heat Affected Zone
RDF	Rib to Deck at Floor Beam
aSSE	all Sandwich Steel Element
SSP	Sandwich Steel Panel
HLAW	Hybrid Laser Arc Welding
DSM	Direct Stiffness Method
CAE	Complete Abaqus Environment
SLD	Safe Life Design
LBB	Leak Before Break
LEFM	Linear Elastic Fracture Mechanics
EPFM	Elasto Plastic Fracture Mechanics
SSY	Small Scale Yielding
ASTM	American Society for Testing and Materials
SIF	Stress Intensity Factor
FLM	Fatigue Load Model
CT	Compact Tension Specimen
XFEM	eXtended Finite Element Method
ANOVA	Analysis of Variance

List of Symbols

Symbols	Description	Units
N_f	Cycles to Failure	-
J	J-Integral	MPa mm
W	Strain Energy density	kJ/m^3
u	displacement vector	mm
K_I	Mode-I Stress Intensity Factor	MPa $mm^{0.5}$
K_{II}	Mode-II Stress Intensity Factor	MPa $mm^{0.5}$
ΔK_I	Range of Mode-I Stress Intensity Factor	MPa $mm^{0.5}$
ΔK_{II}	Range of Mode-II Stress Intensity Factor	MPa $mm^{0.5}$
ΔJ	Range of J-Integral value	MPa mm
δ	Panel displacement	mm
E_w	Modulus of elasticity of foam	MPa
σ_{app}	Applied stress	MPa
σ_y	Yield stress	MPa
w_l	Lane Width	m
U	Displacement	mm
S	Stress	MPa
γ_y	Average Shear strain	1 or radian
δ_y and δ_x	Relative distortions	mm
h	height of the sandwich panel	mm
2p	Pitch of corrugation	mm
k	rotational stiffness of weld	kNm/rad
W	Strain energy density	J/m^3
T	traction vector	-
	CT Specimen	
W	Width	mm
P	Applied Load	N
t	Thickness of specimen	mm
K	Stress Intensity Factor	MPa-mm
β	Geometry correction factor	-
a	Crack size parameter	mm
S	Nominally applied stress	MPa
	T-Joint	
a_1	Length of root gap (left)	mm
a_2	Length of root gap (right)	mm
b_f	Breadth of top face plate	mm
t_f	Thickness of face plate	mm
h_w	Height of web	mm
t_w	Thickness of web plate	mm
l_s	Length of specimen	mm
t_{weld}	Thickness of weld	mm
C and m	Constants in the regression equation	$MPa^{4.55}mm^{4.55}$ and -
	Elastic Constants	
D_x	Bending stiffness in x-direction	Nm
D_y	Bending stiffness in y-direction	Nm

D_{xy}	Twisting Stiffness	Nm
D_{Qx} and D_{Qy}	Transverse Shear stiffness	N/m

1 Introduction

1.1. General Overview

Orthotropic bridge is a wide-spread and conventional method of bridge deck construction. Othrotropic Steel Decks (OSD) have tremendous reserve strength for local lateral loads, such as wheel loads, due to phenomenon of membrane stiffening [10]. It was first proposed in Germany and the name is derived from the ORTHOgonal anisoTROPIC behaviour of these bridges [22]. They have a very high degree of orthotropy due to large ratio of longitudinal to transverse bending stiffness [25]. This is pretty much evident by looking at uni-directional longitudinal stiffeners below the deck plate. Such a structural arrangement of stiffened deck plate, cross beams and longitudinal girders is an optimal way to carry loads. As for the orthotropic bridge deck itself, low self-weight makes it an optimal choice for a deck. The individual components of bridge superstructure, namely, top plate, longitudinal stiffeners, cross girders and longitudinal girders are all connected to each other by welding.

In the past, such bridges were not covered by majority of bridge codes. This is due to the fact that, the stress analysis and fatigue classification of welded connections are too complex [22]. This has resulted in early fatigue failure of welded connections of bridge decks. Also, this type of bridge has suffered from extensive fatigue damage due to their complex welding details and sensitivity to local loading [7]. A promising concept as a substitute for conventional orthotropic plate is Sandwich Panels. For investigation in this thesis we focus on one specific type of sandwich panel - Corrugated Core Sandwich Steel Panel (CCSSP), hereafter referred to as just *sandwich panel*. Previous research, as in [20] and [35], have concluded that sandwich system forms an attractive alternative due to reduced welding and ease of construction.

1.2. Fatigue Problems in Orthotropic Bridges

The main disadvantage of orthotropic bridge decks from fatigue point of view is presence of large number of welded joints. Welds introduce large shrinkage effects and thus a tendency to weld cracking [22]. There are large number of sites where a crack may initiate. One such critical site is a partial penetration weld connecting longitudinal stiffener with deck plate. Due to geometry and inherent torsional strength a deck is subjected to local secondary deformations and stresses that makes them vulnerable to fatigue at the intersection with Floor Beams (FB) [10]. This joint is commonly referred as RDF joint, meaning Rib to Deck at Floor beam. At these locations, a crack could initiate at weld root. Over time the crack progresses to surface where it become visible only after the cracking of pavement layer. Cracks like these were observed in Van Brienenoord bascule bridge. After just seven years of service, fatigue cracks were noticed in most heavily loaded lanes [5]. The fatigue durability of the web-to-deck joint is adversely affected by the range of possible wheel positions on the deck as different wheel load combinations could lead to moment reversals [7].

Although there are other weld locations where a crack could initiate and propagate, stiffener to deck plate crack originating at weld root are by far the most critical. Problem is that these crack are not visible until they have reached the surface. Ultrasonic testing has been applied to the detection of

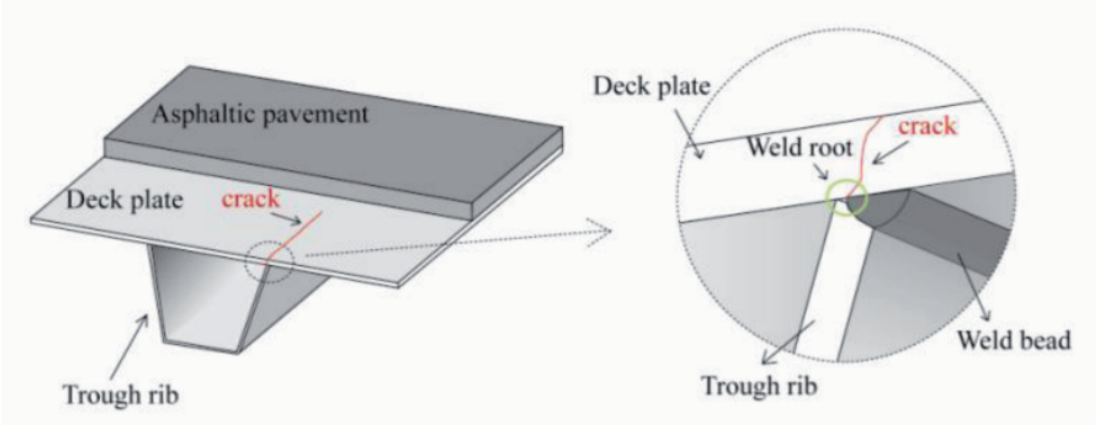

Figure 1.1: Fully grown crack originating from weld root (Location - Rib to Deck weld) [18]

through-deck type cracks [18]. Although these cracks do not endanger the safety of overall structure, in-situ repairs are difficult, time consuming and expensive [7].

1.3. Corrugated Core Sandwich Steel Panel

The idea to develop a better structural system is not new. After the Van Brienenoord trough to deck surface crack was observed, the ministry in Netherlands decided to start an overall project `Fatigue Problems on Steel Bridge decks` ("Problematiek Stalen Rijvloeren" in Dutch) [21]. Under this initiative proposals for repair and rehabilitation were developed to tackle existing fatigue cracks in steel bridges. As for development of better alternatives, the only hindrance was absence of a suitable welding technique to aid rapid production of complex structural members. This problem was solved with advent of Hybrid Laser Arc Welding (HLAW). One structural solution made possible by laser welding is sandwich steel panel. In a typical sandwich panel a steel core is put in between two steel face plates. Some typical core shapes are shown in Figure 1.2. In present study, focus is on corrugated core only. The steel plates above and below the core are called `Top Face plate` and `Bottom face plate` respectively.

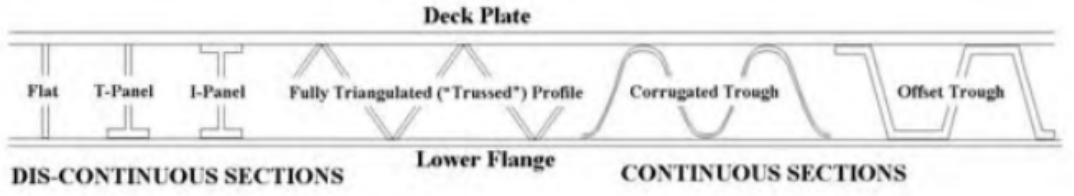

Figure 1.2: Different types of core possibilities in a sandwich panel [7]

The main idea behind development of a new deck is to reduce the difference between shear stiffness in longitudinal and transverse direction. Low transverse stiffness between two troughs of an orthotropic deck prevents uniform load distribution. This results in high peak stresses within directly loaded stiffeners, with negligible stress elsewhere [7]. Corrugated core sandwich panel avoids this poor load distribution, owing to its better ratio of longitudinal to transverse shear stiffness. For a sandwich panel, core provides continuous support to loaded plate (i.e. Top Face Plate) in the longitudinal direction. In transversal direction this support is periodic. Connection type between core and face plates also affects the behaviour of sandwich panel. In the present study, we will consider a sandwich panel where top and bottom face plates are connected to the core by dual stake laser weld.

Figure 1.3: Corrugated Core Sandwich Steel Panel, Nilsson et al. [25]

1.4. Aim of Present Research

The aim of this research is to quantify the bending behaviour & fatigue performance of sandwich panel (empty and foam-filled). The structure is assumed to be made through HLAW. Bending behaviour of panel is affected by the location and type of welded joint.

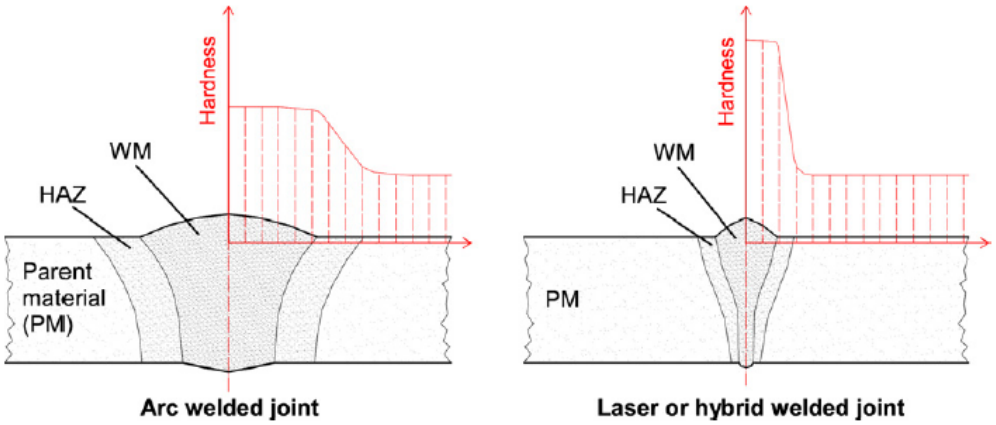

Figure 1.4: Fusion Zone Shape and Hardness Distribution is Arc and Laser Weld [25]

Research Objectives

After a careful study of empty and foam-filled sandwich panels the following objectives were formulated -

Objective 1 - Model Validation

Validation study to develop a FE model to accurately estimate bending response of a sandwich panel.

Approach for Objective 1

For validation study, a sandwich panel dimension and boundary condition from published research work will be used. The purpose of this validation is to develop a simplified FE model which could predict bending response with reasonable accuracy.

Objective 2 - Foam Selection

Selection of foam filling for sandwich panel

Approach for Objective 2

A full 3D FE analysis of foam filled corrugated core sandwich steel panel is challenging, but suitability of different foams could be addressed quantitatively by looking at increase in stiffness properties of the panel. To simplify FE models, multi material steel-adhesive-foam interface will not be considered. Analytical formulae and FEA results together will be used to rank different foams based on the performance improvement imparted by them. Foam filling will be judged on the basis of three criteria -

- Increase in Transverse Shear Stiffness, D_{Qy} - Benefit of Foam Filling
- Decrease in Surface Stresses - Benefit of Foam Filling
- Increase in self weight - Drawback of Foam Filling

Reason for considering D_{Qy}

Even though sandwich panel solves some of the problems of OSD, it still has limitations. One such limitation is difference between two Transverse Shear Stiffness, D_{Qx} and D_{Qy}. Foam filling will reduce this gap to some extent with very little increase in self weight thus maintaining stiffness to weight ratio. Foams are attractive option as filling material for sandwich panels due to the following reasons

- Foam is a light weight material and hence it doesn't significantly affect the high stiffness to weight ratio of existing structure.
- Foam filling utilizes empty space inside the panel. Thus, foam filling will not lead to increase in panel height.

Reason for considering Normal Stresses

Normal stresses in the top face plate will cause Model I crack near the toe of the top face plate - core laser weld. One way to quantify performance improvement due to foam is by measuring the reduction in normal stresses on the top face plate.

Objective 3 - `J-Integral` as a Fatigue Strength Assessment Parameter

J-Integral based local approach to estimate cycles to failure

Need for snubbing global approaches and instead considering a local approach

As pointed out in previous research, a joint in sandwich panel experiences a mixture of tensile, bending and shear stresses simultaneously [15]. Specifically for a web core sandwich panel critical joint in the panel has one notch in tensile stress, whereas the other is in a compressive stress state [12]. This makes nominal stress approach unfeasible (because of large scatter of results). One possible solution is to use local approach for fatigue strength assessment to account for stress and strains at the tensile notch tip where the fatigue crack initiates [12].

1.5. Limitations

Some of the critical limitations of this study are discussed below.

- Normal Stresses - Rotational stiffness of weld will not be considered in analysis. This will lead to underestimation of maximum normal stresses on the top face plate near the laser weld.

- Foam - Adhesive - Steel Interface - In FEA of foam filled sandwich panel, multi-material interface of steel-adhesive-foam is simplified. An accurate modelling of this interface would require properties of all the constituent materials along with actual thickness of the adhesive layer.
- Parameters *C* and *m* - Cycles to failure (N_f) will be calculated from J-Integral value at critical tensile notch of critical joint using regression equation $N_f = C(\sqrt{\Delta J})^{-m}$ established in previous experimental research on web core sandwich panels. It was assumed that this regression equation and the parameters, $C = 294MPa^{4.55}mm^{4.55}$ and $m = 9.1$, are also applicable to corrugated core panel. This assumption might induce some error. In future when value of parameters C and m becomes available for corrugated core panel, more accurate estimate of N_f could be obtained by simply using J-Integral results from this study.

1.6. Research Methodology

Experimental results for a corrugated core sandwich panel was taken from Tan et al. [33]. Using same dimensions as panel tested in experiments, a simplified FE Model was developed in Abaqus/CAE. A second FE model of ASTM CT Specimen was developed to accurately estimate J-Integral at notch tip. The technique from these two well validated models were utilized further to compare fatigue performance of empty and foam filled sandwich panel. To determine performance improvement in fatigue, we make use of $\sqrt{\Delta J}$ as a fatigue strength assessment parameter. Using a small sandwich panel, 3D FEA was carried out under static loading. A submodel driven by results of this full 3D FE model was utilised to calculate value of J-Integral at tensile notch of critical joint. Using critical J-Integral value cycles to failure will be estimated through the regression equation suggested in [12]. Preliminary sizing and parametric study of sandwich panel to assess the effect of geometry of sandwich panel on elastic constants will be presented in the end.

1.7. Thesis Outline

This thesis is divided into 6 chapters. The present chapter deals with introducing the subject matter and describing the research questions.

In Chapter 2 - A brief literature review will be presented

In Chapter 3 - Verification Study will be presented.

In Chapter 4 - A foam selection guide will be presented based on simplified Finite Element Analysis of a small sandwich panel.

In Chapter 5 - Efficient deck sizing guidelines based on criteria of maximizing critical elastic constants will be presented.

In Chapter 6 - Conclusions of this study and recommendations for further research will be presented.

2

Literature Review

2.1. Corrugated Core Sandwich Steel Panels(CCSSP)

2.1.1. Introduction to Sandwich Panels

A sandwich panel is composed of two steel plates, called top face plate and bottom face plate separated by a thick layer of foam material. For heavily loaded structures, foam is replaced with steel core layer where a single unit repeating itself at some pitch (p) makes up the core. This type of sandwich has been called card-board box construction, and also double skin construction [23]. Various options are available for use as a core in a sandwich steel panel. In shipbuilding industry, web-core sandwich steel panel is more common while for use as a bridge deck ongoing investigation suggests CCSSP (hereafter referred as *sandwich panel*) as a better alternative.

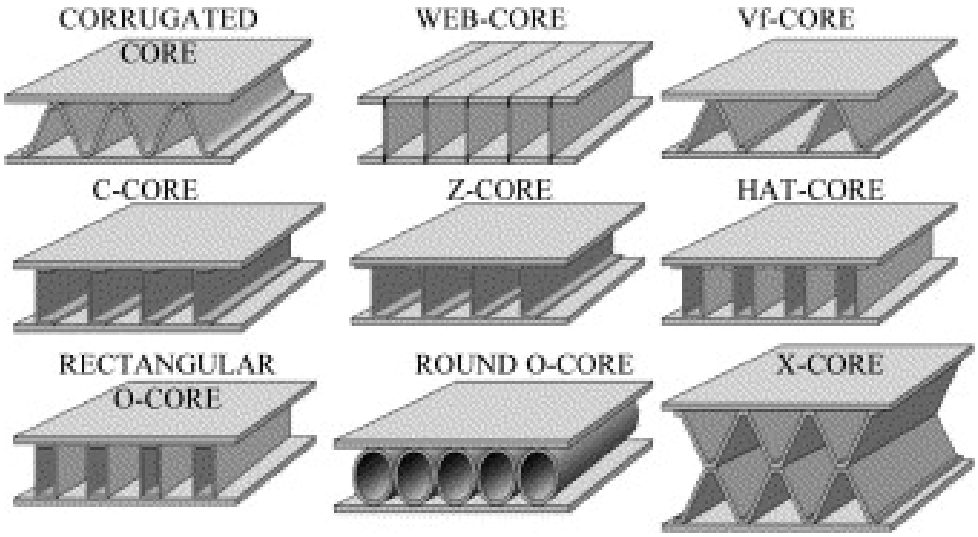

Figure 2.1: Different types of all-metal sandwich panels [29]

2.1.2. Transverse Shear Stiffness, D_{Qy}

A single cell of a sandwich panel loaded by transverse shear (Q_y = 1) and horizontal force of magnitude p/h is shown in Figure 2.2. The deflected shape of cell is shown in Figure 2.3. The transverse shear stiffness is then given by Equation 2.1 (Refer [23] for derivation).

$$D_{Qy} = \frac{1}{\gamma_y} = \frac{1}{\frac{\delta_y}{h} - \frac{\delta_z}{p}} \tag{2.1}$$

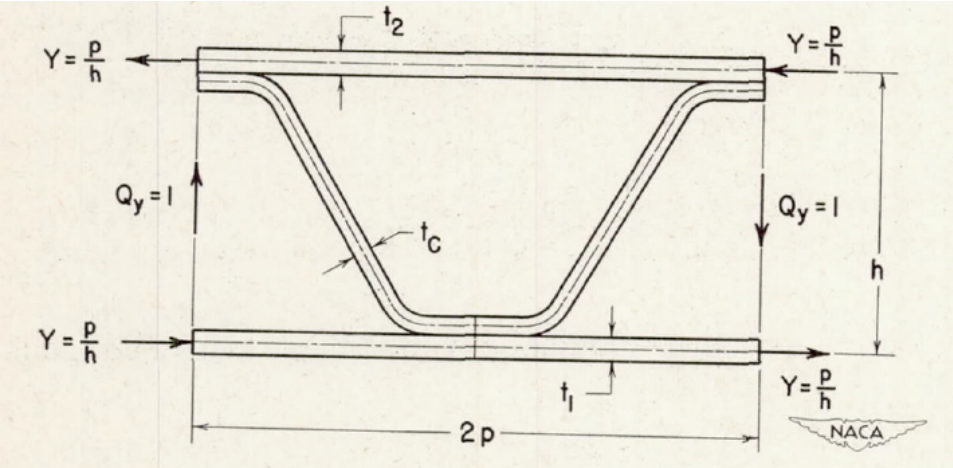

Figure 2.2: Loading on a single cell of sandwich panel [23]

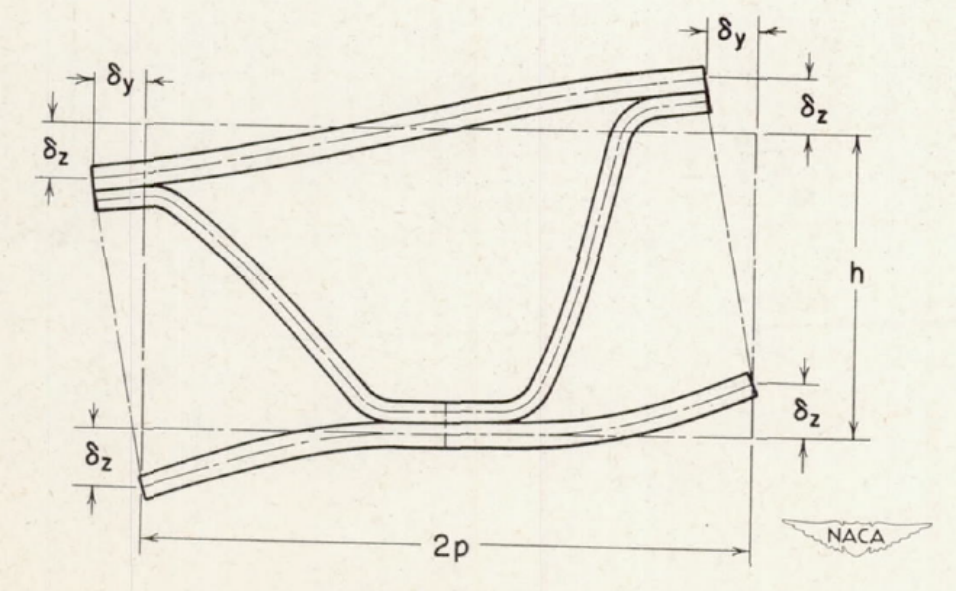

Figure 2.3: Deformed shape of single sandwich panel cell [23]

2.1.3. Rotation Stiffness of weld

Out of the two transverse shear stiffness D_{Qx} and D_{Qy}, the critical one is D_{Qy}. In [25], a Direct Stiffness Method (DSM) is discussed to develop an analytical model for calculating D_{Qy}. The developed model was then verified using FEA of single cell and multi-cell sandwich beams. For each of the two, single cell and multi cell, sandwich panel studied using FEA, four different geometries were considered. The comparison between analytical calculations and FE Model results are shown in the Figure 2.4. These result show how three parameters - transverse shear stiffness, normal stresses in face plates and normal stresses in core layer are affected by change in rotation stiffness of welds. The results of Figure 2.4 could be described in two points -

- Transverse shear stiffness (D_{Qy}) of a sandwich panel is not influenced significantly by the weld rotational stiffness. So for studies where determination of transverse shear stiffness (and response quantities dependent primarily of it) is important it makes sense to disregard the rotation stiffness of weld in the FE model. This is the case when core is joined to top and bottom face plates using dual laser stake welds.
- While considering maximum normal stresses in the top face plate in the region surrounding the laser weld, it was observed that these stresses are considerably influenced by rotational stiffness

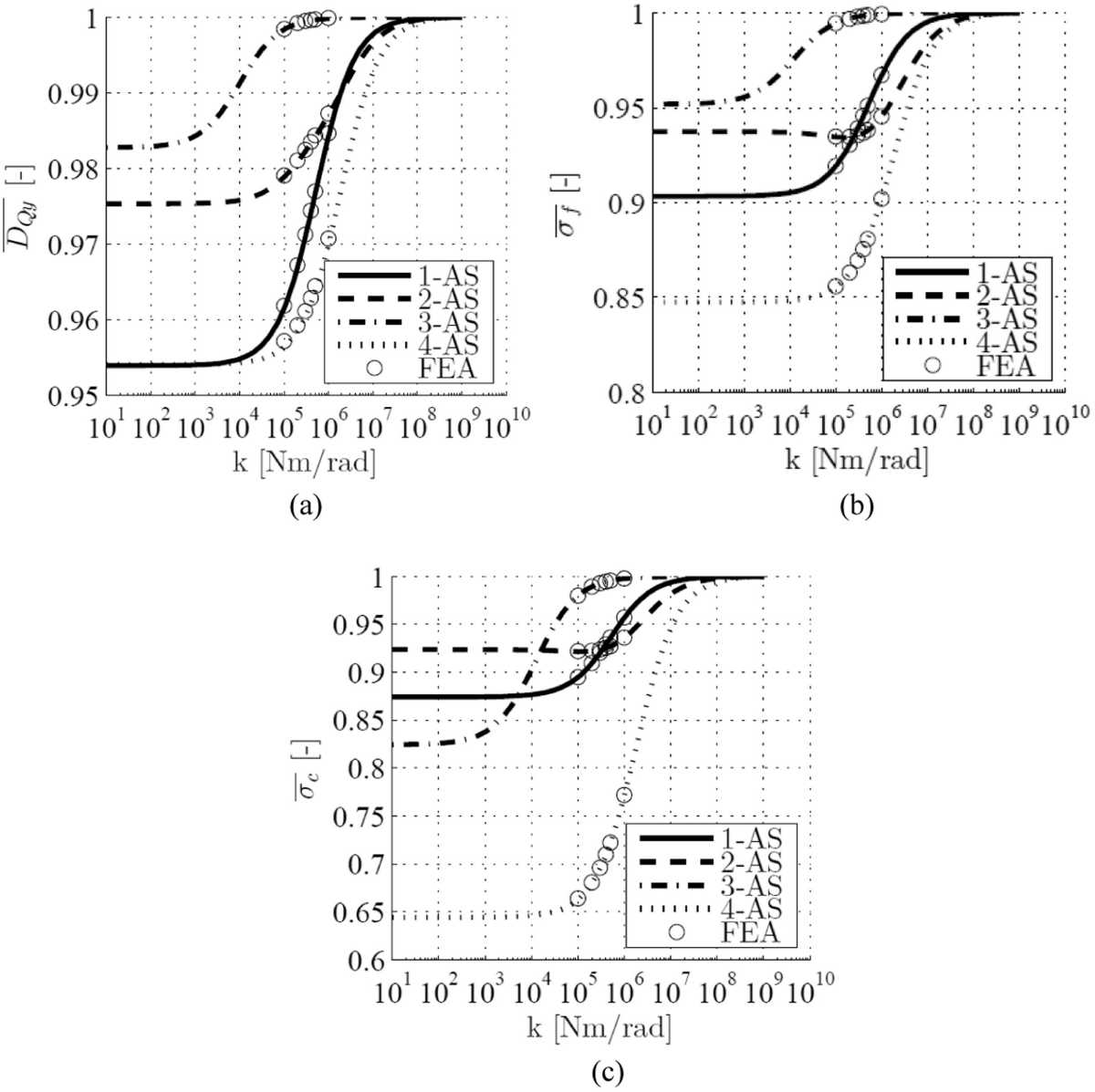

Figure 2.4: Normalized Response as a function of weld region stiffness, (a) Transverse Shear Stiffness, (b) Normal Stresses in top face plate near weld, and (c) Normal Stresses in the core near the weld, AS - Analytical Solution and FEA - Finite Element Analysis Solution for the corresponding parameter. [25]

of the weld. So for cases where accurate estimation of normal stresses is of relevance, it would be prudent to incorporate the rotational stiffness of weld in the FE model.

2.1.4. Analysis of Sandwich Panels

The corrugated core keeps the face sheets apart and stabilizes them by resisting vertical deformations, and also enables the whole structure to act as a single thick plate by virtue of its shear strength [9]. For simple loading and boundary conditions it is possible to analyse sandwich panels and obtain closed form solutions for displacement and stresses in the panel using Mindlin-Reissner Plate theory. Other ways to analyse these panel is by using commercially available FE software. Both shell (S8R element) and solid continuum elements (C3D8R and C3D20R) are known to give good results.

2.1.5. Homogenization of Sandwich Panels

A full 3D Finite Element analysis of a sandwich panel is both time consuming and computationally expensive. For panels without any local load it is possible to reduce 3D FE model of panel to an

equivalent 2D FE model. A 3D sandwich panel FE model could be reduced to equivalent 2D FE model using *Homogenization* technique. The sandwich cross section is homogenized to a thick orthotropic plate. This plate could then be analysed using *Lamina* option of Abaqus/CAE. The input required to carry out analysis using *Lamina* option in Abaqus/CAE can be easily calculated using expressions derived in [23].

2.2. Fatigue and Fracture

Fatigue is failure of a structure or a part of it due to repeated cyclic loading. The failure occurs due to slow elongation of crack with each loading and unloading cycle. Apart from cyclic loading, there are other ways by which an initial defect could grow (and subsequently cause failure) such as stress corrosion cracking, creep, corrosion fatigue, liquid metal embrittlement etc, but in this study we consider the cyclic loading as main criteria for crack growth.

2.2.1. Difference between Fatigue and Fracture

The term fatigue is confused with fracture quite often but they have different meaning. In engineering design, fatigue is a problem that could be handled with careful considerations during design and good detailing. Fatigue cracks are permissible in structures as long as they do not endanger the safety of the structure and are limited in size and growth rates. On the other hand risk of fracture is kept to a bare minimum in engineering design. The reason for this is failure by fracture is brittle in nature and occurs without warning even in ductile materials. In general, unstable fatigue crack growth ends in fracture. Another difference between fatigue and fracture is on the basis of loading characteristics. Fatigue is commonly associated with slow crack growth under cyclic loading while fracture is characterised by rapid crack growth under high amplitude loading.

2.3. Fatigue Assessment

EN 1993, Part 1-9 suggests that fatigue assessment should be undertaken using either *Damage tolerant method* or *Safe Life method*. Both approaches deals with fatigue in a different manner. Damage tolerant approach allows for fatigue cracking provided that inspection and maintenance regime is implemented throughout the design life of a structure to detect and correct for fatigue damage. The fatigue resistance is calculated using fatigue strength curves (or S-N curves). The nominal stress used in fatigue assessment are calculated at the site of potential fatigue initiation.

2.3.1. S-N Curves

Also called the Wohler curves, S-N curves are obtained through experiments. The terms S represents Nominal Stress while the term N represent Cycles to Failure. These curves are plotted on a logarithmic scale, with stress S on the vertical axis and number of cycles N on the horizontal axis. Data points are obtained from experiments to plot these S-N curves. To take care of the scatter in experiment results, a curve is fitted for data points obtained for a particular detail. One such curve which represents 5% failure probability is called a characteristic S-N curve. A S-N curve based on statistical evaluation is shown in Figure 2.5

2.3.2. Detail Categories

Different elements and welds are characterised in terms of Detail Categories in EN 1993, Part 1-9. A detail category of 100 means that the said detail is capable on withstanding two million cycles under the constant amplitude direct stress range of 100 N/mm^2. But, these detail categorisation and S-N curves are available for standard details only. A constant amplitude stress range is used during testing but real structure experiences variable stress ranges during the service life. This makes sequence of loading quite important. Figure 2.6 shows Fatigue strength Curves for direct stresses.

As discussed in Section 1.4, a joint in sandwich panel experiences a mixture of tensile bending and shear stresses simultaneously [15]. Due to large scatter of results nominal stress approach fails. That's why need for a local approach arise. In Section 2.4 one local approach based on J-Integral will be discussed.

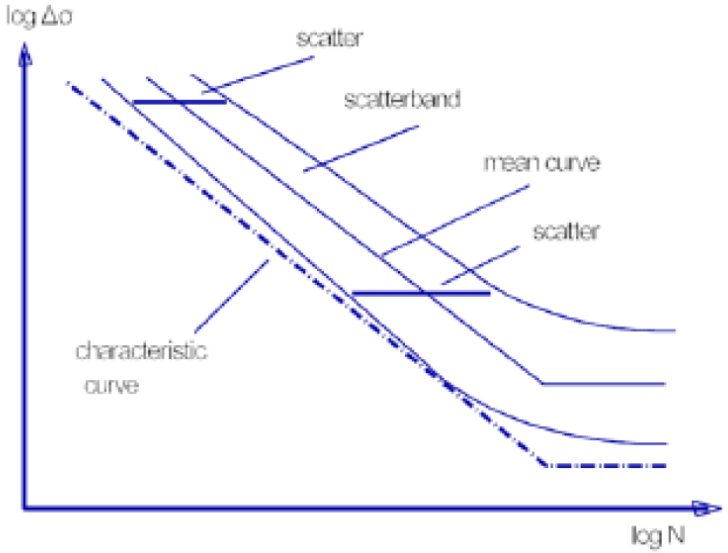

Figure 2.5: S-N curve based on statistical evaluation of welds [16]

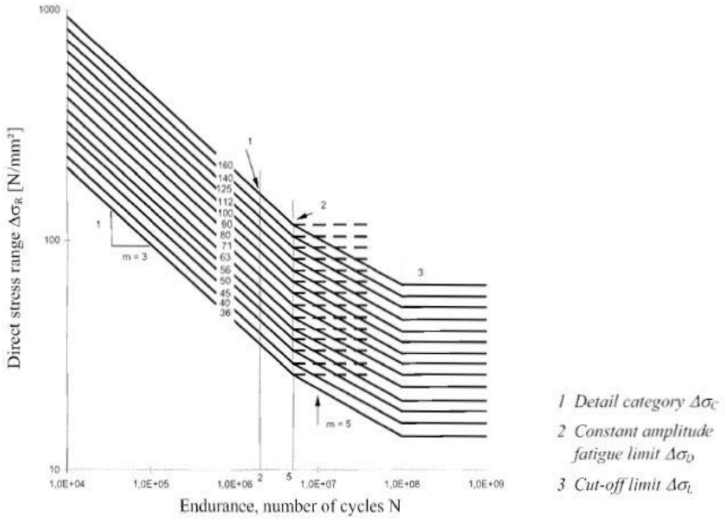

Figure 2.6: Fatigue Strength Curves [8]

2.4. J-Integral

J-Integral is a path independent contour integral which gives us an average measure of crack tip elastic - plastic field. It is applicable irrespective of the material model being linear or non-linear elastic. J-Integral is widely accepted as a quasi-static fracture mechanics parameter for linear material response. In Abaqus, under `Contour Integral` option a number of crack tip integral, including J-Integral, could be evaluated. J-Integral is used to compute energy flow to the crack tip, to estimate crack opening and is used as part of failure criteria for ductile materials [34]. In the present thesis we will make use of *Contour Integral* option to get accurate estimate of J-Integral value at tip of critical tensile notch of the critical joint. The expression for J-Integral as presented in [26] is as follows -

$$J = \int_{\Gamma} \left(W dy - T \frac{du}{dx} ds \right) \tag{2.2}$$

In equation 2.2, W refers to strain-energy density, T refers to a traction vector defined according to outward normal along Γ, u is the displacement vector and ds is an element of arc length along ds

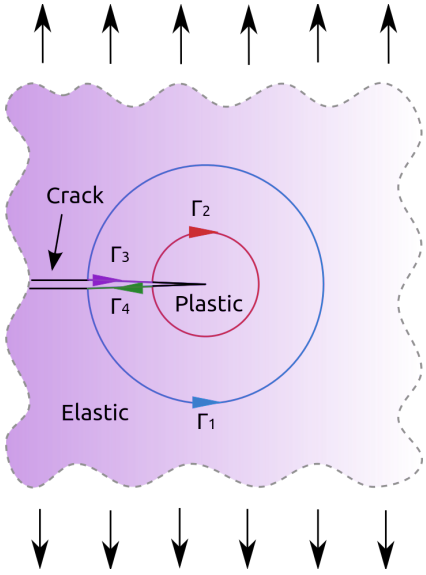

Figure 2.7: Paths for J-Integral calculation around a notch in a two-dimensional elastic-plastic material [26]

is an element of arc length along Γ, Γ refers to a curve surrounding the notch tip. J-Integral is a path independent integral but its path independence is valid only when crack faces are not loaded. When crack faces are loaded or when crack is curved, this property of J-Integral no longer holds true. In this thesis, J-Integral will be calculated at notch tip (where we expect crack to originate) before actual crack initiation. Tendency for a crack to originate at critical tensile notch of the critical joint will be captured via J-Integral value.

For general loading the J-Integral could be obtained as a superposition of Mode - I, II and III Stress Intensity Factors, with the following expression -

$$J = \frac{K_I^2}{E'} + \frac{K_{II}^2}{E'} + \frac{K_{III}^2}{E'(1-\mu)} \tag{2.3}$$

where, E' varies and depending on whether the case is plane strain or plane stress. Also, this expression is valid under the condition that a plane initial crack remains planar and maintains a constant shape as it grows [3].

2.4.1. Application of J-Integral

J-Integral based Local Approach for Fatigue Strength Assessment

In this thesis $\sqrt{\Delta J}$ is used as a fatigue strength assessment parameter. From review of previous research [12], it is clear that because of large scatter in results nominal stress approach won't work for fatigue assessment of a sandwich panel. Local approach for fatigue assessment are needed to solve this problem. Available local approaches are - Effective Notch Stress, J-Integral and Strain Energy Density. To the best of author's knowledge, there has been no research to confirm which approach works better. Therefore, in this thesis we will use J-Integral based local approach for fatigue strength assessment of sandwich panel.

When applied to sharp cracks, J-Integral or *J* refers to a value which is obtained by integration around a crack tip [15]. J Integral will be evaluated at all notches of critical joint of sandwich panel. But, for use in regression equation only critical J-Integral value (i.e. the value of J-Integral at critical tensile notch) will be considered. This scalar value represents *energy release rate* for crack growth. $\sqrt{(\Delta J)}$ will be used as a fatigue strength assessment parameter to make sure that complex state of mixed fracture mode loading is accurately accounted for [15].

The regression equation which will be used to obtain N_f from J-integral value at critical tensile notch of the critical joint is as follows -

$$N_f = C\sqrt{\Delta J}^{-m} \tag{2.4}$$

where, N_f refers to cycles to failure, C and m are constants related to $\sqrt{\Delta J}$ vs N_f based regression equation. A regression equation based on experiments conducted on web core sandwich panel gives the following value for constants - C = 284 $MPa^{4.55}mm^{4.55}$ and m = 9.1.

2.4.2. Contour Integral in Abaqus

J-Integral value at crack-tip is calculated using *Contour Integral* option in Abaqus/CAE. Before requesting contour integral it is important that a crack front is configured by selecting entities from the assembly. Abaqus uses the crack front and one layer of elements outside it to calculate first contour integral. It is possible to request integrals for more than one contours around the crack-tip. When contour integral is requested at more than one contour, a single layer of element is added to the group of elements that were used to calculate the last contour integral. Figure 2.8 shows this process visually.

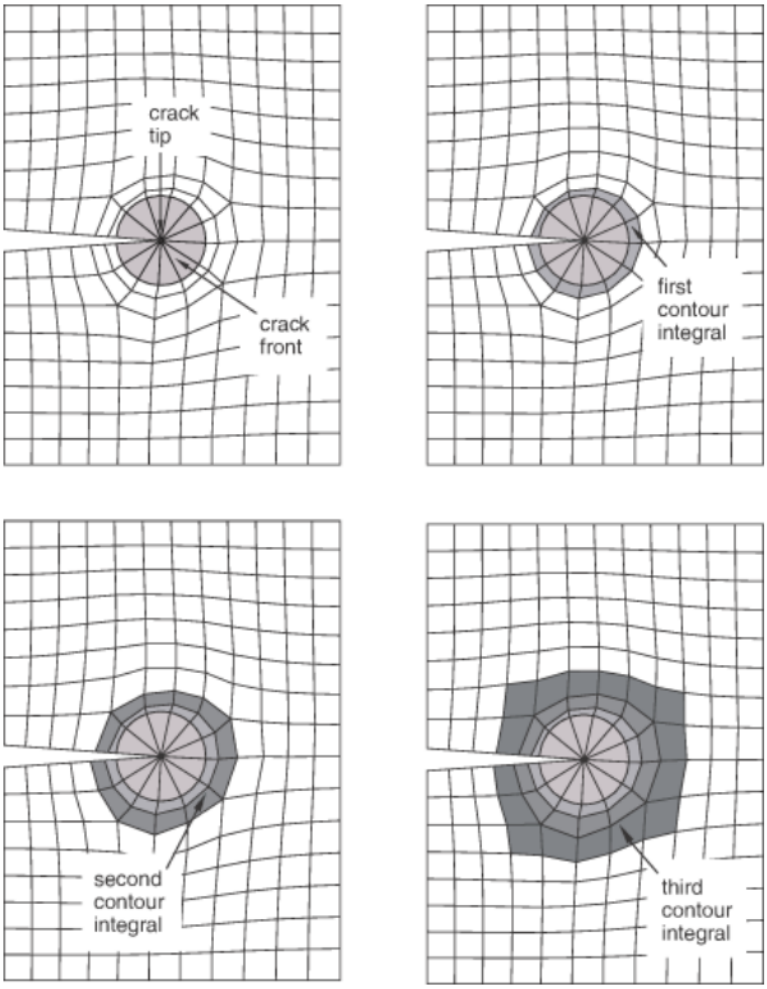

Figure 2.8: Evaluation of successive contour integrals in Abaqus [2]

2.4.3. Controlling the singularity at crack tip

Contour integral was estimated at tip of a notch (sharp crack) created by dual stake laser welding. For regions defined with a sharp crack strain field is observed to be singular. This negatively affect the analysis results. To improve the accuracy, it is recommended that crack-tip singularity be included in analysis. It is also recommended to use collapsed element with mid-side nodes shifted by a quarter point near the crack tip to mesh the contour integral region.

Implementation

Three types of strain singularity could be added to crack tip - $1/\sqrt{(r)}$ strain singularity also called, square root singularity, $1/r$ strain singularity and a combined $1/\sqrt{(r)}$ & $1/r$ strain singularity. In this thesis for calculating J-Integral we have included $1/\sqrt{(r)}$ strain singularity. For Linear Elastic case, it is recommended to use square root singularity. The implementation of this in Abaqus/CAE is quite simple and is as follows. In the *Contour Integral* option, choose the following parameters to include this singularity, Toggle ON - `Collapse Element Side, Single Node`, refer Figure 2.10. Apart from this it is also recommended to shift element nodes from center to quarter-point location, called *quarter point spacing*. This can be achieved by giving a value of 0.25 to *Midsize node parameter* during crack definition. The effect of this is shown in Figure 2.9.

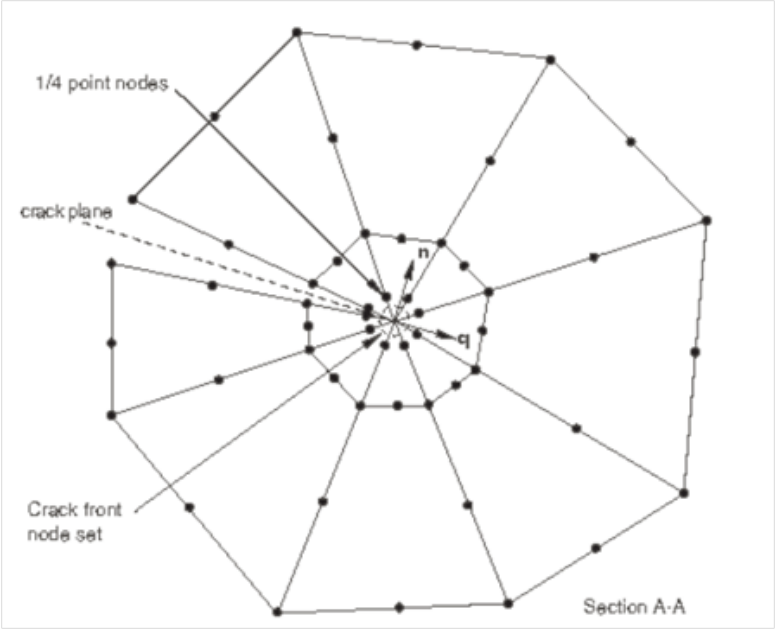

Figure 2.9: Including Quarter-Point spacing in elements of crack front [2]

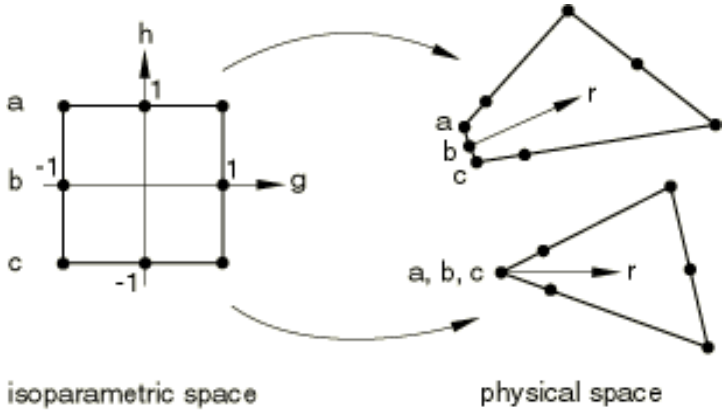

Figure 2.10: Collapsed Element [2]

2.5. Strengthening Technique for Sandwich Panels

It was discussed in Section 1.4 why strengthening a sandwich panel by a filling material is a good choice. Two categories of foam filling has been considered by researchers in the past, namely - (a) Metallic foams and (b) Polymeric foams. In the case of metallic foams, aluminium foam filling is an

option. For polymeric foams available options are Divinycell, Rohacell, Polyurethane and Polystyrene.

Experimental studies conducted in the past on web core sandwich panels have demonstrated improvements due to foam filling. In experiments conducted in [4], the load level at 2 million cycles increased by a factor of 8.5 when the beams were filled with a low-density PVC (polyvinylchloride) foam (like Divinycell H80) [19] when compared to empty sandwich beams under 3-point bending test. To best of author's knowledge no experimental studies have been conducted so far to quantify the effect of foam filling on sandwich panel. Finite element analysis in relation to fatigue test results is also not performed due to the fact that modelling of multi-material interface would require cyclic properties of all the constituent materials (like adhesive layer, steel member and foam filling) along with actual thickness of the adhesive layer [19].

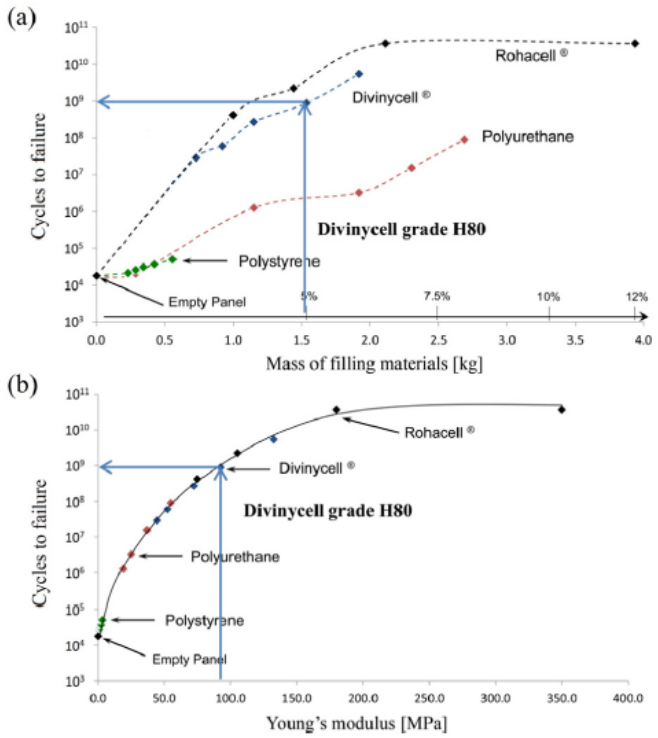

Figure 2.11: Comparison of cycles to failure for various foams in terms of (a) Mass of filling material and (b) Young's Modulus [19]

2.5.1. D_{Qy} for foam filled sandwich panels

An empty sandwich panel has five elastic constants - Two in Bending (D_x and D_y) One in twisting (D_{xy}) and two in transverse shear (D_{Qx} and D_{Qy}). For foam filled sandwich panels these constants should be modified. Romanoff et al. [28] discussed analytical formulation to modify these constants. D_{Qy} is a critical elastic constant and in this study we make use of analytical formulation to calculate increase in D_{Qy} due to foam filling. A five step process to calculate D_{Qy} for foam filled sandwich panel is given in [28] - (Refer Appendix 4).

2.6. Shell, Solid and Planar Elements

2.6.1. Shell Elements

Shell elements are used in FE analysis when one dimension is much smaller than other two dimensions. There are two kinds of shell elements in Abaqus/CAE - conventional shell element and continuum shell elements. Conventional shell elements discretize the object of analysis by defining its geometry at the reference surface while the continuum shell elements discretize an entire 3D body. Conventional shell elements have displacement and rotational degree of freedom while continuum shell elements have

displacement degrees of freedom only. The difference between the two is presented graphically in Figure 2.13. Triangular and rectangular conventional shell elements are shown in Figure 2.12.

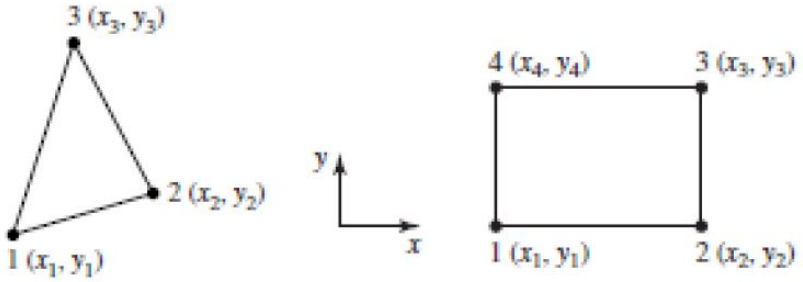

Figure 2.12: Triangular and rectangular conventional shell elements [17]

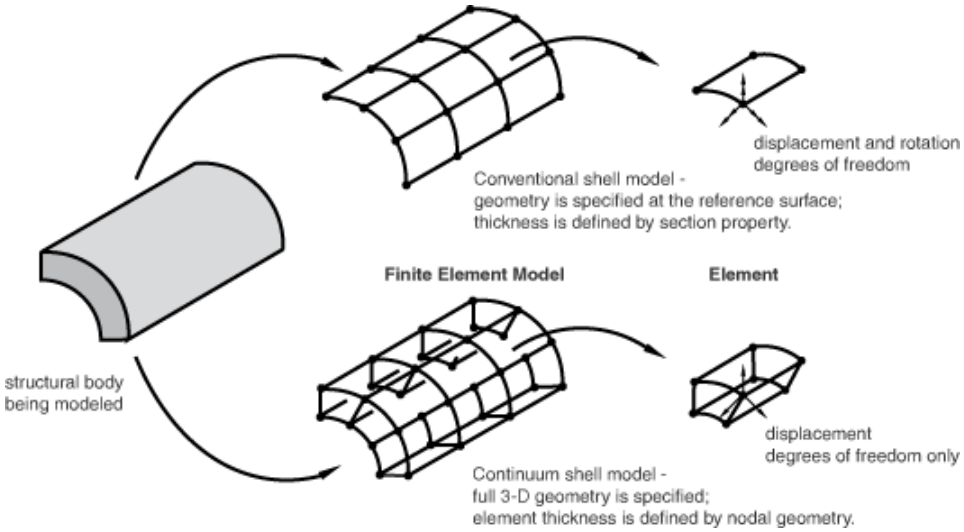

Figure 2.13: Conventional and continuum shell elements [2]

In this thesis we have used conventional shell elements. They are computationally less intensive and known to give good results. The geometric shape of shell element could be triangular or rectangular. A triangular element could be used to discretize complex curves easily while with rectangular elements such a discretization will require large number of elements along the curve. Within conventional shell elements we have choice of linear or quadratic interpolation. Higher interpolations (like cubic) are also possible in theory. But in Abaqus/CAE available S4R and S8R shell elements use linear and quadratic interpolation respectively. In the present thesis for shell models, we used S8R conventional shell element. S8R is a double curved 8-nodes thick shell element with reduced integration. A typical 8-noded conventional 3D shell element and location of its integration points are shown in Figure 2.14.

2.6.2. Solid Elements

Solid elements in Abaqus/CAE can be used for linear analysis involving contact, plasticity and/or large deformations. Only displacement degrees of freedom are active for these elements. The elements shapes available are tetrahedral (4-noded or 10-noded) and brick (8-noded or 20-noded). These are shown in Figure 2.15. Solid elements are computationally much more intensive. Part of the reason is because for same interpolation, a solid element has higher number of nodes. Also, to capture the behaviour of a member using solid elements fine mesh is recommended. This leads to increase in computation time and cost. Solid elements offers a number of advantages over shell elements. Solid elements could take into account through thickness variation of properties and they can provide vari-

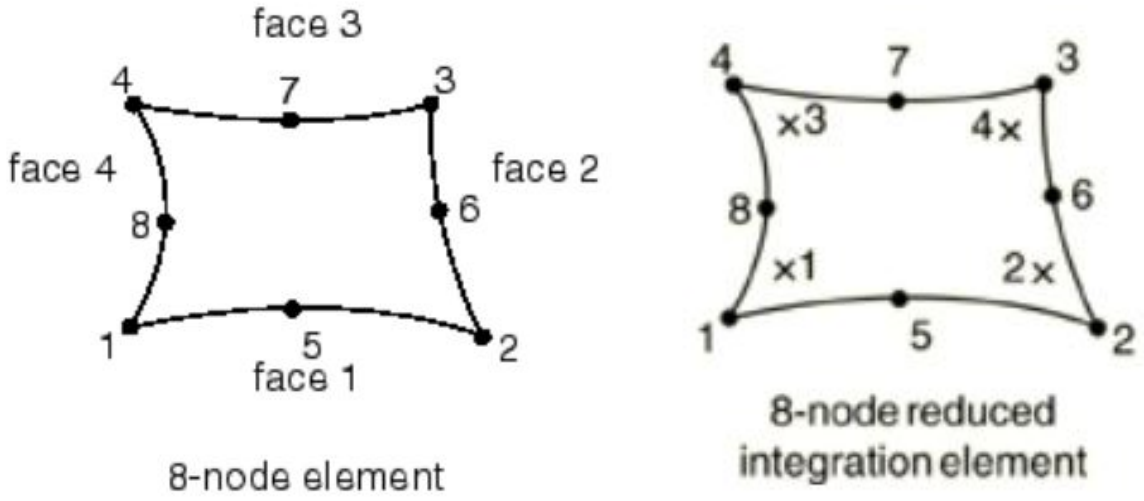

(a) Typical 8-noded shell element

(b) Integration points for reduced integration case

Figure 2.14: Typical 8-noded 3D conventional shell element [2]

ation of stresses through the member thickness which is not possible with shell elements.

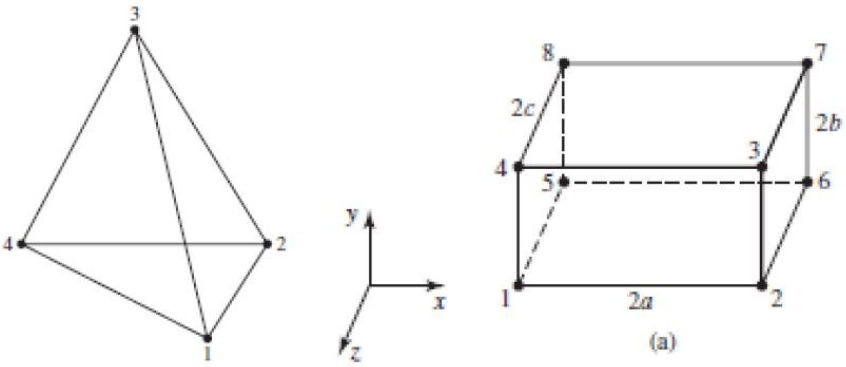

Figure 2.15: Solid tetrahedral and brick elements [17]

2.6.3. Planar Elements

Planar elements are either plane stress or plane strain type depending on the problem being modeled. CPS8R is a general purpose plane stress element while CPE8R is a general purpose plane strain element. These elements are special case of shell elements. Generally the coordinates in z-direction is zero. Just like in the case of shell element, the plane stress (or plane strain) element is expanded into a C3D20 or C3D20R element as shown in Figure 2.16

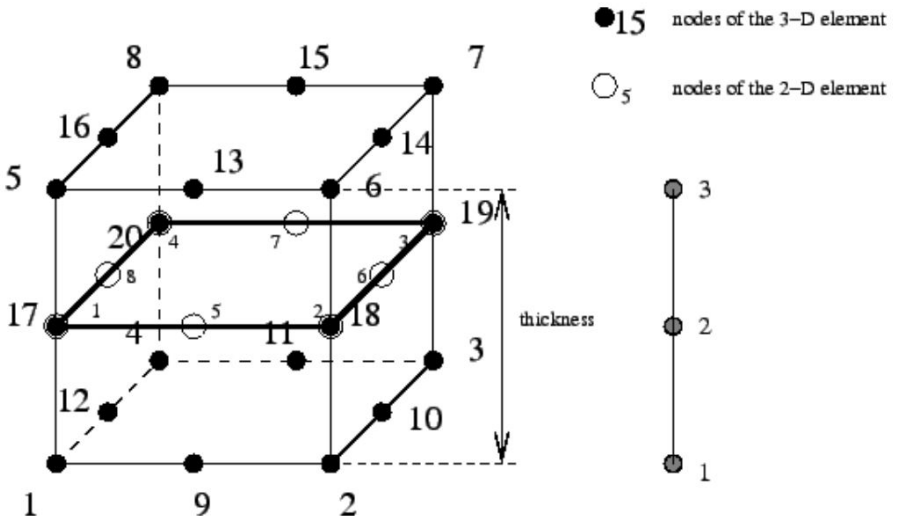

Figure 2.16: Expansion of a 2D 8-node element into a 3D brick element [1]

2.7. Review - Previous Research

A lot of research has been carried out on web-core sandwich panels. Though this thesis focuses on corrugated core panel, still there are plenty of similarities with web-core sandwich panel.

- In both of these panels, a relatively new laser welding technology was employed, namely, HLAW.
- In both the cases, there is an option to improve the panel performance using a suitable filling material
- Both the structures have low self-weight and thus are suitable for application where low self weight is critical.
- Although, fatigue performance is better as compared to conventional bridge decks there is still need to carry out detailed experimental analysis to get the S-N plots for these laser welded joints.

From Section 2.7.1 to Section 2.7.4, highly relevant research work will be reviewed in brief .

2.7.1. Fatigue Performance of laser welded steel bridge decks [6]

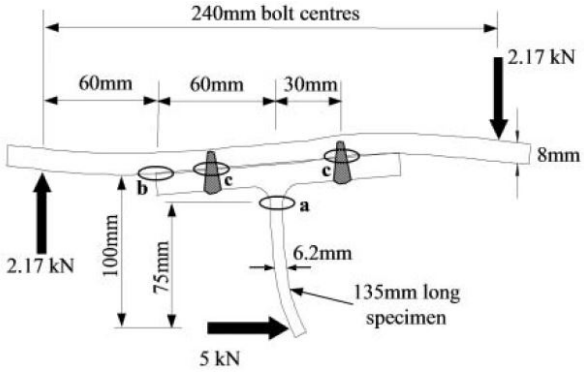

Figure 2.17: Free Body Diagram for joggle test and possible crack locations [6]

This paper examines the fatigue performance of laser stake welds. Location of crack initiation and subsequent propagation directions were obtained from a series of experiments conducted on samples extracted from an I-core sandwich panel. Samples are shown in Figure 2.20. Testing setup for *Deck*

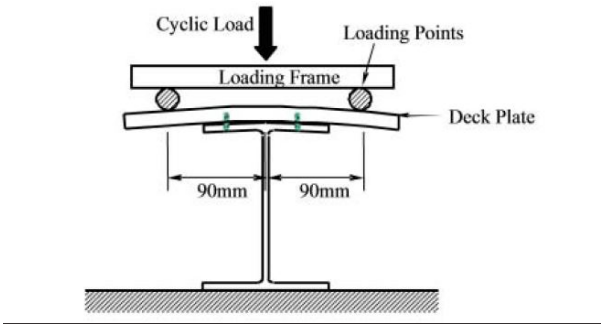

Figure 2.18: Test setup for deck bending test [6]

bending test is shown in Figure 2.18.

Samples of I-core sandwich panel were tested under two different loading configuration. One was *Deck Bending Test* and other was *Joggle Test*. The are shown in Figure 2.18 and Figure 2.17 respectively.

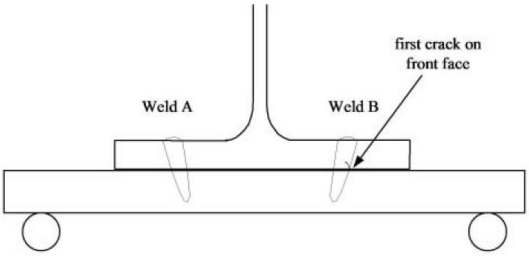

Figure 2.19: First crack originating on the front face of specimen [6]

From existing experimental work on web core sandwich panels (refer [27] and [14]) it is known that fatigue crack propagates through weld metal instead of base metal. This is in contrast with the case for conventional arc welds. In experiments conducted by Bright and Smith in [6] same conclusion was found. First crack started at the edge of weld at core - face plate junction as shown in Figure 2.19. It was observed that initially crack moved in a vertical direction but after propagating by a few mm it tended towards a 45°. This was explained as follows - during initial propagation transverse bending stresses were significant but later shear stresses became significant in the weld body [6].

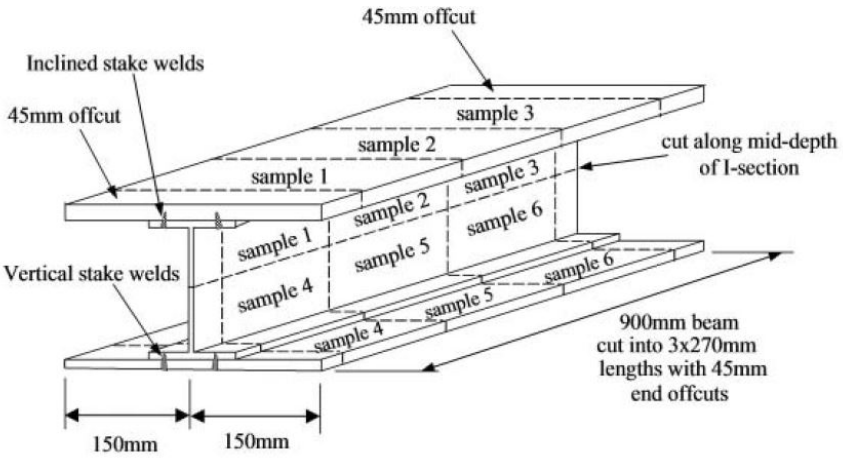

Figure 2.20: Samples taken from an I-Core sandwich panel [6]

Important insights on location of crack initiation and propagation direction were obtained from this paper. Two important conclusion of this paper are as follows - For deck bending test weld detail with 4 welds per joint exhibited inferior fatigue performance and is more expensive to manufacture. For deck bending a two-stake weld configuration could be approximated to a Class C S-N curve of BS 5400 [6].

2.7.2. Fatigue life improvement using filling material [12]

This paper estimated the relative improvement in fatigue life due to foam filling in web core sandwich panel. J-Integral was used as a fatigue strength assessment parameter. The performance improvement in foam-filled panel was characterised with respect to fatigue life of an empty panel. Two different categories of foam filling was considered - PUR and Divinycell.

FE Model

Material properties in FE model were - Young's Modulus (E) 206 MPa and Poisson's Ratio (μ =) 0.3. Geometric Non-linearity was considered during analysis.

To calculate J-Integral value, a two stage FE analysis was carried out. First a global model of panel (with shell elements to model steel member and solid elements to model foam) was analyzed and then a 2D model driven by the displacements of global model was developed. The definition of a 2D FE model is shown in Figure 2.21.

Foam for this FEA was modeled using 8-noded solid element while in 2D FEA the whole section was modeled using 8-noded 2D Plane Strain elements. For 2D submodel analysis was carried out using *Displacement Control*. Nodal displacements from global analysis at Nodes M, N & O were applied in the 2D model as shown in upper part of Figure 2.21. Rotations were applied in 2D model by rotating the boundary cross section.

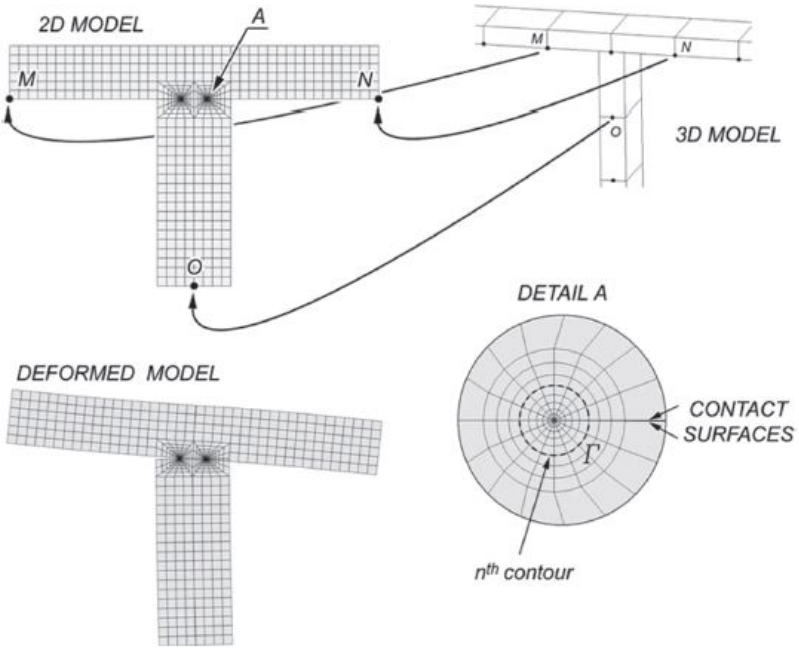

Figure 2.21: 2D FE Submodel and its definiton [12]

Results

Fatigue life assessment was obtained using regression equation, $N_f = C\sqrt{\Delta J}^{-m}$, where m (=9.1) is the slope of fatigue resistance curve and C (=294 $MPa^{4.55}mm^{4.55}$) represents the material constant.

Computed fatigue life for a constant specimen geometry and loading ($\Delta F = 6kN$) is shown in Figure 2.22. The results show an increase in fatigue life by a factor of 500 with only 2% increase in weight.

	Filling				Critical joint	
Case	Density [kg/m^3]	Young's modulus [MPa]	Poisson's ratio	Mass [kg]*	$\sqrt{\Delta J}$ [MPa$^{0.5}$ mm$^{0.5}$]	Fatigue life, N_f [cycles]
EMPTY	0	0	0	0.0	0.636	18,026
PUR15	15	1	0.33	0.3	0.626	20,913
PUR60	60	19	0.33	1.2	0.399	1,268,334
PUR100	100	25	0.33	1.9	0.359	3,274,644
PUR120	120	37	0.33	2.3	0.303	15,475,030
PUR140	140	55	0.33	2.7	0.249	90,490,102
H35	38	44.5	0.4	0.7	0.283	28,775,058
H45	48	52.5	0.4	0.9	0.261	59,730,156
H60	60	72.5	0.4	1,2	0.221	270,390,869
H80	80	92.5	0.4	1.5	0.194	888,523,982
H100	100	132.5	0.4	1.9	0.159	5,434,562,360

*All panels have the area of 0.48 m^2.

Figure 2.22: Computed fatigue life from $\sqrt{\Delta J}$ value, load ΔF = 6kN [12]

2.7.3. Fatigue Strength of laser welded foam filled beams [19]

Beams of web-core sandwich panel with H80 foam and empty ones were tested under 3-point bending test. The purpose of these experiments were to determine stiffness, ultimate strength and fatigue life for empty and filled beams.

Beam Dimensions

Each web-core sandwich beam was 50 mm wide, 46 mm in height. Each beam consisted of 4 cells with web spacing of 120 mm. Total length was 480 mm. Face plates were 3 mm thick and web plate was 4 mm thick. Material for face plates was S355J2G2 and web plates were made of S235JR [19]. The foam was joined adhesively to the steel plates. For details of samples preparation reference could be made to Section 2.2 of the paper under discussion.

Fatigue Testing

Sample tested for *Stiffness* and *Ultimate Strength* were under displacement control with a constant rate of 10 mm per minute. For fatigue testing, force control was employed with a load ratio of 0.05. The fatigue life of sample was assessed using the regression relation - $N_f(\sqrt{\Delta J})^m = C$ with $m = 9.1$ and $C = 294MPa^{4.55}mm^{4.55}$. The results of fatigue testing is shown in Figure 2.23.

Results

Results of the experimental investigation could be summarized as follows -

- 3 x increase in stiffness
- 6% increase in self-weight
- 2.7 x increase in ultimate strength
- slope of fatigue resistance curve, m increase from 4.508 to 7.321
- 8.5 x increase in load at 2 million cycles at load ratio 0.05

2.7.4. Improving the shear properties of web-core sandwich structures [27]

It is well understood that web-core or any other similar sandwich panel imparts a high degree of orthotropy in the structure. For example, in case of web-core sandwich panel, the shear stiffness in the

Fatigue data. Failure locations: IT/IB = Intermediate Top/Bottom joint between indenter and roll support. ST/SB = Support Top/Bottom joint. Load ratio was $R = 0.05$.

Specimen ID	F_{max} [N]	Cycles to failure	Failure location
Empty 1	264	1,204,000	ST & SB
Empty 2	290	281,200	IT & SB
Empty 3	320	496,200	IT & SB
Empty 4	350	388,500	IB & SB
Empty 5	350	201,400	IT & SB
Empty 6	375	136,900	IT & SB
Empty 7	400	147,300	IT & SB
Empty 8	400	183,000	IT
Empty 9	450	64,500	IT & SB
Filled 1	1000	2,590,000	(Runout)
Filled 2	2250	435,500	IB
Filled 3	2250	590,200	IB
Filled 4	2500	209,600	IB
Filled 5	2500	265,700	IB
Filled 6	2750	74,300	IB
Filled 7	2750	137,100	IB & IT
Filled 8	3000	70,500	IB

Figure 2.23: Results of fatigue testing on empty and filled beams [19]

direction of core could be orders of magnitude higher than the shear stiffness in the direction perpendicular to the core. This difference in shear stiffness create problems by inducing normal stresses in the web and face plates. By filling foam in space between webs, it is possible to improve shear properties of a sandwich panel.

This paper considers shear stiffness, shear induced secondary normal stresses and the ultimate strength of foam - filled web core sandwich panels. Divinycell foams were used as a filling material with density ranging from 80 kg/m^3 to 200 kg/m^3. Web and face plates were joined together by laser welds while foam was bonded adhesively to the surrounding steel plates. Foam filled beams were then tested under four-point bending.

Dimensions

The dimensions of beams tested were as follows: Length - 1080 mm, Breadth - 50 mm, face plate thickness - 2.52 mm, web plate thickness - 3.97 mm and height of web plate - 40 mm. The spacing of web plates were 120 mm and in total there were 9 web plates along the beam's length. In the paragraph below we discuss the FE model and results.

FE Model

FE Analysis was carried out in two steps. First, the linear elastic response of the beam was evaluated using 20-noded solid element (C3D20R). Later, plane strain element models were used to assess the ultimate strength behaviour. Unlike previous FE models, here the rotational stiffness of weld was considered in the model. Equivalent weld thickness of 2 mm was used to model the rotational stiffness. Foam behaviour was taken as orthotropic. Non-Linear analysis was carried out in Abaqus using *Riks* option in Abaqus.

Results

Normal stresses on the top surface of the top face plate are shown in Figure 2.24 and Load deflection behaviour in Figure 2.25. Compared to empty beams, foam filled beams showed less deflection. H200 foam showed less deflection as compared to H80 foam. As for y-direction normal stresses (Refer Figure 1 of the reference paper) the results showed substantial reduction in the peak stress value. For the beam under four-point bending test the peak normal stress reduced from 120 N/mm^2 to 40 N/mm^2 for H80 foam filling. For H200 foam filling reduction was even more pronounced with stress reducing

from 120 N/mm^2 to approximately 15 N/mm^2. Ultimate strength also showed *2.5 x* and *3.5 x* increase for H80 and H200 foams respectively.

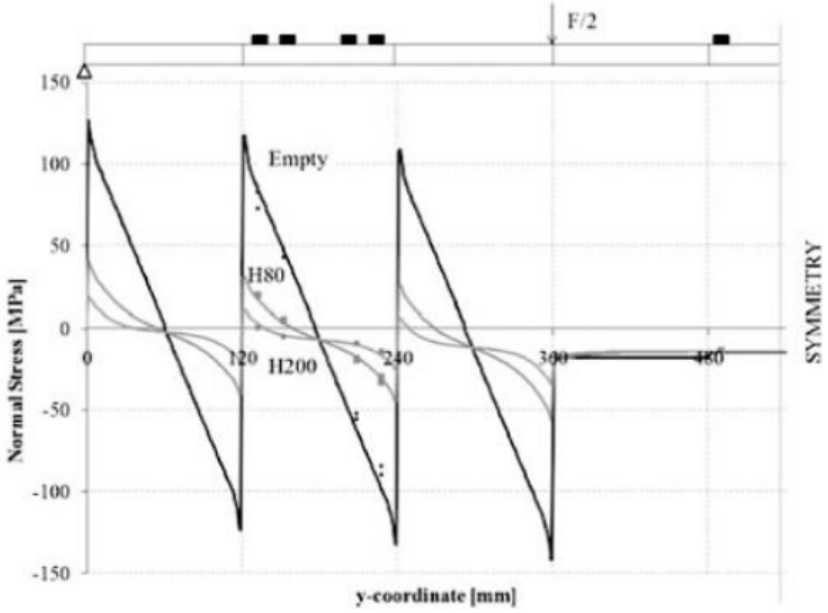

Figure 2.24: Comparison of normal stresses on the top surface of top face plate [27]

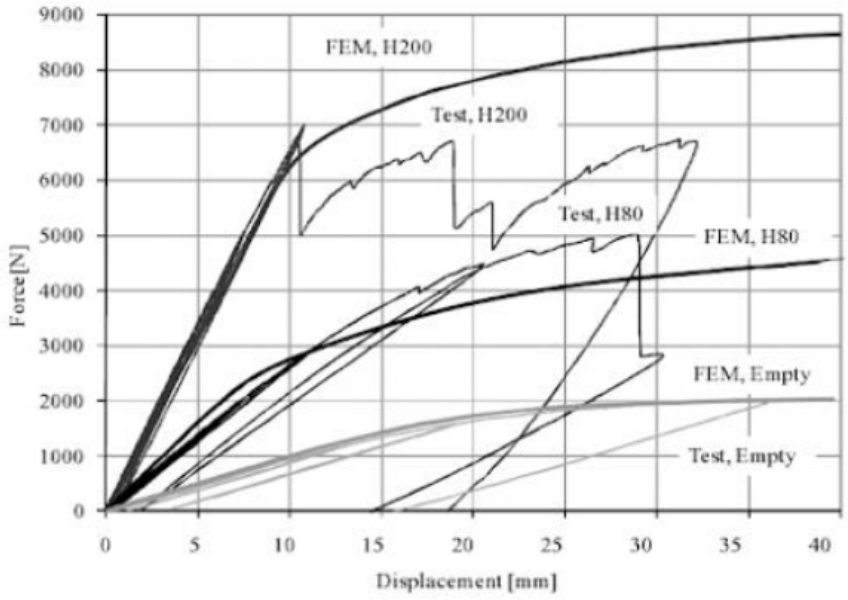

Figure 2.25: Comparison of Force vs Displacement plots for empty, H80 and H200 beams [27]

3

Verification Study

3.1. Introduction

This chapter deals with development of various FE models. The results obtained from these models will be compared with published experimental results for the purpose of validation. For verification study 1, the panel dimensions and experimental results were taken from Tan et al. [33] (referred as *Tan KH* in this thesis). For validation study 2, ASTM-CT specimen was modelled in Abaqus/CAE to validate the J-Integral calculation technique using *Contour Integral* option. For validation study 3, joint of a web core sandwich panel was modelled. The aim of this is to get a good estimate of J-Integral at tensile notch of the welded joint.

3.2. Verification Study - Sandwich Panel

A sandwich panel consists of three components - top face plate, core layer and bottom face plate. The core could be of various shapes. Possible core shapes are shown in Figure 2.1. Only sandwich panel with corrugated core is investigated in this thesis. A corrugated core sandwich panel of plan dimension 5996 mm x 2120 mm was chosen to carry out validation study. Dimension, loading, boundary condition and material properties were taken from Tan et al. [33]. These will be discussed in Section 3.2.1 and onwards.

3.2.1. Panel Geometry

The sandwich panel is made up of 2.5 mm thick mild steel plates. The core is of symmetric corrugated type with 12 mm thick end plates all around the panel. The components of sandwich panel are joined together using spot welding. One deviation of this verification study with Tan et al. [33] is the type of welding. In this verification study we assumed that top face plate and bottom face plates are welded respectively to core by dual stake laser weld. The plan dimensions of the panel and cross section geometry of a single cell are shown in Figure 3.1 and Figure 3.2 respectively.

3.2.2. Material Properties

The material model was assumed to be Linear-Elastic. Non-linearity was not included in FE analysis and reason for this is described in Section 3.2.4.3. The panel is made up of mild steel. The properties of the steel used in FE model is as follows -

1. Young's Modulus - 209 GPa
2. Poisson's Ratio - 0.3

3.2.3. Loading and Boundary Conditions

Load was applied on the top face plate. Two different loads, one 5.5 kN/m^2 and other 6.9 kN/m^2 was applied as uniform pressure load on two models. The experimental and closed formed solutions in Tan et al. [33] are given in terms of panel deflection (for load of 5.5 kN/m^2) and stresses or strains (for load of 6.9 kN/m^2). This is why in this validation study it was necessary to have two different loads.

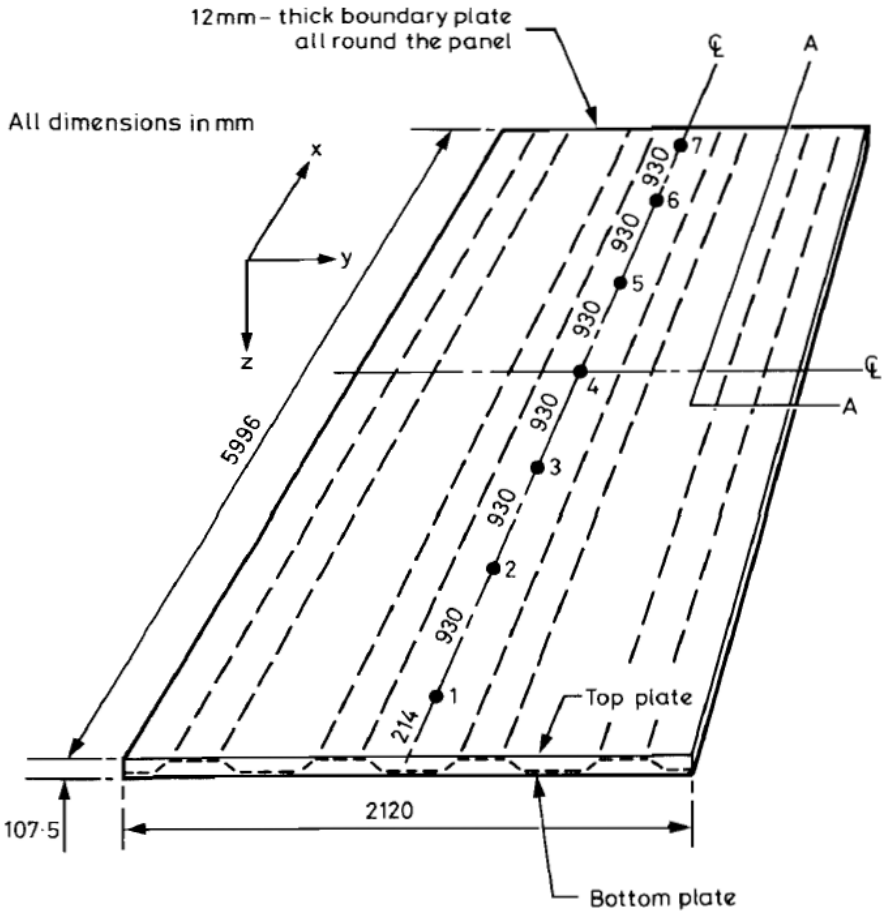

Figure 3.1: Global dimensions of Sandwich Panel used in verification study, from Tan et al. [33]. Black dots shows location of strain gauges. These are not relevant for this thesis.

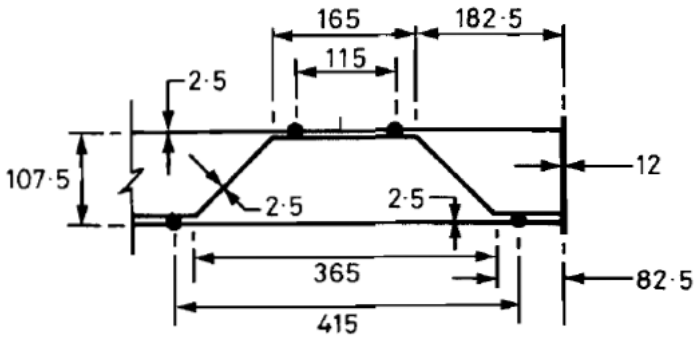

Figure 3.2: Cross section A-A of Sandwich Panel used in verification study, from Tan et al. [33]

The applied load on FE model is shown in Figure 3.14.

Two different boundary conditions were considered in this validation study. One where two smaller sides are simply supported and other where panel is simply supported on all sides. The former case is referred as *SS ends only case* in this thesis while the latter is referred as *All sides SS case*. The panel is doubly symmetric in plan and therefore only one fourth of the full panel was modelled. Boundary condition and the quarter part modelled is shown in Figure 3.3 and Figure 3.4 respectively.

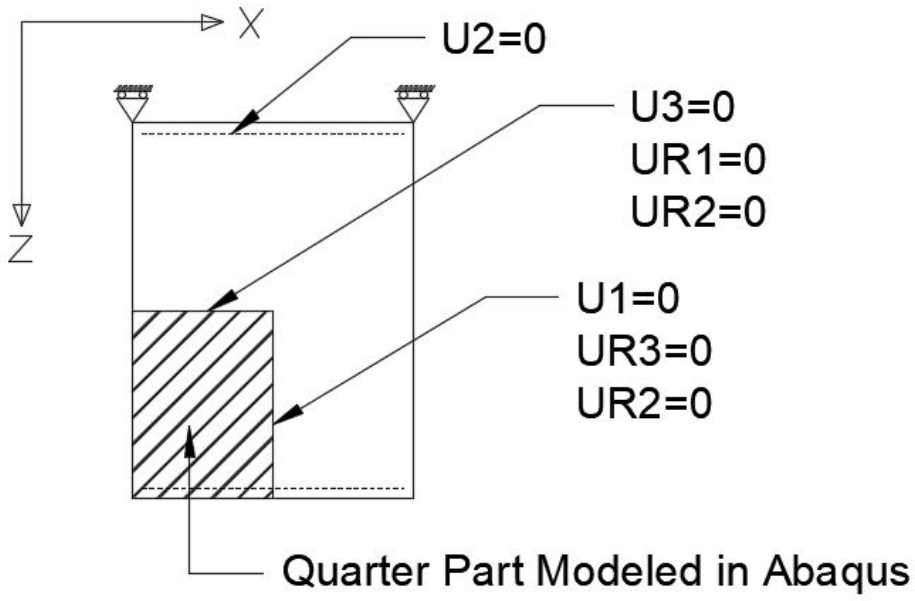

Figure 3.3: *SS Ends only* case - Quarter Model and boundary condition

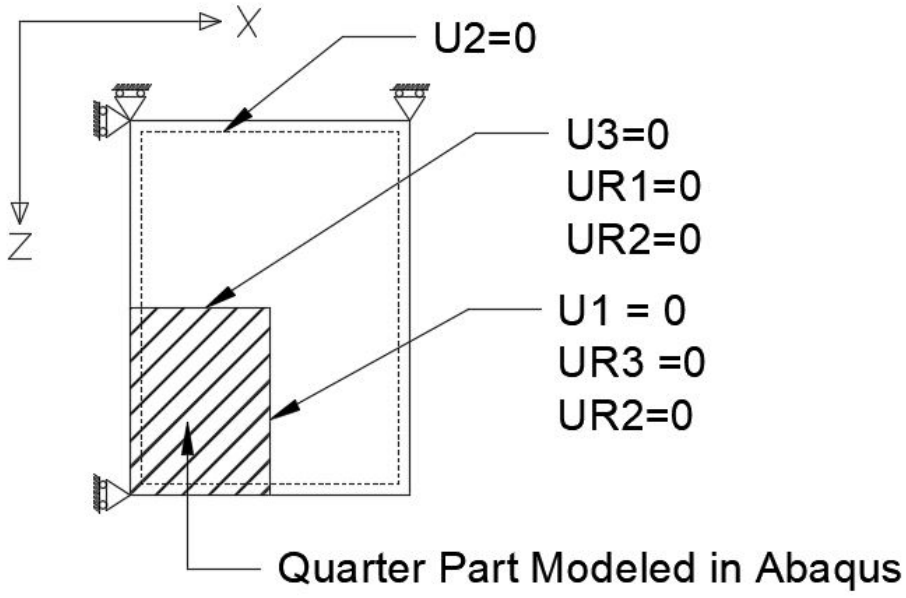

Figure 3.4: *All Round SS* case - Quarter Model and boundary condition

3.2.4. FE Modelling in Abaqus/CAE

Aside from geometry and material properties, some tools from *Interaction* module of Abaqus/CAE was also used to create FE model. This section explains the following parts in more detail - Use of *Offset* for shell models, use of interaction module, shell element local axis and whether to consider geometric non-linearity in analysis or not. The knowledge of shell element local axis is important for correct interpretation of the Abaqus/CAE output.

Offset

A reference geometry should be created first with individual parts modelled as *Shells*. Once reference geometry is ready Abaqus/CAE *Offset* tool could be used to capture the thickness of the solid model

that our shell model is replacing [2]. Appropriate offsets were assigned to top face plate, core layer and bottom face plate. Top face plate was offset by *-0.5*, bottom face plate by *+0.5*. Inclined parts of core were at *0* offset. Parts of core that were in contact with bottom face plate were at an offset of *+0.5* and parts which were in contact with top face plate were at an offset of *-0.5*. The FE model reference surface and post offset cross section is shown in Figure 3.6. Individual offsets are shown in Figure 3.5. The modelled height of the sandwich panel is 105 mm and is shown in Figure 3.7.

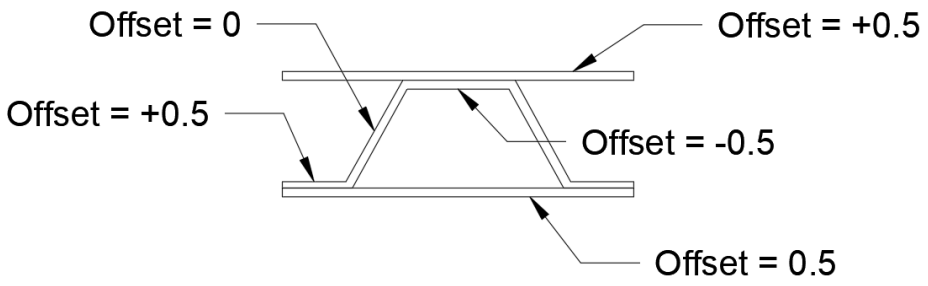

Figure 3.5: Offsets given to individual parts of sandwich panel

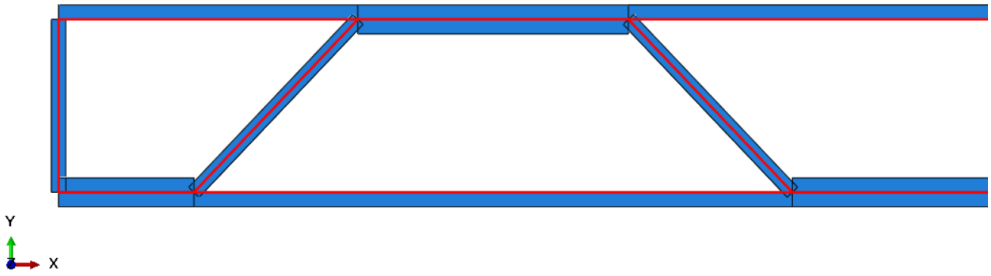

Figure 3.6: Cross Section of Shell Model (Red line shows shell reference surface) and post offset orientation of various parts

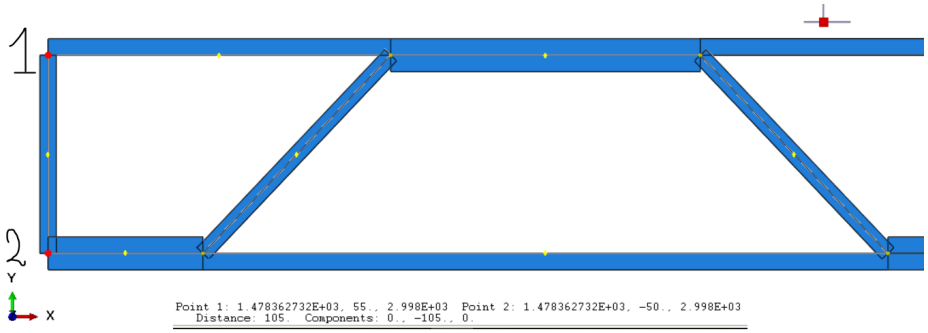

Figure 3.7: Modelled height of sandwich panel, distance between point 1 and 2 is 105 mm.

Modelling Interactions

In this verification study the effects of welds as well as interaction between steel plates during analysis were incorporated using *Interactions* module of Abaqus/CAE. To simulate the effect of welding *Tie Constraints* were used. Contact between steel plates during analysis were handled through *surface to surface* interaction. Within Abaqus surface-to-surface contact definition, *Finite Sliding* option was

chosen. Contact interaction property was further refined with frictionless *Tangential* behaviour and Hard Contact for *Normal* behaviour. These two interactions are shown in Figure 3.8 and Figure 3.9 respectively. Both of these interactions were implemented in the FE model.

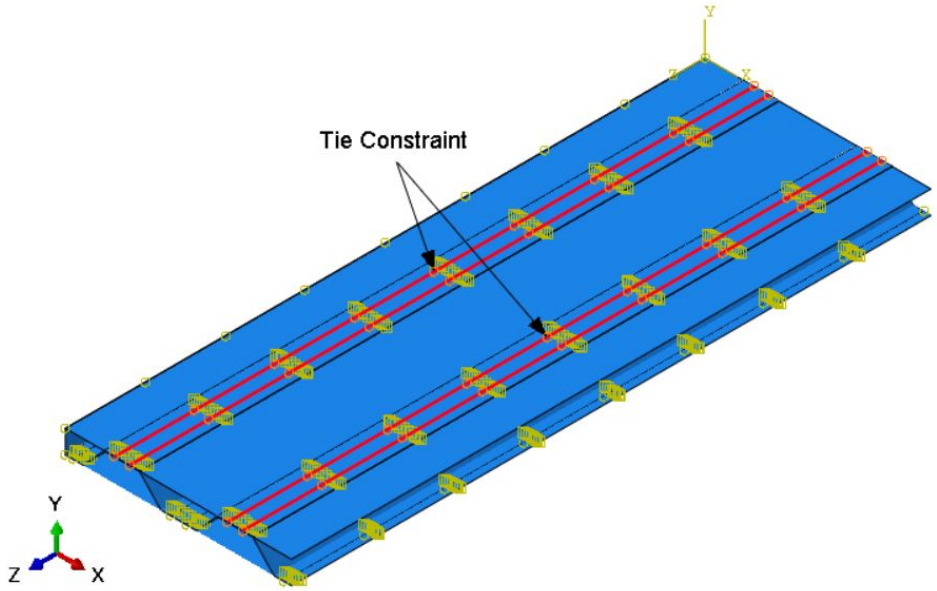

Figure 3.8: Application of tie constraints to simulate the effect of continuous weld

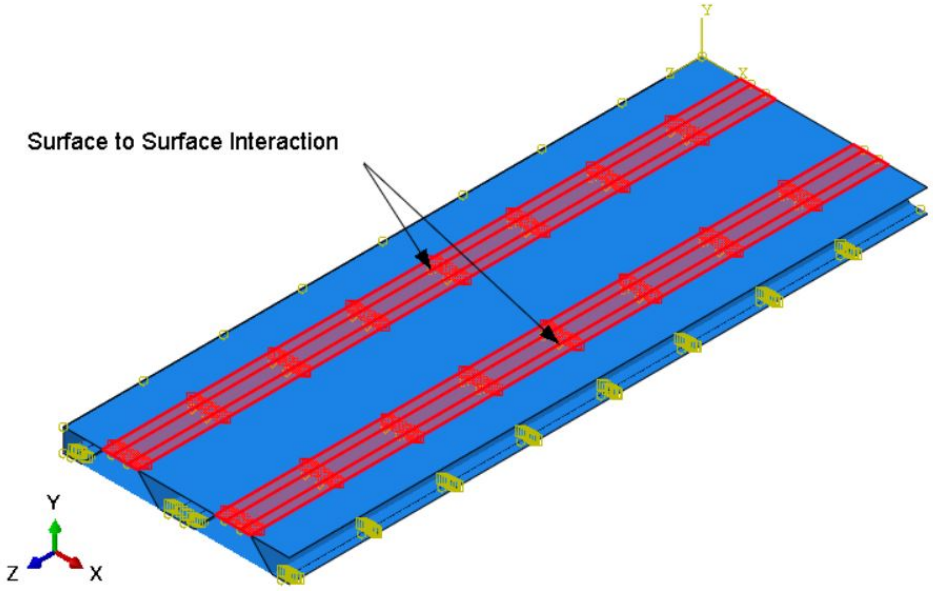

Figure 3.9: Surface to Surface interaction between top face plate and core

Geometric Non-Linearity in Analysis

A trial analysis was run to ensure that results for geometrical non-linear analysis case are not substantially deviating from the linear first-order analysis. Comparison of peak displacement U2 and peak stresses S11 and S22 are shown in the Table 3.1 below for the two cases, one with NLGEOM (geometric non linearity) - OFF and other with NLGEOM - ON. Table. 3.1 shows result for *Both Sides SS* case and Table. 3.2 shows result for *All Sides SS* case. Results for both the cases show that geometric

non-linearity only marginally affects the output. For small deflection cases, we can disregard geometric non-linearity. From previous research, refer Section 1.3 of [28], we know that for deflection to be considered small it should be in the range of 0.1 to 0.5 of the panel height. In this verification study maximum deflection observed was approximate 23.00 mm which is less than 0.5 x panel height.

It is evident from the comparison results (see Table 3.1 and Table 3.2) that difference between linear analysis and geometric non-linear analysis is quite insignificant. Only for the case of *Stress, S11* is the observed difference a bit high. For all other parameters of interest, error is within limits. The maximum strain in the whole model is equal to 0.041% for *SS Ends only case* and 0.18% for *All Sides SS Case*. As a rule of thumb, if strain is less than 5%, geometrical non-linearity could be disregarded in analysis. Therefore, in this verification study geometrical non-linearity will not be considered.

	without NLGEOM (abs.)	with NLGEOM (abs.)	% difference
U2 max (abs.)	23.00	23.40	1.71
Stress, S11 (max), (abs.)	52.96	64.34	17.68
Stress, S22 (max), (abs.)	83.20	85.20	2.35

Table 3.1: Comparing Results for Linear and Geometrically Non-Linear Analysis for *Both Sides SS* case

	without NLGEOM (abs.)	with NLGEOM (abs.)	% difference
U2 max (abs.)	6.83	6.90	1.01
Stress, S11 (max), (abs.)	147.5	155.5	5.14
Stress, S22 (max), (abs.)	56.23	60.72	7.39

Table 3.2: Comparing Results for Linear and Geometrically Non-Linear Analysis for *All Sides SS* case

Shell Element Local Axis

Unlike continuum elements, shell elements use material directions local to each element. Knowledge of local direction are important while interpreting results of FEA. In the description below, the term *axis* refers to global coordinate axis while the term *direction* refers to local coordinate axis.

The output of FEA with shell elements are given in terms of local directions. The local material 1- and 2- directions lie in the shell plane while the 3- direction is perpendicular to it given by *right hand thumb rule*. The default local 1- direction is projection of the global 1- axis onto the shell surface. For a specific case where global 1- axis is perpendicular to the shell surface, local 1- direction is projection of the global 3- axis on the shell surface.

FE Model

To create a full 3D sandwich panel, three separate parts were drawn in Abaqus *Parts* module. These three parts were then assembled using the assembly option of Abaqus. To select an appropriate element for discretization both the reference paper ([33]) and Abaqus User's Manual (Sec 3.6.1) were referred. User's Manual states that Non negligible transverse shear flexibility is required for this element to function properly; hence the element (element term here means S4R and S8R shell elements) is suitable for the analysis of composite and sandwich shells [2]". A regular mesh geometry was used in case of S8R elements as irregular meshes of this element converge very poorly because of severe transverse shear locking.

To get an appropriate mesh size for our FE model, a mesh convergence study was also carried out and is discussed in Section 3.2.6. Based on this study it was decided that an element size of 20 mm is suitable. The model, boundary condition and it's meshing is shown in Figure 3.12a and Figure 3.12b below. The two FE models developed are shown in Figure 3.10 and Figure 3.11 for *SS Ends only case* and *All Sides SS Case* respectively.

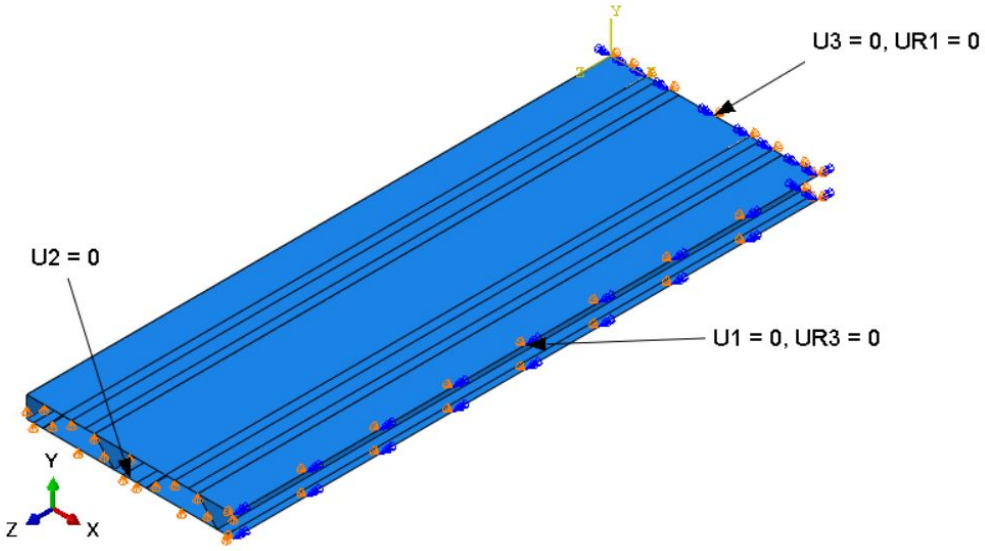

Figure 3.10: FE Model - Boundary Condition for *SS Ends only case*

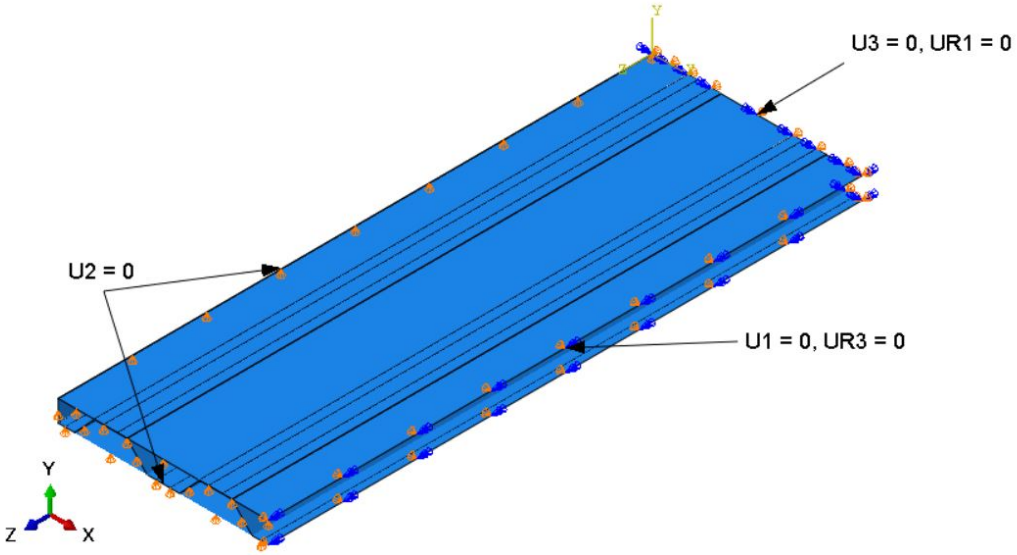

Figure 3.11: FE Model - Boundary Condition for *All Sides SS Case*

3.2.5. Analysis Results

SS Ends Only Case

The maximum deflection on the top face plate is 23.00 mm while from Figure 7 of [33] we get a deflection of 23.50 mm. Observed difference is 2.13% only. The stress S22 on the top compression plate are shown in Figure 3.16, the maximum observed stress is equal to 104.4 N/mm^2 compared to the reference result of 95 N/mm^2. This higher difference in stresses could be attributed to the way core to face plate connection is modelled. In the reference case, beam elements were used to model spot welds, while in the present FE model, the weld joining core to face plates were continuous laser welds and were modelled using tie constraints. Experimental data from the reference study shows that the stresses obtained in this FE Model are conservative. The stresses, S22 on the bottom tension plate are shown in Figure 3.17. The maximum stress, S22 on the bottom plate is 111.6 N/mm^2 while for the reference case maximum stress value is 95 N/mm^2. In Figure 3.18 a comparison is shown between maximum panel deflection obtained in our FE Analysis compared with experimental results obtained in [33]. The deflection along x-symmetric boundary condition line (Refer Figure 3.3) is com-

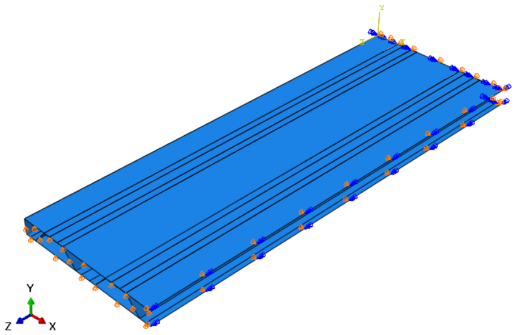

(a) Global Model and Boundary Condition for SS ends only case

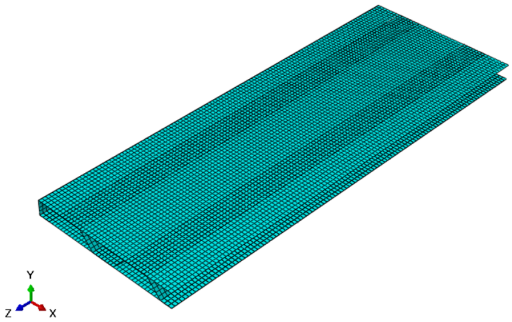

(b) Meshing in Quarter Model for SS ends only case

Figure 3.12: Quarter Panel for the SS ends only case modelled in Abaqus

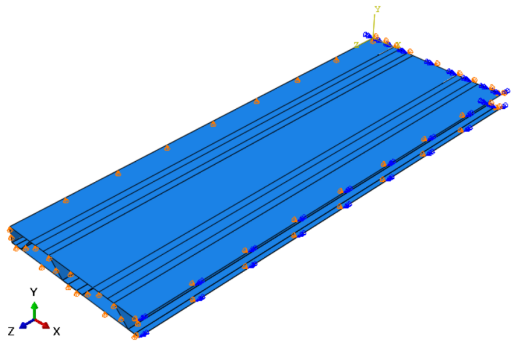

(a) Global Model and Boundary Condition for *All sides SS* case

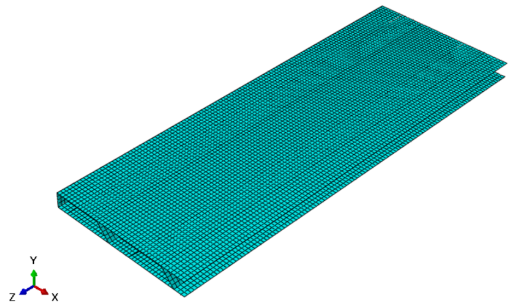

(b) Meshing in Quarter Model for *All sides SS* case

Figure 3.13: Quarter Panel for the *All sides SS* case modelled in Abaqus

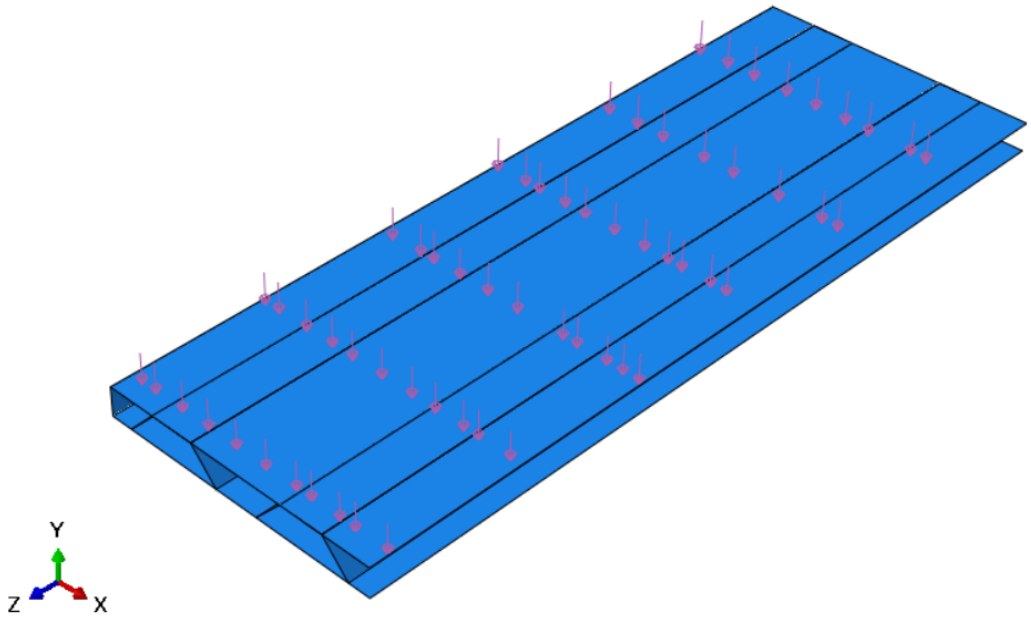

Figure 3.14: Uniformly distributed pressure applied on top face plate, 5.5 kN/m^2 for deflection measurement and 6.9 kN/m^2 for stress - strain verification

pared with TanKH - experimental and TanKH - FEA results. This comparison plot is shown in Figure 3.19.

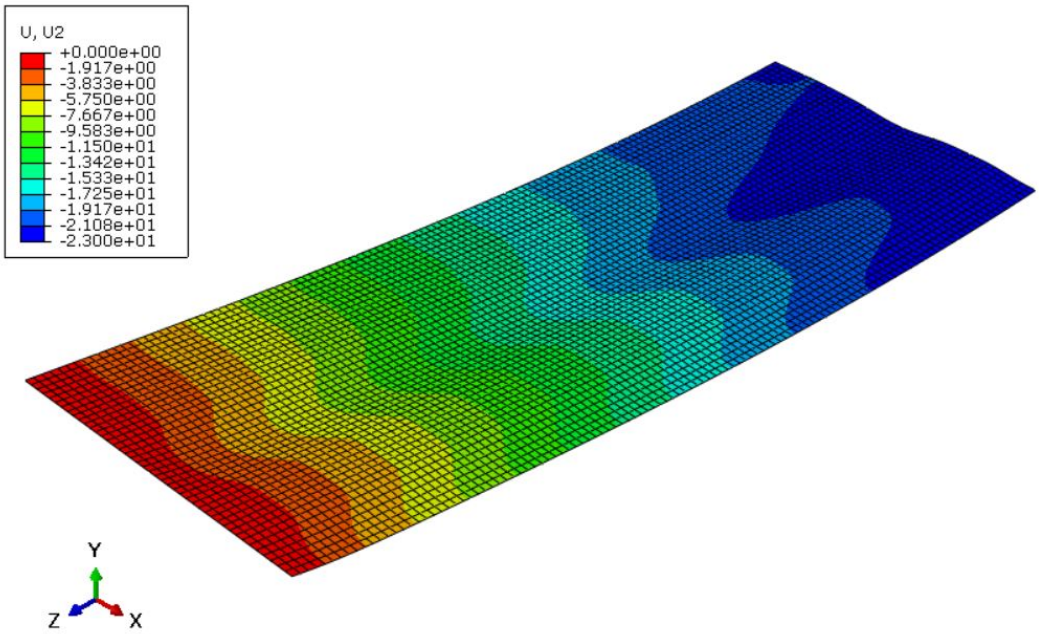

Figure 3.15: Deflection U2 on top compression plate for udl of 5.5 kN/m^2 for SS ends only case

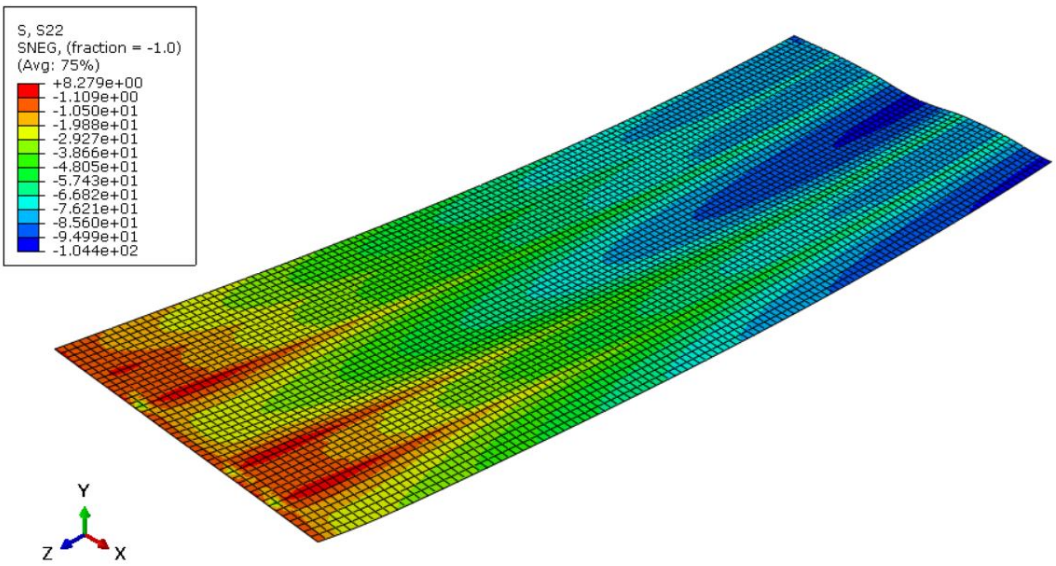

Figure 3.16: Stress, S22 on the top compression plate for udl of 6.9 kN/m^2 for SS ends only case

All Sides SS Case

The boundary condition for this part is shown in Figure 3.4 and the FE model and meshing is shown in Figure 3.13a and Figure 3.13b respectively.

The displacement in the bottom face plate is shown in Figure 3.20. Stresses, S22 on the top and bottom face plates are shown in Figure 3.21 and Figure 3.22 respectively. The deflection obtained in the present FE Analysis is compared with Experimental and FE Analysis results of the reference paper. The comparison shows good agreement overall as can be seen in Figure 3.23. The comparison

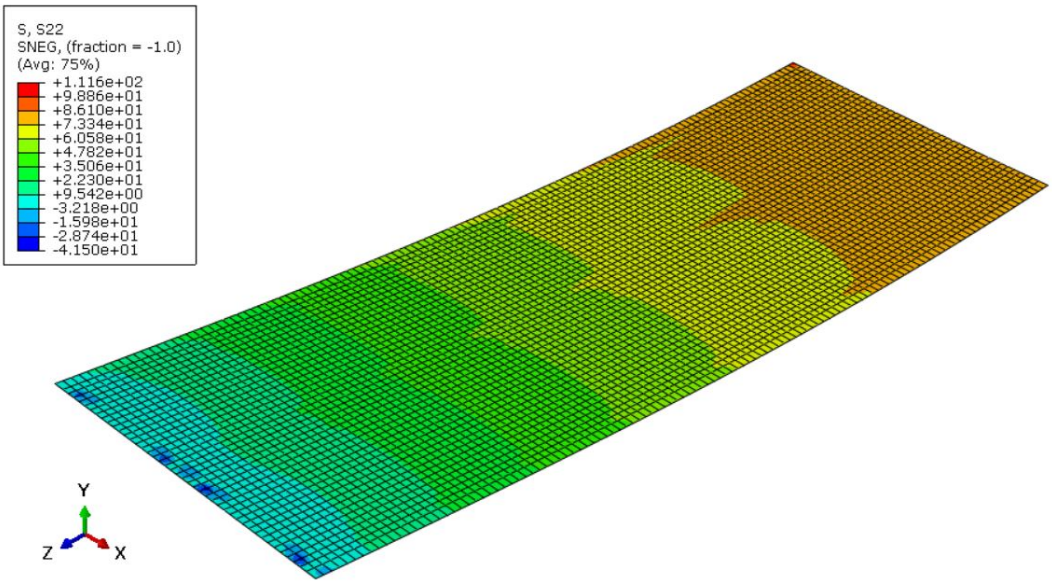

Figure 3.17: Stress, S22 on the bottom tension plate for udl of 6.9 kN/m^2 for SS ends only case

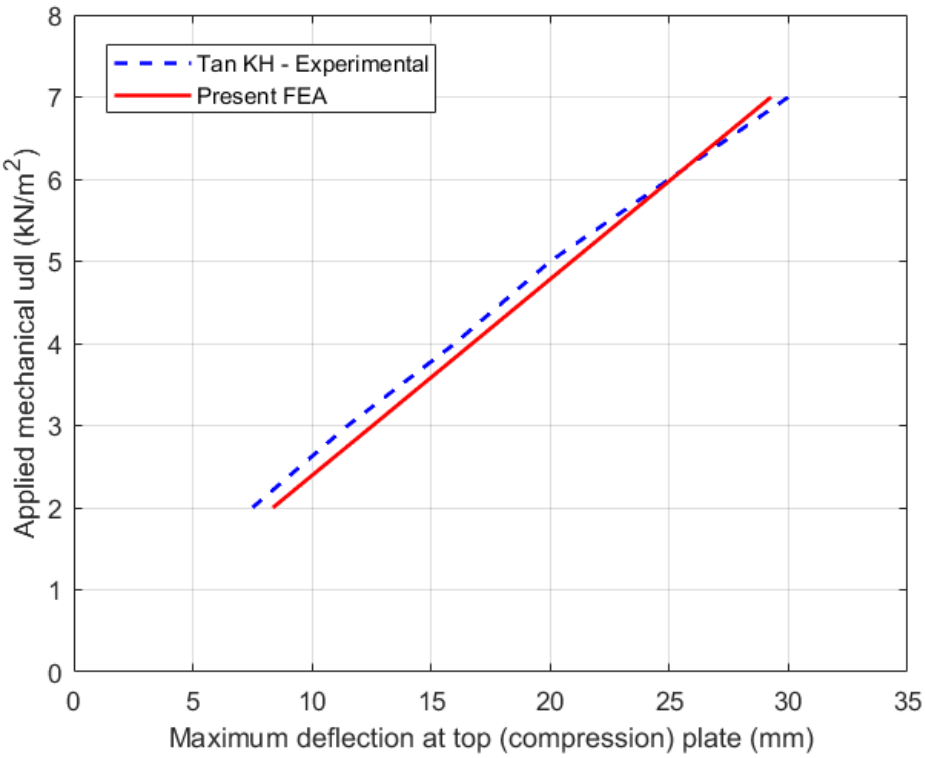

Figure 3.18: Comparison of FE Analysis results obtained in this study with experimental data from [33] for *SS ends only case*. Here Tan KH refers to results obtained from Tan et al. [33].

between applied load and corresponding maximum panel deflection for *All Sides SS* case is shown in Figure 3.24. The present FE analysis correlates well with experimental results of reference paper.

3.2.6. Mesh Convergence

In this section mesh density will be increased gradually to check for convergence in obtained solution. For *Both Sides SS* case, convergence will be checked for maximum deflection in y-direction for the top

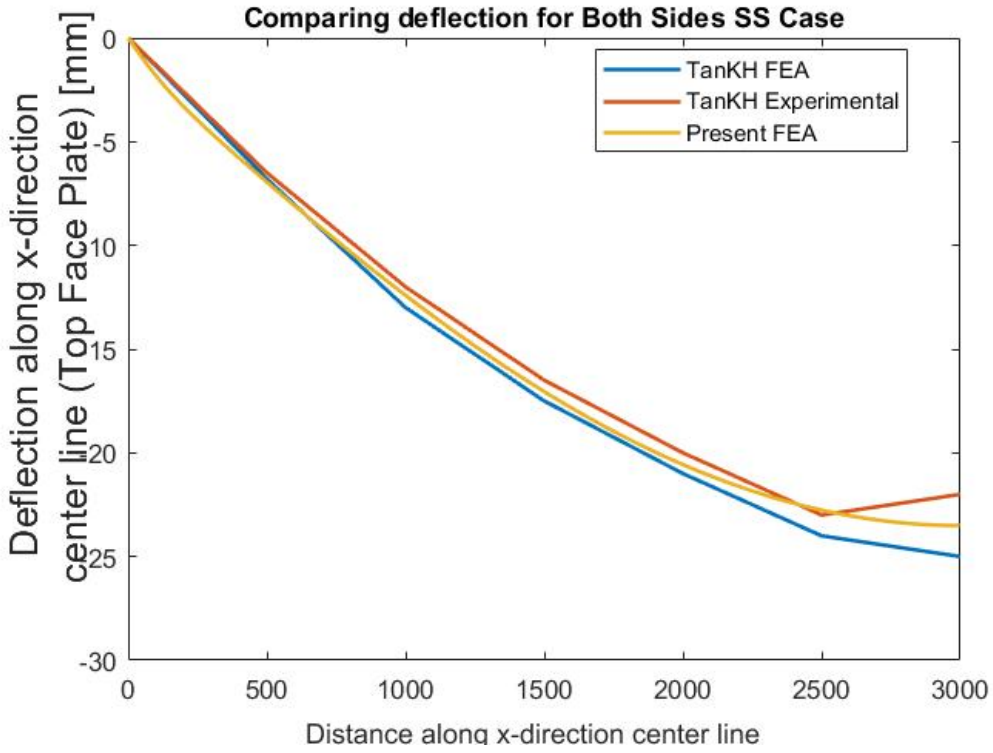

Figure 3.19: Comparison of deflection along x-symmetric BC line for *SS ends only* case. Here Tan KH refers to results obtained from Tan et al. [33].

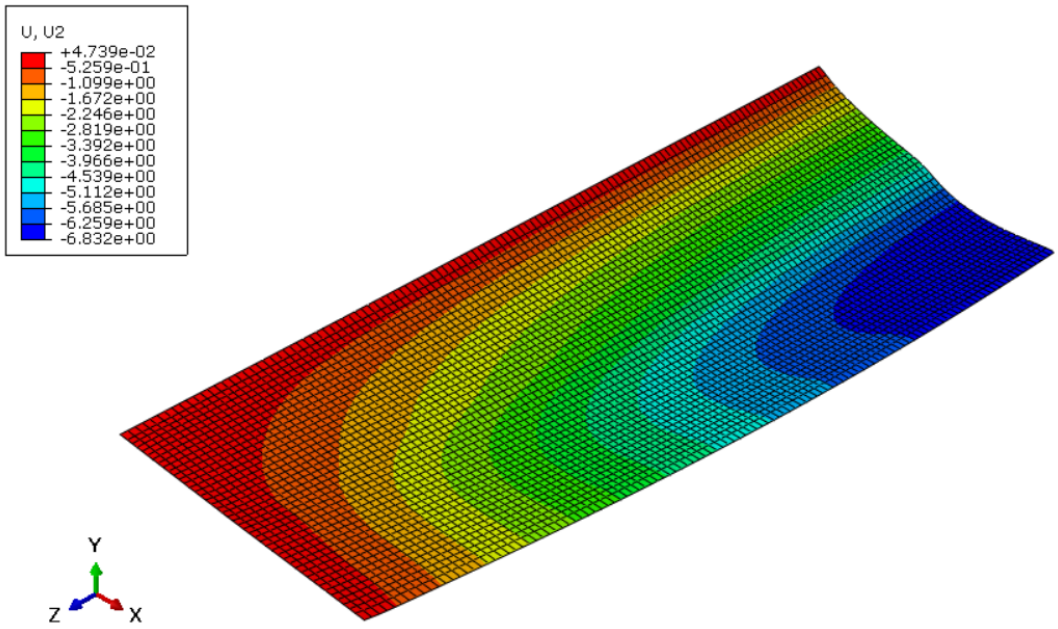

Figure 3.20: Deflection U2 on the bottom plate for udl of 5.5 kN/m^2 for *All Sides SS* case

face plate. For *All Sides SS* case, maximum deflection for the bottom face plate will be checked for convergence. In Table. 3.3 the convergence results are shown for *SS ends only case* and 3.4 shows the convergence results for *All Sides SS Case*. Convergence is obtained at mesh size of 20 mm and the converged deflection is equal to 22.98 mm and 6.83 mm for beam and plate behaviour case. From the mesh convergence study shown in Table. 3.3 and Table. 3.4 it was observed that a global mesh size of

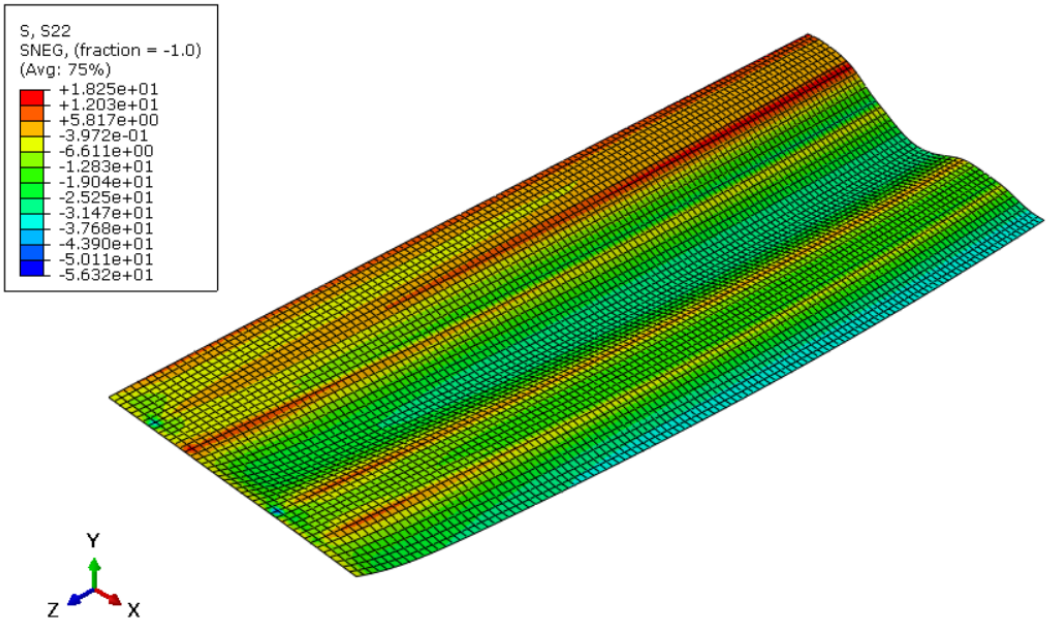

Figure 3.21: Stress S22 on top face plate for udl of 6.9 kN/m^2 for *All Sides SS* case

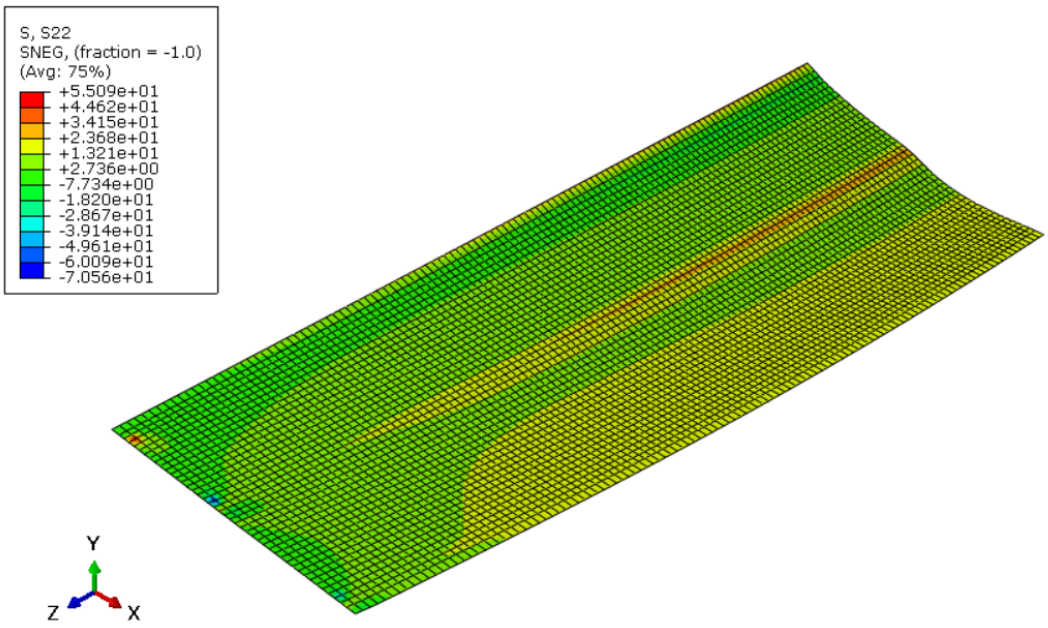

Figure 3.22: Stress S22 on bottom face plate for udl of 6.9 kN/m^2 for *All Sides SS* case

20 mm gives good results. Therefore, for verification study 1, a global mesh size of 20mm was used.

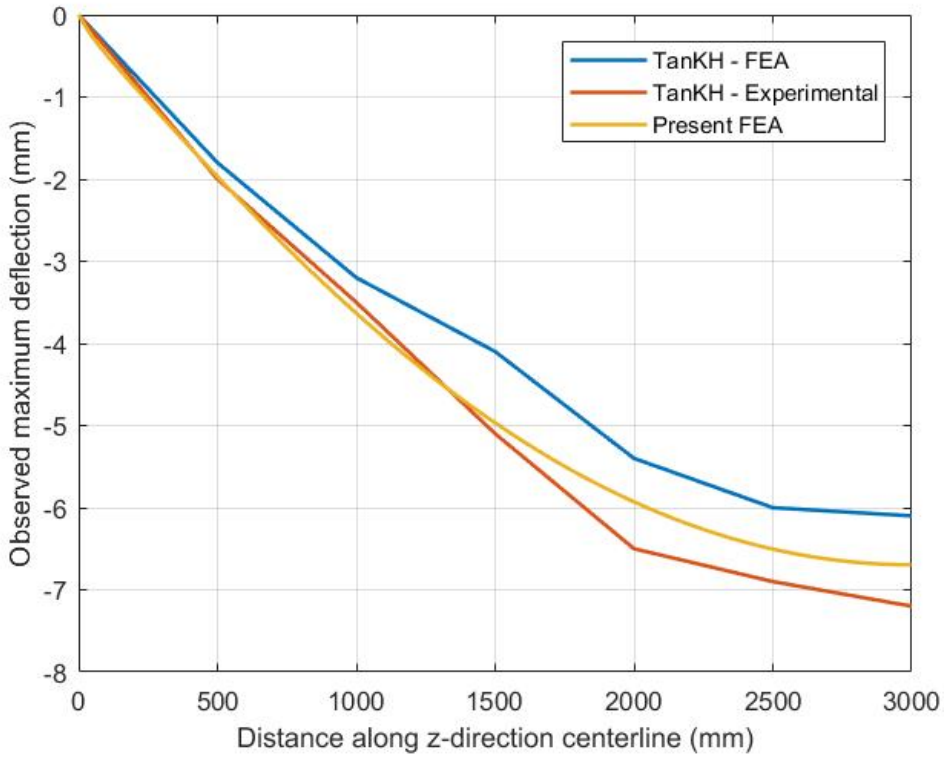

Figure 3.23: Comparison of deflection along z-direction centreline for *All Sides SS* case. Here Tan KH refers to results obtained from Tan et al. [33].

	Mesh Size (mm)	U2 (mm)
1.	100	23.16
2.	50	23.08
3.	25	23.00
4.	20	22.98
5.	15	22.96

Table 3.3: Mesh Convergence Check for udl of 5.5 kN/m^2 and *SS ends only case*, U2 (mm) on the top face plate

	Mesh Size (mm)	U2 (mm)
1.	100	6.87
2.	50	6.84
3.	20	6.83
4.	25	6.82
5.	15	6.82

Table 3.4: Mesh convergence check for udl of 5.5 kN/m^2 and *All sides SS case*, U2 (mm) on the bottom face plate

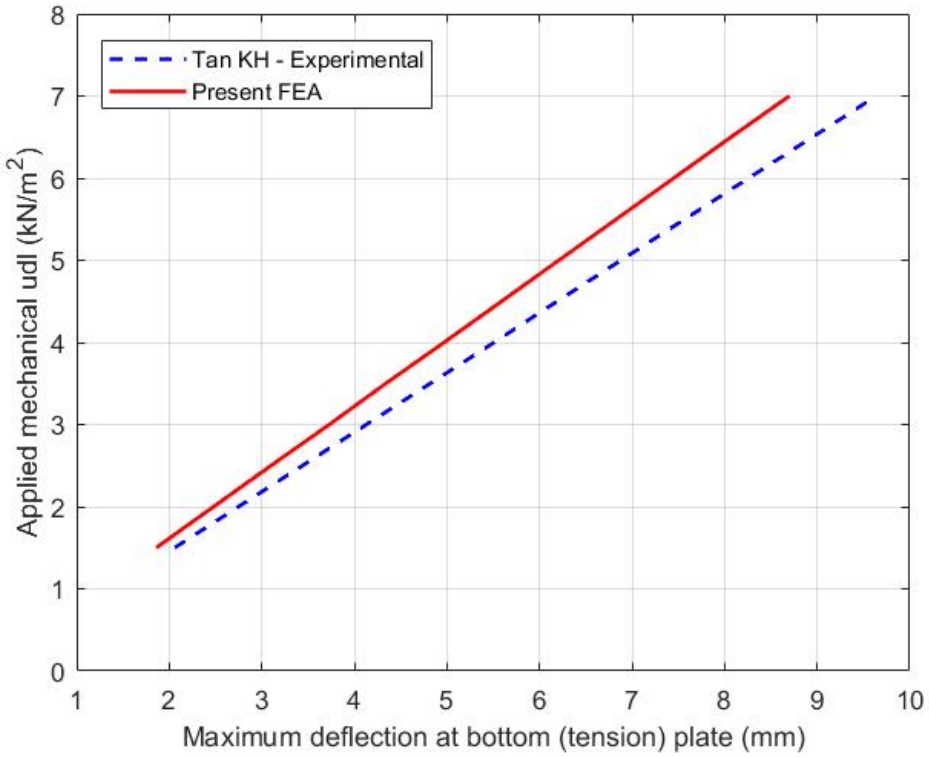

Figure 3.24: Comparison between present FEA and experimental data of Load - max deflection plot for *All Sides SS* case. Here Tan KH refers to results obtained from Tan et al. [33].

3.3. Verification Study - J-Integral

In this section, verification study on ASTM - Compact Tension (CT) Specimen will be carried out. For ASTM - CT specimen, there are empirical expressions (Refer Equation 3.1 and 3.2 and 3.3) available for calculating Stress Intensity Factor (SIF) values. From this SIF values we can calculate J-Integral values using Equation 3.4. The purpose of this verification study is to see if a good match can be obtained between J-Integral values obtained using ASTM empirical equations and Abaqus FE Model - Contour Integral option.

The expression for SIF for CT Specimen is taken from [32] and is as follows -

$$K = \beta S \sqrt{\pi a} \tag{3.1}$$

$$S = \frac{P}{Wt} \tag{3.2}$$

$$\beta = \frac{\left(2 + \frac{a}{W}\right)}{\left(1 - \frac{a}{W}\right)^{1.5} \left(\frac{\pi a}{W}\right)^{0.5}} \left[0.886 + 4.64\left(\frac{a}{W}\right) - 13.32\left(\frac{a}{W}\right)^2 + 14.72\left(\frac{a}{W}\right)^3 - 5.6\left(\frac{a}{W}\right)^4\right] \tag{3.3}$$

The expression to calculate J-Integral from SIF value is as follows -

$$J = \frac{{K_I}^2}{E'} + \frac{{K_{II}}^2}{E'} + \frac{{K_{III}}^2}{2\mu} \tag{3.4}$$

where, E′ = E for plane stress and E′ = E/(1-μ^2) for plane strain

A CT specimen is tested under tensile loading and therefore, the SIF obtained is for Mode - I only. K_{II} = 0 and K_{III} = 0.

3.3.1. Specimen Geometry

ASTM CT specimen is a notched sample and is made in accordance with ASTM standards. There are two reasons why this specimen is chosen for present verification study. First, there are simple empirical expressions available to calculate SIF (or J-Integral) for this specimen second, the specimen contains a discrete crack. Due to presence of a discrete crack, there is no need to define damage model for crack initiation. The geometry of CT specimen with relative size is shown in Figure 3.25. In present verification study W = 45 mm, crack length is taken as 10 mm which makes a = 23.68 mm and thickness t = 0.5 mm.

3.3.2. Material Properties

The material model was assumed to be Linear-Elastic. It is assumed that specimen is made up of aluminium. The properties of the material used in FE model is as follows -

1. Young's Modulus - 70 GPa
2. Poisson's Ratio - 0.33

3.3.3. Loading and Boundary Condition

Tensile load in applied on the specimen as shown in Figure 3.25. In the FE model in Abaqus/CAE, a concentrated point load (P = 200 N) was applied at the centre of the upper circle. The loading and boundary condition are shown in Figure 3.26. At reference point 2 (or RP-2) Ux = 0 and Uy = 0 boundary condition was applied while at reference point 1 (or RP-1) only Uy = 0 boundary condition was applied.

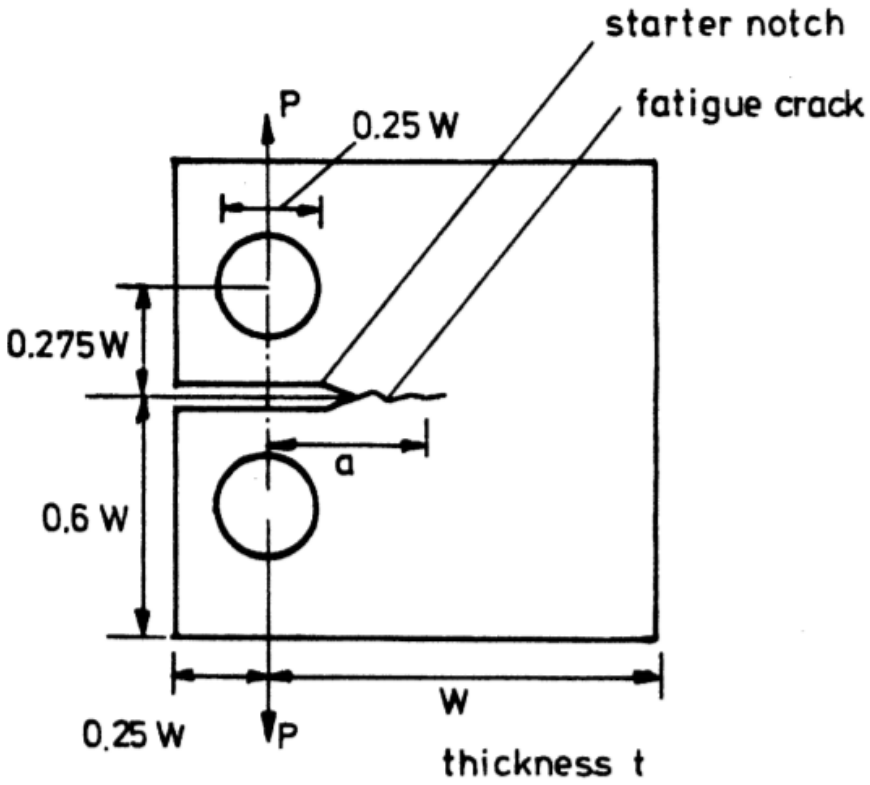

Figure 3.25: ASTM Standard Compact Tension (CT) Specimen [32]

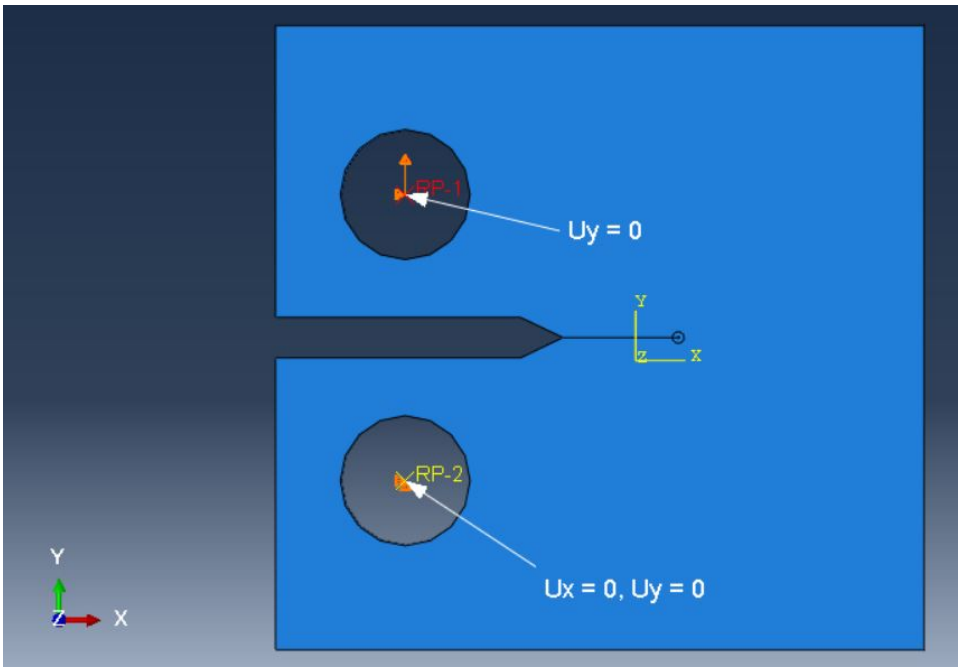

Figure 3.26: Loading and Boundary Condition in the 3D CT Specimen Model

3.3.4. FE Modelling in Abaqus/CAE

Before discussing the results of FEA, some important concepts like *Interactions* and *Contour Integral* will be discussed.

Modelling Interactions

To assign boundary condition in the model, first two reference points were created at the centre of 2 circles in the FE model called RP-1 (Reference Point 1) and RP-2 (Reference Point 2). These were then coupled with the internal surface of circle around them using *Coupling* constraint available within Abaqus/CAE *Interaction* module. First a reference point (named RP-1) was created. Then using the *Coupling* tool all degrees of freedom of the inside surface of the circle was coupled with RP-1. This is shown in Figure 3.27.

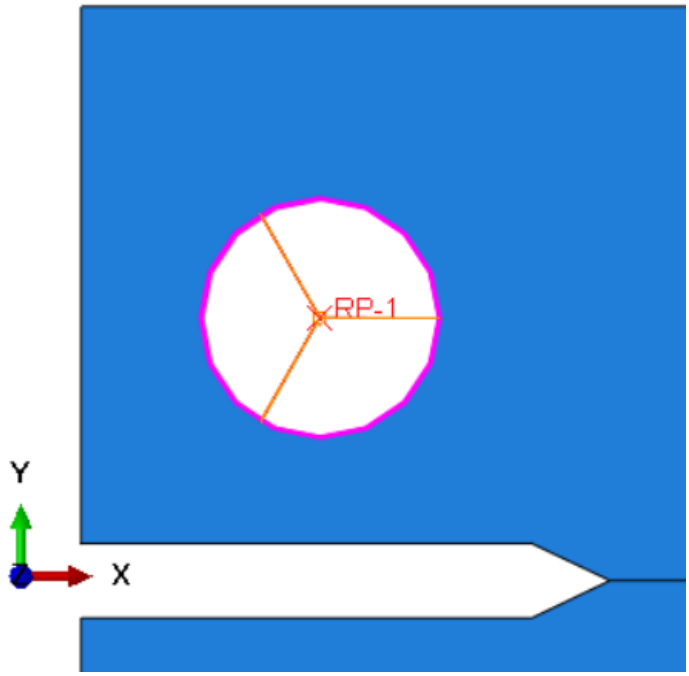

Figure 3.27: Coupling Interaction in Abaqus/CAE

Crack Definition

When using *Contour Integral* option in Abaqus, first an uncracked specimen in created in Abaqus/CAE *Parts* module. The crack is then inserted using *Partition* geometry tool and *Sweep/Extrude* tool. This generates a cracked specimen. For Abaqus/CAE to realize the location of existing crack the crack face is defined as *Seam*. A seam is allowed to open up during analysis thus simulating an existing crack. Once cracked specimen model is ready, a crack is defined using *Create Crack* tool. If the mesh around crack-tip is fine then *crack front* is taken as a line otherwise *crack front* is defined as small zone around the crack-tip. 3D FE model of cracked CT specimen is shown in Figure 3.28.

Element type and meshing

Both C3D8R (8-noded linear brick element with reduced integration and hourglass control) and C3D20R (20-noded quadratic brick element with reduced integration) solid elements are suitable for meshing. To get good estimates, the techniques discussed in Section 2.4.3 should be utilised for meshing around the crack tip. In the present validation study a comparison was made between results obtained using C3D8R, C3D20R and plane stress elements (CPS4R and CPS8R). Use of *Hex-Dominated Sweep* meshing is recommended in the contour integral region. Element size was chosen based on the mesh convergence study of Section 3.3.6. Since very little change is observed in value of output, a mesh size of 0.5 mm was used in the present FE model.

Contour Integral

Contour Integral option in Abaqus offers a simple way to calculate J-Integral at crack tips. Once crack definition and meshing is complete, J-Integral can be requested as an output using *History Output*

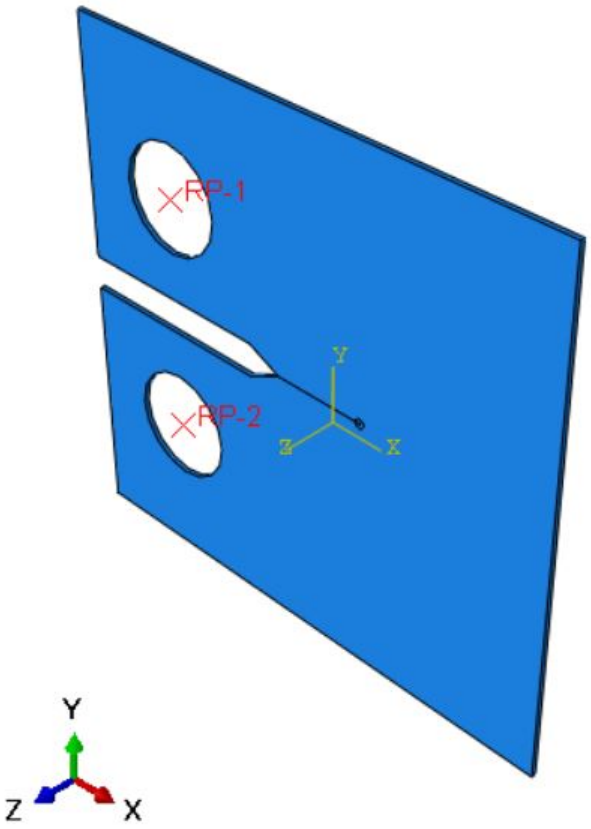

Figure 3.28: Cracked CT Specimen

Request in Abaqus. J-Integral was requested at crack-tip. It is recommended to request output for more than one contour. In the present validation study, J-Integral was requested for five contours around the crack tip. Generally, the estimate obtained for first two contours is ignored and the mean of remaining contours is taken as J-Integral value. A typical J-Integral output is shown in Figure 3.29.

While modelling, we have option to use a 2D Planar model or 3D Solid model. The difference in values obtained from 2D or 3D model is usually negligible. The benefit of using a 2D model is that meshing is simple and quick. Comparison between J-Integral estimate from 3D and 2D models of CT specimen is shown in Section 3.3.5. It is acceptable to use either a 2D or 3D Model as long as sufficiently fine mesh (around the crack tip) is defined. Two concepts related to meshing around crack-tip are *Quarter point singularity* and use of *Collapsed element* in the contour integral region. These are described in Section 2.4.3.

FE Model

Fully meshed 3D CT specimen model is shown in Figure 3.30 and details of meshing around the crack tip is shown in Figure 3.32. Collapsed Element was used around crack tip for meshing and quarter point singularity was included in analysis by shifting the mid-side nodes by quarter-point towards the crack tip. The resulting shift in nodes is shown (see *Red* nodes) in Figure 3.31.

3.3.5. Analysis Results

Both 3D and 2D FE Models were made in Abaqus to calculate J-Integral at crack tip. Different meshing techniques were applied around the crack-tip to see whether it affects the output. Types of model, meshing and element type used in this validation study are shown in Table. 3.5. The result of J-Integral estimate for all eight models is shown in Table. 3.6. J-Integral Estimate (Analytical, using Equation.

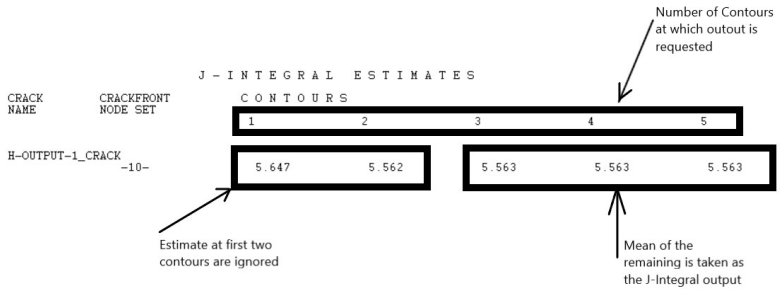

Figure 3.29: Reading Abaqus J-Integral output

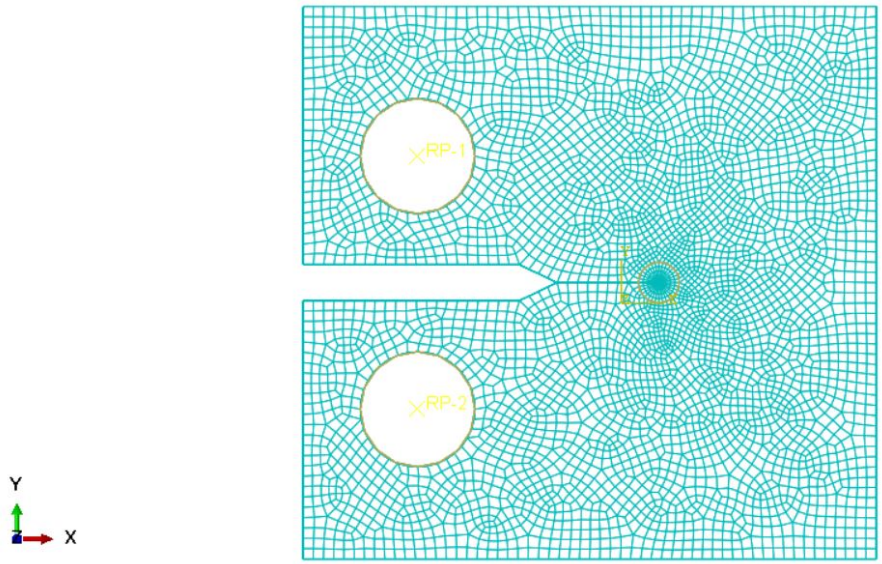

Figure 3.30: Meshing in 3D CT Specimen model

3.1, 3.2, and 3.3) is 5.0347. Error in 3D CT specimen FE models with respect to analytical solution is 15.31%.

SNo	FE Model	Element	Mesh Type	Quarter Point Singularity (Y/N)	Spider Web Meshing (Y/N)
1	3D	C3D20R	Hex Dominated - Sweep	Y	Y
2	3D	C3D8R	Hex Dominated - Sweep	N	Y
3	3D	C3D20R	Hex - Sweep	Y	N
4	3D	C3D8R	Hex - Sweep	N	N
5	2D	CPS8R	Quad Dominated - Sweep	Y	Y
6	2D	CPS4R	Quad Dominated - Sweep	N	Y
7	2D	CPS8R	Quad - Free	Y	N
8	2D	CPS4R	Quad - Free	N	N

Table 3.5: Description of different types of CT Specimen FE Model

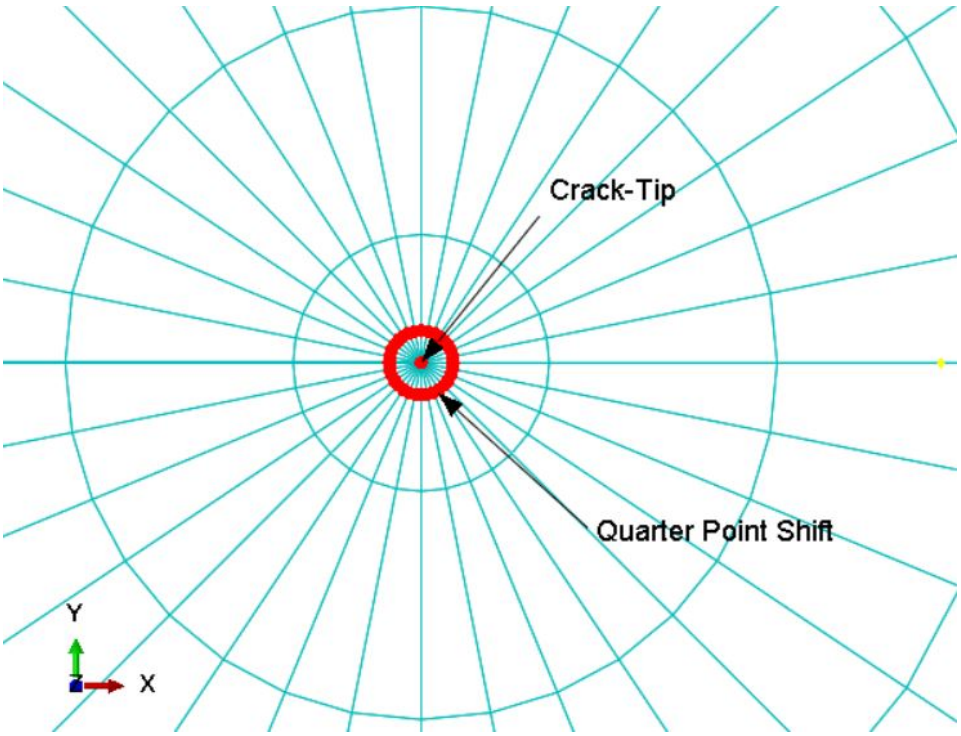

Figure 3.31: Mid Nodes shifted by a a quarter point towards the crack tip in 3D CT Specimen Model.

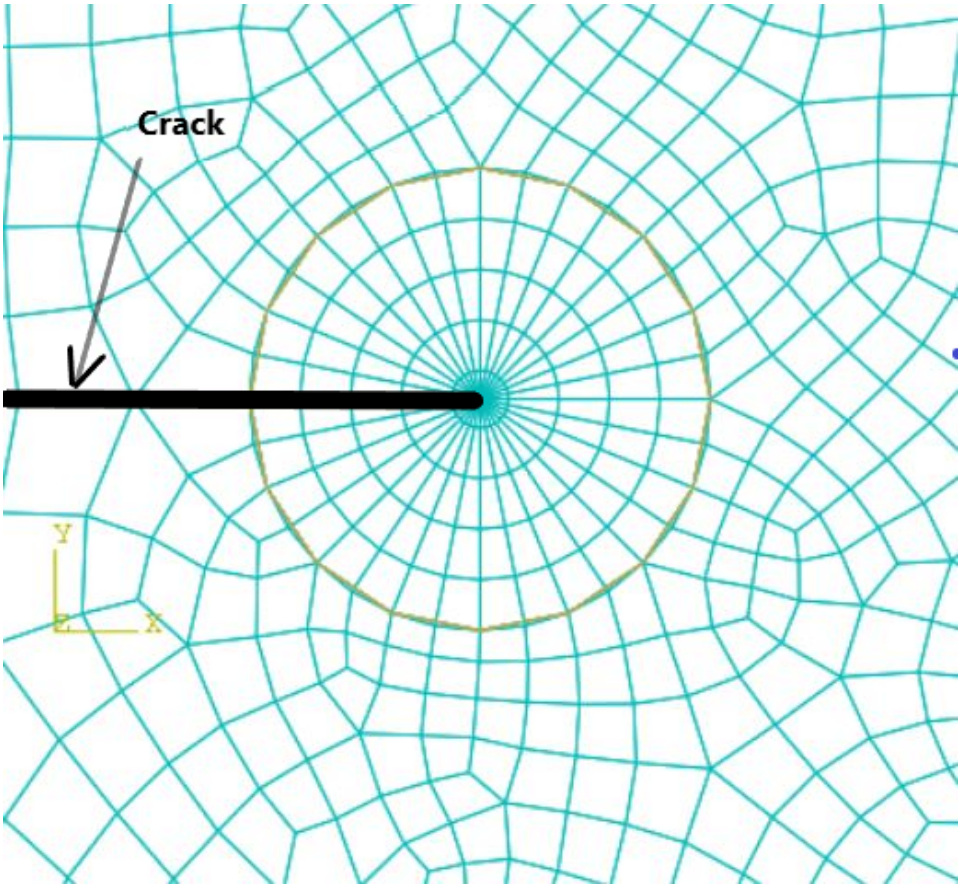

Figure 3.32: Spider web like meshing around the crack tip

SNo	FE Model	Element	J-Integral Estimate	Error (%)
1	3D	C3D20R	5.806	-
2	3D	C3D8R	5.739	1.15
3	3D	C3D20R	5.803	0.05
4	3D	C3D8R	5.800	0.10
5	2D	CPS8R	5.568	4.09
6	2D	CPS4R	5.515	5.01
7	2D	CPS8R	5.563	4.18
8	2D	CPS4R	5.556	4.30

Table 3.6: J-Integral estimate for all eight CT specimen FE Models

3.3.6. Mesh Convergence

Mesh around the crack tip and global mesh size outside the crack zone was reduced gradually to check convergence. The results of mesh convergence study are summarised in Table. 3.7. Negligible change was observed in value of J-Integral with reduction in mesh size. Choice of 0.50 mm as average element size gave satisfactory and converged results.

Average element size (mm)	J-Integral Estimate [MPa mm]
0.50	5.806
0.33	5.805
0.25	5.801
0.20	5.799

Table 3.7: Results for Mesh Convergence Study

3.4. Verification Study - Joint of web core sandwich panel

A joint of web core sandwich panel will be considered in this validation study. Due to welding between top face plate and web, two notches are formed at the weld ends. When top face plate is loaded one notch of the T-joint experiences compression while other will be in tension. This is shown in Figure 3.36b. A tensile crack originates at tensile notch or at critical tensile notch (if more than one tensile notch are present in a critical joint). J-Integral will be estimated at two notches (one tensile and one compressive notch) of T-Joint of a web core sandwich panel.

A 2D FE model of a T-Joint of a web core sandwich panel will be analysed in detail in Abaqus/CAE. A priori 3D analysis (Refer [13]) confirms that out of plane shear stresses have very little contribution to cracking. This implies that contribution to J-Integral (at the crack tip) is only due to Mode I and Mode II cracking. Due to this, choice of 2D FE model is satisfactory. The 2D model in this verification study will be based on T-joint tested for fatigue strength in [13]. The experimental set-up is shown in Figure 3.33.

3.4.1. T-Joint Geometry

A T-Joint of FWA series (T8 x 8 x 24A) was selected for this study (Refer Frank et a. [13] for details of FWA or other series of T-joint). The thickness of web plate (t_w) is 8 mm, thickness of face plate (t_f) is 8 mm and the length of specimen (l_s) is 24 mm. The results of the experimental work conducted in past on T-joint of a web core sandwich panel is shown in Frank et al. [13]. The J-Integral values were shown in terms of Mode I and Mode II Stress Intensity Factors. Under plane strain (meaning Mode III contribution is insignificant) and linear-elastic conditions J-Integral can be expressed by Eq. 3.5. The geometry of the T-joint, geometric parameters, and weld eccentricity are shown in Figure 3.34. The

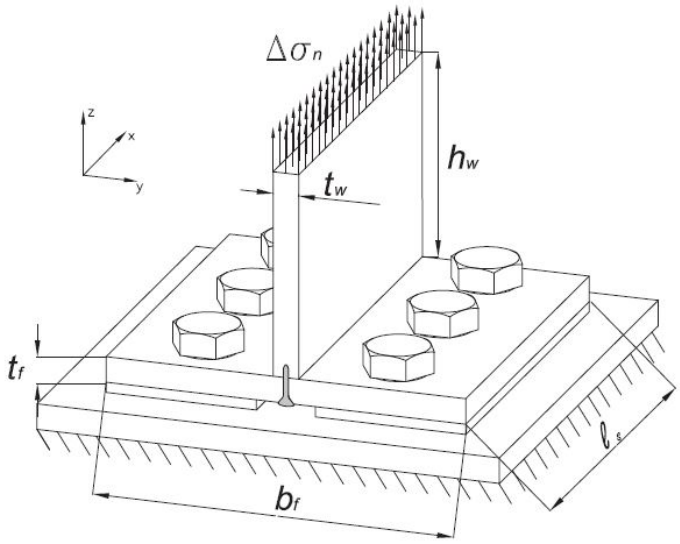

Figure 3.33: Test Setup for determining Fatigue Life [13]

dimensions adopted in this verification study are shown in Figure 3.35.

$$\Delta J = \frac{1-\mu^2}{E}\left(\Delta K_I^2 + \Delta K_{II}^2\right) \tag{3.5}$$

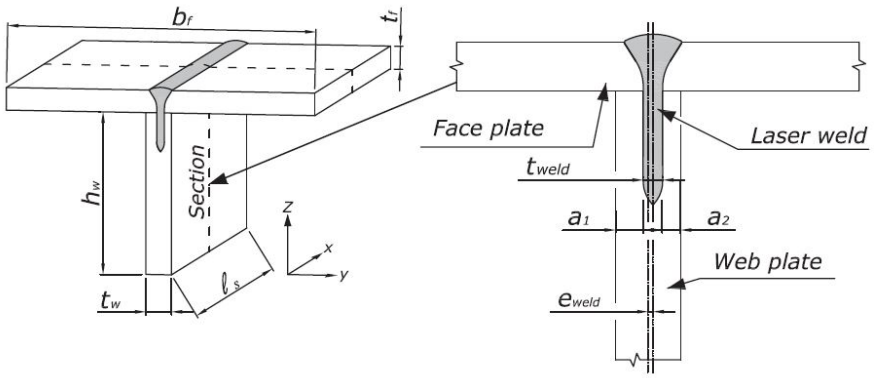

Figure 3.34: Details of T-Joint, dimensions and weld eccentricity [13]

The weld eccentricity (as determined from values of *root gap length* a_1 and a_2) shows quite a spread even for a single specimen of a series. This can be observed in Table A1 of [13]. The root gap lengths for this verification study is taken as a_1 = 2.15 mm and a_2 = 2.34 from Table A1. Since weld is not perfectly aligned (which is rarely the case even for a well controlled welding process) the joint will rotate on application of load. Due to this rotation, one side of the joint will experience tension and other compression. This is visible in Figure 3.36a. This will create a tensile and compressive notch. The J-Integral value will be calculated for both tensile and compressive notch.

3.4.2. Material Properties

The material model was assumed to be Linear-Elastic. Non-linearity was not included in FE analysis. The panel is made up of mild steel. The properties of steel used in FE model is as follows -

1. Young's Modulus - 209 GPa
2. Poisson's Ratio - 0.3

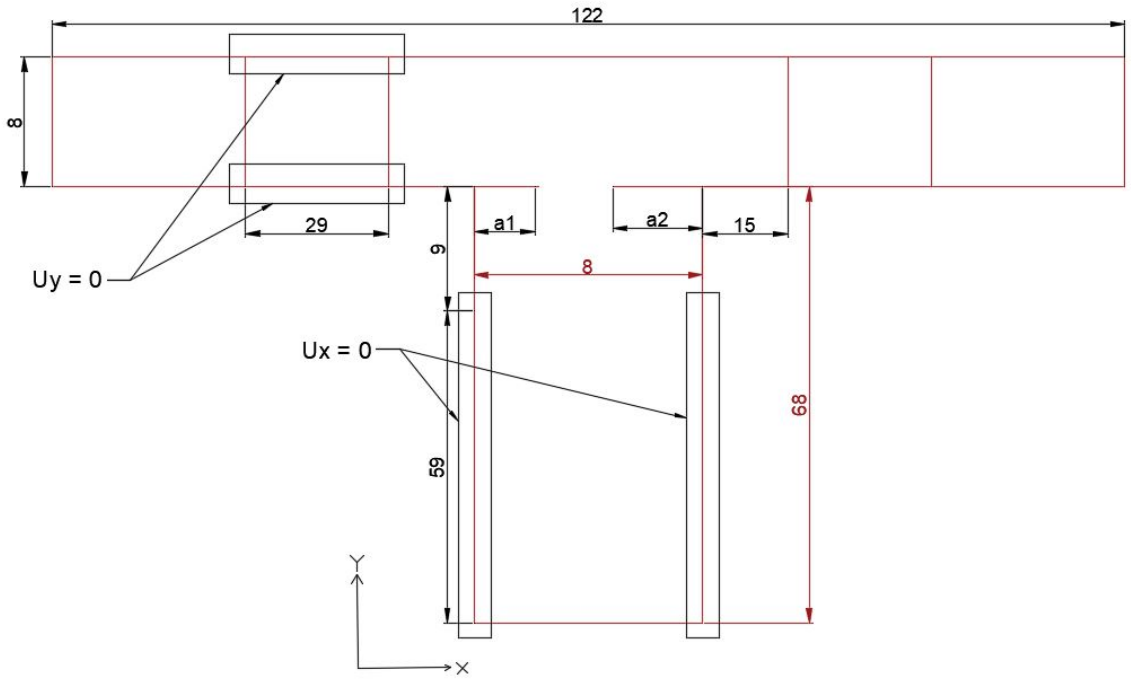

Figure 3.35: Dimensions selected for this verification study - T Joint Model

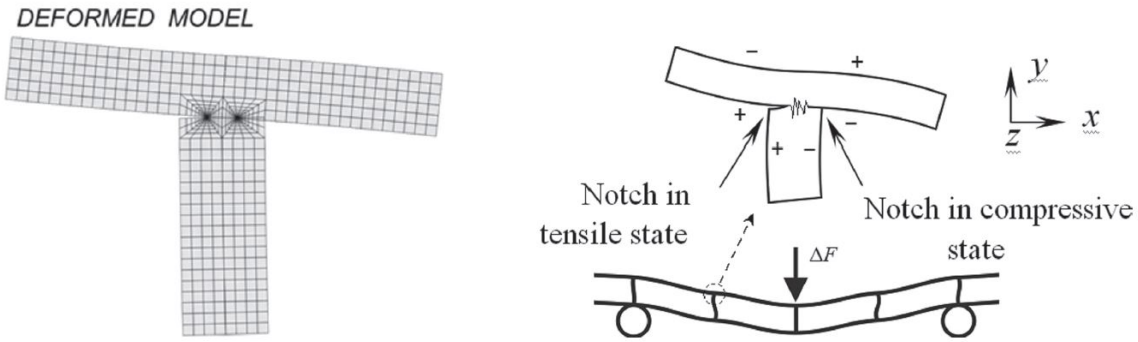

(a) Deformed 2D FE Model of T-Joint [13]

(b) Compressive (-ve) and Tensile (+ve) notch in T-Joint of web core sandwich panel [13]

Figure 3.36: (Left) Deformed 2D model and (Right) Creation of Compressive and Tensile Notch due to loading on Top Face Plate.

3.4.3. Loading and Boundary Condition

A pressure load of 187.5 N/mm^2 was applied at the bottom of the web in the negative y direction. The boundary condition for the FE model was determined from the experimental set-up shown in Figure 3.33. Boundary condition for the FE model are shown in Figure 3.37 and 3.35.

3.4.4. FE Modelling in Abaqus/CAE

The geometric information, material properties, loading and boundary condition necessary for the FE model were described in Section 3.4.1, 3.4.2 and 3.4.3. Interaction are discussed below.

Modelling Interactions

The T-joint specimen discussed so far is an uncracked specimen. But, to avoid defining a damage model we assumed that there is a tendency for crack to originate at the two notches created by laser welding. To incorporate this in FE model, the root gap lengths were embedded in the model by *Partition* tool. Both of these notches were then defined as *Seam*. Crack definition was done in the same way as

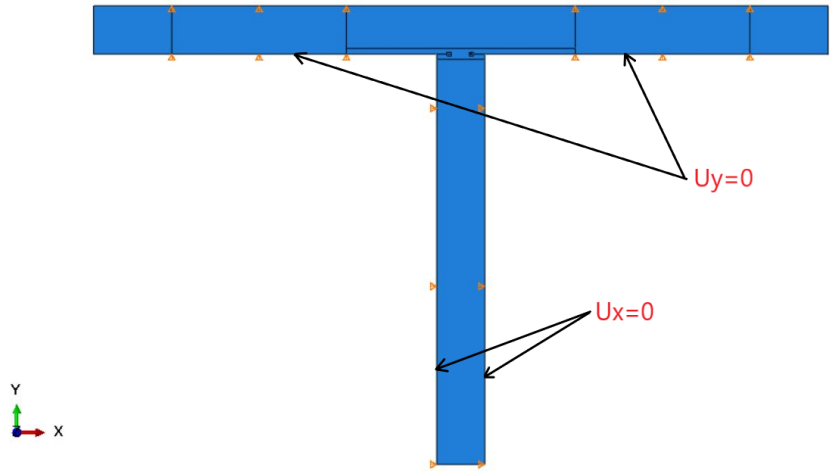

Figure 3.37: Boundary Condition in the 2D FE Model

described in previous verification study.

Element Type and Meshing

Plane strain elements CPE4R (4-node bilinear elements with reduced integration & hourglass control) and CPE8R (8-node bi quadratic elements with reduced integration) were suitable for meshing. These elements come from Abaqus/CAE 2D solid element library. CPE8R element was used in the present FE model. The meshing around the crack tip i.e. within the *Contour Integral* region was *Quad dominated - Sweep* mesh. Use of *Collapsed Element* and *Quarter-Point* singularity is important to get accurate J-Integral estimate and hence was incorporated in contour integral region of the FE model. The meshing away from the crack tip an outside the contour-integral region was *Quad-Sweep* type.

The Mesh Type inside the small zone around the crack tip (radius of zone = 0.1 mm) is shown in Figure 3.38. Quadratic Plane strain element CPE8R were assigned to the FE Model for discretization.

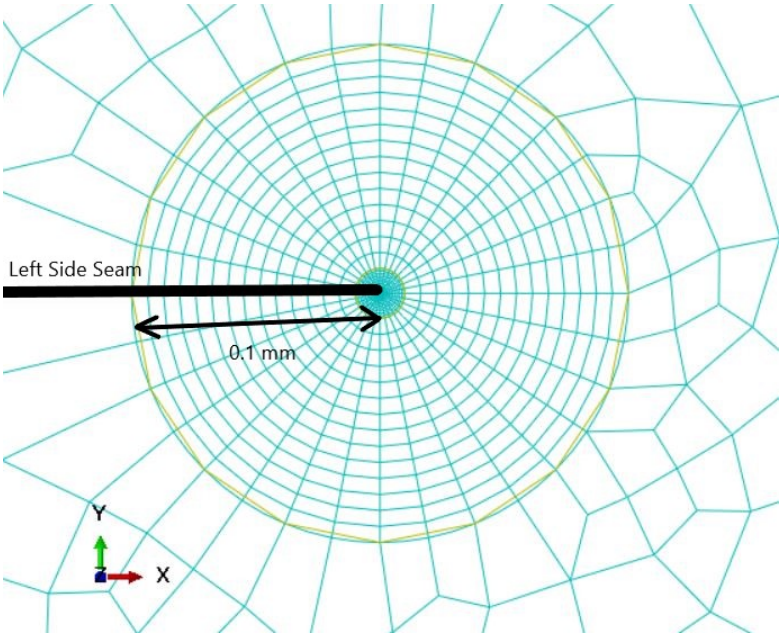

Figure 3.38: Mesh Inside a small zone of radius 0.1mm around the crack-tip

FE Model

A General-Static linear analysis was carried out in Abaqus with J-Integral requested for both right and left cracks in *History Output Request*. J-Integral was estimated using the *Contour Integral* option and value for J-Integral was requested for 9 contours around the crack-tip.

3.4.5. Analysis Results

The results of FEA are shown in Figure 3.39. From all the 9 contours the result of contour 5 was taken as J-Integral estimate for that crack-tip. This is because of the fact that estimate obtained after contour number 4 were stable. The difference in J-Integral values for left and right crack-tip is evident from the deformed shape. The right contour in under higher tensile loading due to the eccentricity of weld. If weld was perfectly aligned same value of J-Integral would be obtained for both right and left notch tips.

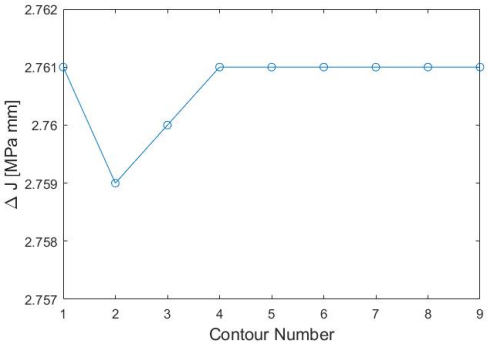

(a) Values of J-Integral range for the left crack-tip ΔJ for different contours

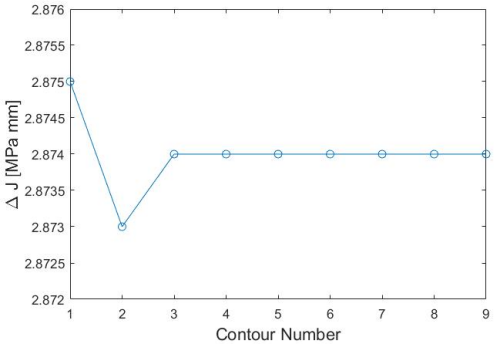

(b) Values of J-Integral range for the right crack-tip ΔJ for different contours

Figure 3.39: Range of J-Integral estimated for contours 1 to 9 for one set of a_1, a_2 values only.

The range of J-Integral estimate obtained from Table 3 of [13] is 1.46 to 3.27. This range was obtained using the Stress Intensity range (MPa $mm^{0.5}$) ΔK_I and Standard deviation of stress intensity range (MPa.$mm^{0.5}$) ΔK_I. Since our estimate of J-Integral lies within the expected range we can safely conclude that the estimate is correct. As a further measure of confidence in technique and results, few more J-Integral values were calculated for other root gap tips. The results are summarised in Table. 3.8. The mean of the estimate given in reference paper is 2.365 while the mean obtained from Table. 3.8 is 2.855. The difference is 17%. Also, all estimates of J-Integral value are within the expected range of 1.46 to 3.27.

SNo	a_1 [mm]	a_2 [mm]	J Integral estimate [MPa mm]
1	2.15	2.34	2.874
2	2.33	2.10	2.871
3	2.37	2.01	2.898
4	2.22	2.03	2.812
5	2.01	1.88	2.731
6	2.21	2.05	2.811
7	2.35	2.01	2.887
8	2.48	2.23	2.956

Table 3.8: J Integral estimate for 8 sets of a_1, a_2 values

3.4.6. Mesh Convergence

The result of mesh convergence study for one set of a_1, a_2 values are shown in Table. 3.9.

Average element size (mm)	J-Integral estimate [MPa mm]
5.0	2.869
2.5	2.869
1.0	2.874
0.1	2.874

Table 3.9: Results for Mesh Convergence Study - T Joint

4

Performance Improvement due to foam filling

4.1. Introduction

Corrugated Core Sandwich Steel Panels (CCSSP) provides considerable structural improvement over Orthotropic Steel Deck (OSD) by reducing the orthotropy (ratio of longitudinal to transverse bending stiffness). Adding foam filling around the core layer will further reduce this orthotropy with little increase in self weight. Foams are lightweight material with low Modulus of Elasticity (E) (generally in the range of 100-200 MPa) and are suitable as a filling material in sandwich panels. Because of their low E value, global bending behaviour of panel is barely affected by foam filling. But, because of tight packing reduction in fatigue relevant local stresses is significant enough to warrant in-depth analysis. It was concluded in Frank et al. [12] that how adding even a low-density filling material could significantly increase the fatigue life of a sandwich panel subjected to lateral loading.

On the basis of experimental investigation and FE analysis on web core sandwich panels in Kartunnen et al. [19], it was concluded that shear induced local stresses were reduced by at least 75% at web to faceplate joint. Load level at 2 million cycles also increased by a factor of 8.5. The governing shear induced normal stresses are due to low transverse shear stiffness in the weak direction i.e. perpendicular to the stiffeners. To study the effect of foam filling on stress distribution along the governing direction i.e. the weak direction, we consider a beam of sandwich panel instead of a rectangular panel.

In previous research (refer [4] and [19]) it was observed that there are two main categories of foams suitable for filling in sandwich panels - Metallic and Polymeric foams. Seven different polymeric foams were considered in this thesis. These foams are assumed to be adhesively bonded to the steel plates of panel. Exact modelling of multi-material interface (Steel - Adhesive - Foam Interface) will be ignored. This is due to the fact that modelling of the multi-material interface (steel-adhesive-foam) would require cyclic properties of all the constituent materials and the actual thickness of the adhesive layer [19]. To avoid these problems, modelling technique derived from [27] (with some simplifications) will be used in this thesis.

4.2. Foam Filling in Sandwich Panels

Fatigue performance of sandwich panels due to lateral loading could be improved further by foam filling. To quantify the extent of improvement possible we use a simplified FE analysis method (will be discussed in Section 4.4). A foam filled panel will be judged on the basis of three criteria - (a) Increase in transverse shear stiffness D_{Qy} (based on analytical calculation, refer Section 2.5.1), (b) Increase in self weight (based on analytical calculation) and (c) Decrease in normal stress (based on FEA) in the top face plate. Results for these three parameters will be measured against the corresponding value for an empty panel. This preliminary exercise will be used to quantify possible improvement in sandwich panel behaviour due to foam filling.

4.3. Polymeric Foams - Material Properties

Mechanical properties of polymeric foam are given in DIAB - Divinycell® technical manual [11]. There appears to be some discrepancy in this data provided by manufacturer, for e.g. tensile strength is higher than compressive strength (Refer Figure 4.1). Verification of this data is beyond the scope of this thesis. The corrected data suitable for FEA is taken from Romanoff et al. [27]. This corrected data is shown in Table 4.1.

Property	H45	H60	H80	H100	H130	H200	H250
Density [kg/m^3]	48	60	80	100	130	200	250
Compressive Properties							
Strength [MPa]	0.5	0.7	1.15	1.65	2.4	4.2	5.4
Modulus [MPa]	45	60	80	115	145	200	240
Tensile Properties							
Strength [MPa]	1.1	1.5	2.2	2.5	3.5	6.3	8.0
Modulus [MPa]	45	57	85	105	135	210	260
Shear Properties							
Strength [MPa]	0.46	0.63	0.95	1.4	1.9	3.2	3.9
Modulus [MPa]	12	16	23	28	40	75	88

Table 4.1: Mechanical Properties of Foam Filling [27]

Property	Unit	H 35	H 45	H 60	H 80	H 100	H 130	H 160	H 200	H 250
Nominal Density 1) ISO 845	kg/m^3	38	48	60	80	100	130	160	200	250
Compressive Strength 2) ASTM D 1621	MPa	0.45 (0.3)	0.6 (0.5)	0.9 (0.7)	1.4 (1.15)	2.0 (1.65)	3.0 (2.4)	3.4 (2.8)	5.4 (4.5)	7.2 (6.1)
Compressive Modulus 2) ASTM D 1621	MPa	40 (29)	50 (45)	70 (60)	90 (80)	135 (115)	170 (145)	200 (175)	310 (265)	400 (350)
Tensile Strength 2) ASTM D 1623	MPa	1.0 (0.8)	1.4 (1.1)	1.8 (1.5)	2.5 (2.2)	3.5 (2.5)	4.8 (3.5)	5.4 (4.0)	7.1 (6.3)	9.2 (8.0)
Tensile Modulus 2) ASTM D 1623	MPa	49 (37)	55 (45)	75 (57)	95 (85)	130 (105)	175 (135)	205 (160)	250 (210)	320 (260)
Shear Strength ASTM C 273	MPa	0.4 (0.3)	0.56 (0.46)	0.76 (0.63)	1.15 (0.95)	1.6 (1.4)	2.2 (1.9)	2.6 (2.2)	3.5 (3.2)	4.5 (3.9)
Shear Modulus ASTM C 273	MPa	12 (9)	15 (12)	20 (16)	27 (23)	35 (28)	50 (40)	73 (50)	73 (65)	97 (81)
Shear Strain ASTM C 273	%	9 (4)	12 (8)	20 (10)	30 (15)	40 (25)	40 (30)	40 (30)	45 (35)	45 (35)
1) Typical density variation +/– 10%.										
2) Perpendicular to the plane. All values measured at +23°C.										

Figure 4.1: Observed discrepancy in tensile strength and compressive strength [11]

4.4. Analysis Method - Review

Experimental and FE analysis were conducted on empty and foam filled sandwich beams by Romanoff et al. [27]. This section deals with a brief review paper.

Geometry
Web core sandwich panel was cut into small beams of length 1050 mm and breadth 50 mm. The cut was made perpendicular to the direction of web stiffeners. Face plates were 2.52 mm thick. Web plates had a height of 40 mm and thickness of 3.97 mm. Spacing of web plates was 120 mm. Each beam had 10 web plates and was thus divided into 9 cells.

Material Properties
In the experimental investigation, face plates and core had different properties. Face plates had E value of 221 GPa, yield strength of 360-368 MPa and tensile strength of 470 - 476 MPa. Web plates had E value of 200 GPa, yield strength of 360 MPa and tensile strength of 398 MPa. The Poisson's ratio for both face plates and web plate was 0.3. For FE analysis the same properties were used.

Loading and Boundary Condition
The beams were tested experimentally under four point bending condition. The beam was simply supported. While performing the experiments the load was increased from 0 N to 400 N and then decreased back to 0 N. Same loading was used in FE analysis.

Element Type and Mesh Size
Two FE models were built for each beam sample. In first FE model linear elastic response of the beam was evaluated using 3D solid elements (C3D20R elements). In second FE model ultimate strength behaviour of beams was analysed using 2D model and meshing of plane strain element (CPE8R).

FE Model
The investigation was carried out on empty and foam filled beams under 4-point bending. FE analysis was carried out using 20 noded solid elements (for 3D Solid Model) and using 8 noded plane strain elements (for Plane Strain Model). FE model is shown in Figure 4.2. Rotational stiffness of core to top face plate and core to bottom face plate joint was also considered through an appropriately sized thick weld i.e. 2mm. Two variants of filling material of Divinycell - H type were considered - H80 and H200. H80 was considered as orthotropic while H200 was considered as isotropic. Non-Linear analysis was carried out in Abaqus using the RIKS method. Foam - Filling was assumed to be bi-linear with yield point at 2% elongation.

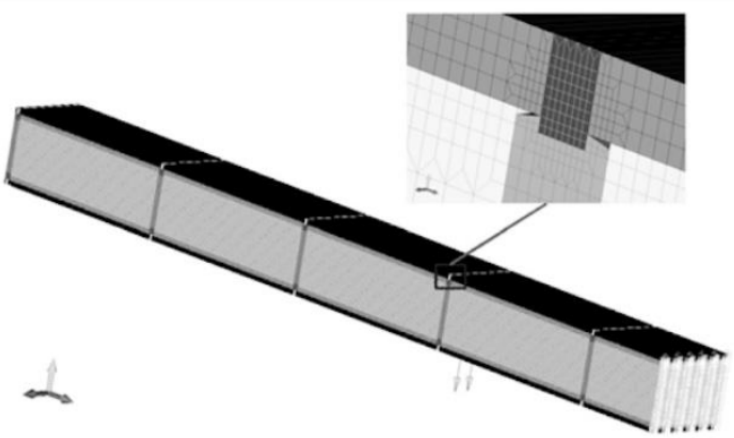

Figure 4.2: 3D FE Model of web core sandwich panel [27]

Results
It is clear from the Figure 4.3 and results of Romanoff et al. [27] that the shear induced normal stresses are considerably reduced when the section is filled with foam. In particular reduction by a factor of 3 and 7 for foam filling of H80 and H200 respectively as compared to empty sandwich beams. Weight increase for H80 and H200 is about 6% and 15% compared to empty sandwich beams. Although both H80 and H200 considerably reduces the normal stresses, performance of H200 is better.

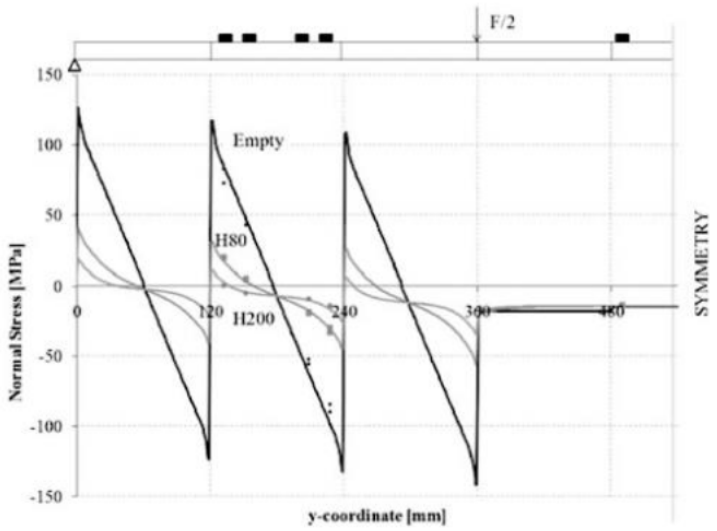

Figure 4.3: Plot showing reduction in normal stresses due to foam-filling (Dot shows the experiment results) [27]

Drawbacks of foam filling

The observed ultimate load for foam filled beams was significantly lower under four point bending. This is because of difference in failure mode of filled and empty beams. Filled beams failed by core shear followed by plastic hinge formation at the laser weld location while empty beams failed directly due to plastic hinge formation at the laser weld [27]. Reduction in ultimate strength was also observed in foam filled beams. This reduction was much more severe for H200 foam filled beams as compared to H80 foam filled beams.

4.5. Normal Stresses

The stresses on the top face of top face plate are important from fatigue point of view. Under local loading this is the most stressed part of top face plate. The stresses here will directly impact the Mode - I tension crack originating at the interface of laser weld and top face plate as shown in Fig. 4.4. Any reduction in normal stresses will affect growth rate of this crack. Based on this consideration, it is quite important to quantify performance of different foam filling on the basis of possible reduction in normal stress.

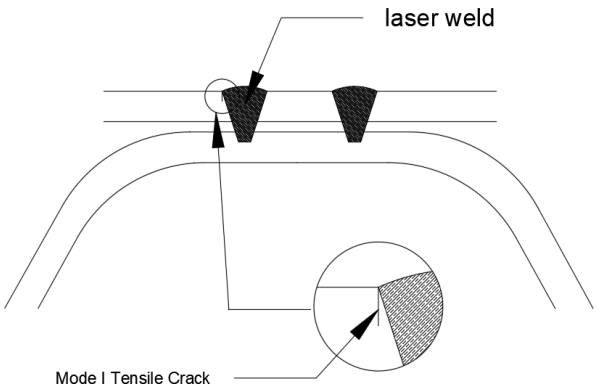

Figure 4.4: Mode I Tensile Crack - Top Face Plate

4.6. 2D FE Model

Input, FE model and results of 2D FEA will be discussed in this section.

4.6.1. Geometry

Using the sandwich panel section dimensions from Nilsson et al. [25], we will carry out our FE Analysis on a 2D beam model. The cross section is shown in Figure 4.5 and numerical value of geometric parameters of sandwich panel is shown in Figure 4.6. t_1 is thickness of bottom face plate, t_c is thickness of corrugated core steel plate, t_2 is thickness of top face plate, h is centre to centre distance between top and bottom face plate, θ is angle of corrugation, R_1 or R_2 is fillet radius of core layer, $2p$ is pitch of corrugation, n_{cells} is number of cells in a panel, t_w is thickness of single laser stake weld and b is thickness of the beam. The plane stress / strain thickness equal to thickness of beam (b = 190 mm) was adopted in 2D FE models.

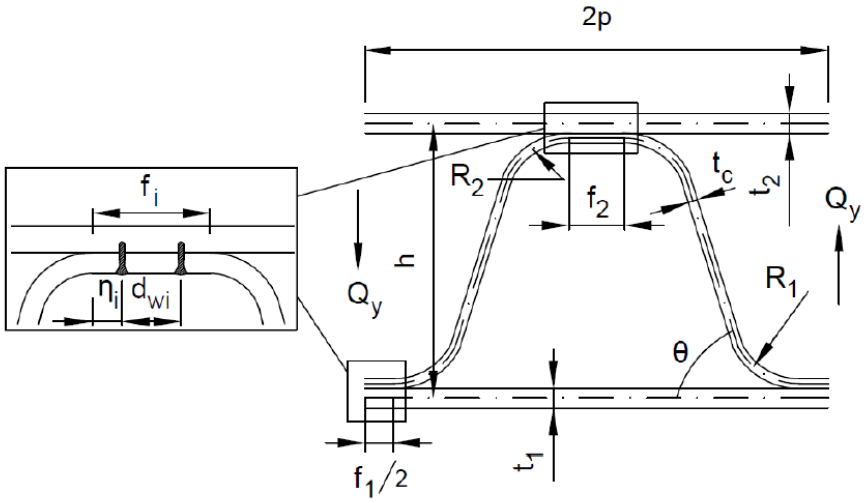

Figure 4.5: Cross section geometric properties of sandwich panel [25]

t_1	t_c	t_2	h	θ	$f_{1,2}$	$d_{w1,2}$	$R_{1,2}$	$2p$	n_{cells}	t_w	b
[mm]	[mm]	[mm]	[mm]	[°]	[mm]	[mm]	[mm]	[mm]	[-]	[mm]	[mm]
5	6	8	132	64.4	60	30	7.4	253	8	1	190

Figure 4.6: Adopted geometric properties of sandwich panel for FEA [25]

4.6.2. Material Properties

For the steel, modulus of elasticity (E) was taken as 210 GPa. Poisson's ratio is equal to 0.3. Density of steel was taken as 7860 kg/m^3. Properties for foam filling were taken from Table 4.1. Both steel and foam were assumed to be *Isotropic*. Young's Modulus for foam filling was taken as mean of compressive and tensile modulus given in Table 4.1. Poisson's ratio of 0.4 was adopted for foam filling.

4.6.3. Loading and Boundary Condition

A concentrated load on 1 kN was applied on the top surface of top face plate as shown in Figure 4.7. The boundary condition for 2D beam FE model is - left support is Ux = 0, Uy = 0 and right support is Uy = 0.

4.6.4. Interaction

To simulate the effect of double stake laser weld *Tie Constraints* were used. The welds were assumed to be 4 mm wide. Surface - to - surface interaction was also implemented using *Interactions* module in

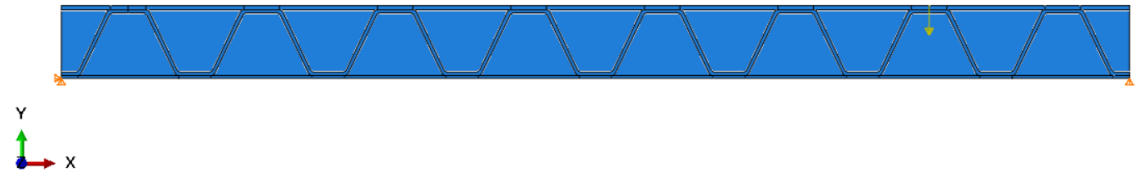

Figure 4.7: Loading and Boundary Condition on 2D Solid FEA

Abaqus/CAE. Within Abaqus surface-to-surface definition, *Finite Sliding* option was chosen. Interaction between steel plates was further refined with frictionless *Tangential* behaviour and Hard Contact for *Normal* behaviour.

4.6.5. Element Type and Mesh Size

Linear plane stress element CPS4R was used in meshing. CPS4R is 2D quadrilateral solid element with reduced integration and hourglass control built-in. For foam region a Quad-dominated free mesh with advancing front *type* was defined. An approximate element size of 1 mm was selected for meshing in all the regions.

4.6.6. Analysis and Results

General Static option was selected for analysis in Abaqus. Neither geometric nor material non-linearity was considered in this analysis.

The analysis results of S11 - surface stresses on the top face plate of empty and foam-filled sandwich panel are shown in Fig. 4.9 and comparison with no foam filling case is shown in Fig. 4.10 The absolute decrease in stress due to foam filling is not substantial. This is because of the very low Modulus (Elastic Modulus & Shear Modulus) combined with low tensile & compressive strength of foam material. Nevertheless, even a small improvement is advantageous as we are utilizing empty space around the core. Also, increase in self weight due to foam filling is negligible (for comparison foams have a density range of 48-250 kg/m^3 while steel has a density of 7860 kg/m^3). All things considered constant, improvement in fatigue performance (when compared to an empty panel) is expected due to reduced normal stresses and due to improved bending stiffness in x- and y-direction.

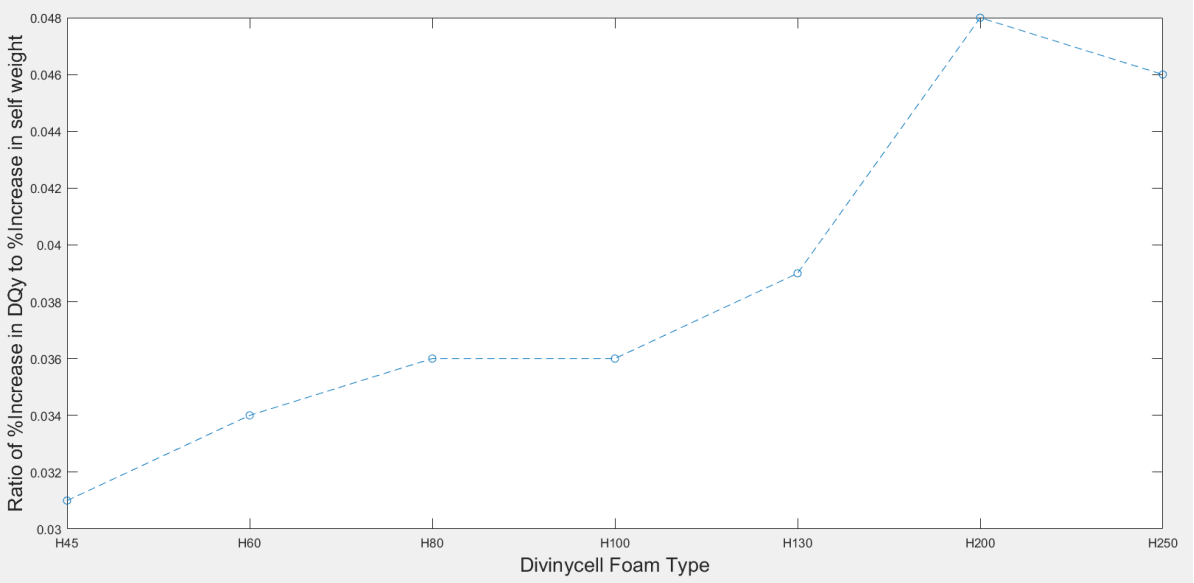

Figure 4.8: Plot of Ratio of % increase in D_{Qy} to % increase in self weight Vs Foam Type

The foam which will give highest ratio of *decrease in surface stress* to *increase in self weight* (signifying highest reduction in surface stresses against lowest increase in self-weight) would be the best choice. A plot or ratio of increase in D_{Qy} to increase in self-weight vs Foam type is shown in Figure 4.8. Higher value of this ratio indicates better foam performance.

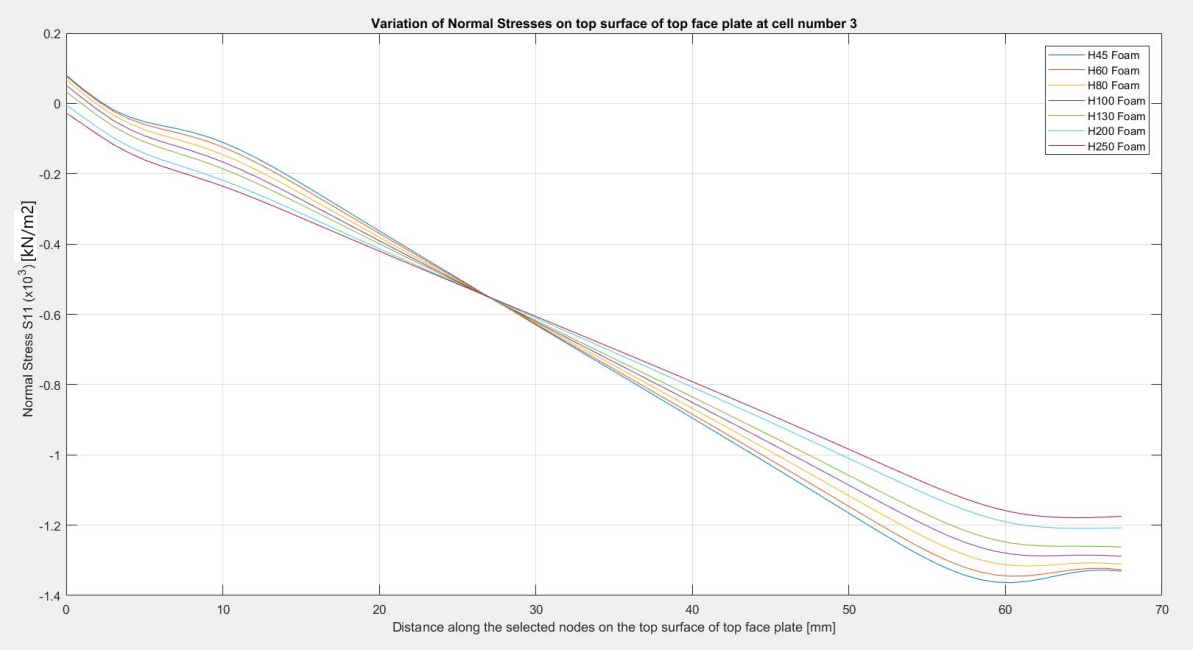

Figure 4.9: Variation of Normal Stress (S11) for different foam filling

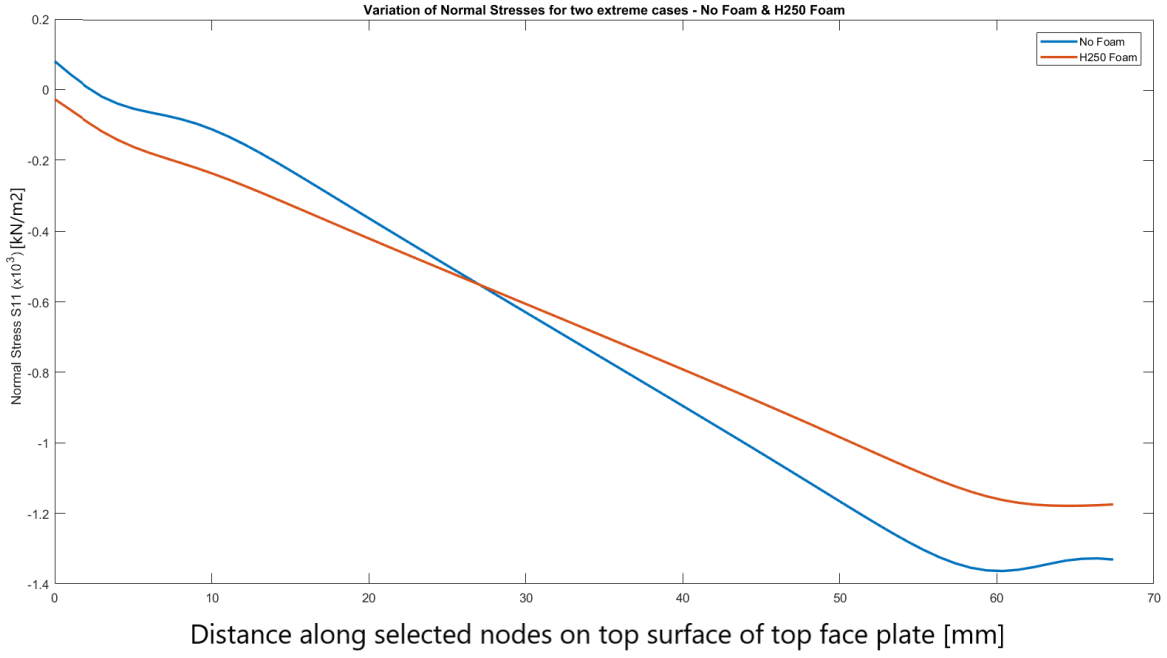

Figure 4.10: Variation of maximum Normal Stresses S11 for case of No Foam and the heaviest H250 Foam

4.6.7. Increase in transverse shear stiffness D_{Qy}

It's clear that foam filling will increase transverse shear stiffness, D_{Qy} with negligible increase in self weight. Here we discuss exactly by how much will D_{Qy} will increase due to different foam fillings using analytical technique given in Appendix A4 of Romanoff et al. [28]. Clearly H250 will cause the largest increase in D_{Qy} value due to high modulus but at the same time this will lead to maximum increase in self-weight. The results of D_{Qy} calculation for panel with and without foam are shown in Table. 4.2. The thickness of panel is taken as 190 mm same as in [25]. The weight of empty panel used in below calculation is approximately equal to 44.27 kg. For comparison the D_{Qx} value of the same panel is of the order of 10^6 N/mm. For detailed calculation, please refer Appendix A. Reference could also be made to Appendix A4 of [28] for derivation of the formulae used in Appendix A.

From Table. 4.2, we can clearly see that as far as increase in D_{Qy} is concerned with minimum possible increase in self-weight, H200 is clearly the best choice followed by H250, H130, H100, H80, H60 and H45.

Property	H45	H60	H80	H100	H130	H200	H250
Density $[kg/m^3]$	48	60	80	100	130	200	250
D_{Qy},steel $[N/mm]$	7097	7097	7097	7097	7097	7097	7097
D_{Qy},fill $[N/mm]$	12	16	22	27	39	73	86
D_{Qy},total $[N/mm]$	7109	7113	7120	7124	7136	7170	7183
D_{Qy} increase [%]	0.16	0.22	0.31	0.38	0.55	1.03	1.21
self-weight increase [%]	5.1	6.3	8.5	10.6	13.8	21.2	26.5
$\frac{\%D_{Qy}}{\%self-weight}$	0.031	0.034	0.036	0.036	0.039	0.048	0.046

Table 4.2: Transverse shear stiffness D_{Qy} - steel plates and foam contribution (Refer Appendix A for calculation details).

4.7. 3D FE Model

So far in this chapter, only a beam was considered for analytical calculations & 2D FEA. A 2D Planar model was developed in Abaqus/CAE and normal stresses on top face plate in cell number 3 (counting from the left side and numbering first cell as 1 were compared. A full 3D FEA of empty and foam filled sandwich panel is presented next.

A two stage 3D FEA was carried out using Abaqus sub modelling technique. The two stage FE analysis definition for web-core sandwich panels is shown in Fig. 4.11. The definition of 2D model driven by results of 3D model is shown in Fig. 2.21. To keep the analysis time reasonably small, we consider similar plan dimensions as in [12] i.e. approximately 1000 mm x 1000 mm. The objective of two stage 3D FEA was to calculate J-Integral value at critical tensile notch tip.

4.7.1. Geometry

A 1265 mm long 1265 mm wide panel was selected for 3D FEA. Such a peculiar plan dimension was necessary to incorporate five full core pitch between the end supports. The cross section geometry of the panel is same as for the previous 2D FEA discussed in Section 4.6.

4.7.2. Material Properties

Material properties for steel and foam remains the same as previous 2D FE Model, refer Section 4.6.2.

4.7.3. Loading and Boundary Condition

Load is applied at the centre of the whole panel. Dimension of loaded area was randomly selected as 100 mm x 100 mm. Uniform pressure load of 24 N/mm^2 was applied on this area. The panel was considered to be simply supported. At one end all translation degrees of freedom were restricted (Ux = 0; Uy = 0; Uz = 0) and on the other end only y-direction translation (Uy = 0) was restricted. Loading and boundary condition is shown in Figure 4.12 and Figure 4.13 for empty and foam filled sandwich panels respectively.

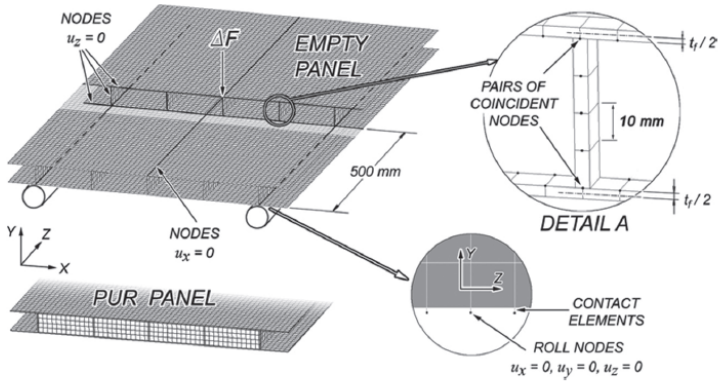

Figure 4.11: Definition of a 3D FE Model - Web Core Panel [12], $\Delta F = 6kN$

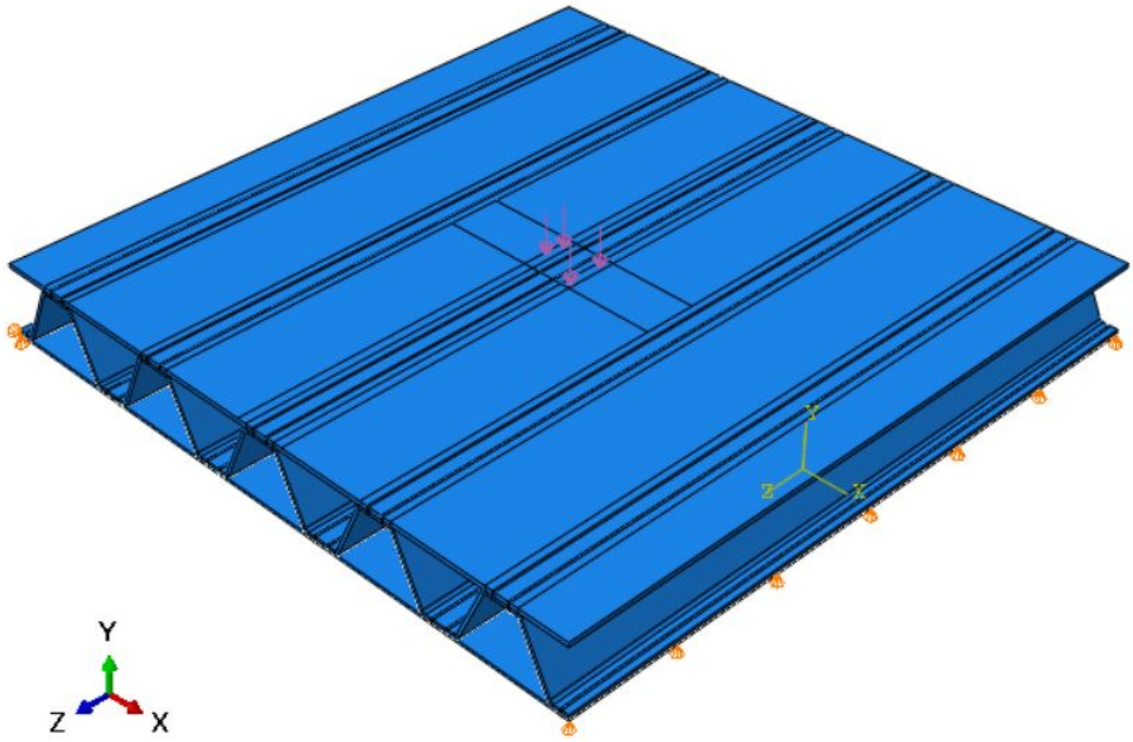

Figure 4.12: Global model of empty sandwich panel

4.7.4. Interaction

To simulate the weld effect tie constraints were used. Two 2mm wide strip were created at the location where welding is expected. These were then connected using tie constraints. Surface-to-surface contact definition stays the same as discussed in Section 3.2.4.2.

4.7.5. Location of Submodel

In 3D global model load was applied at the centre of the top face plate. This makes the joint next to the loaded area critical. The sub model consists of critical joint. We take a 5 mm thick strip of this critical joint and create the 3D FE sub model (Refer Figure 4.14)

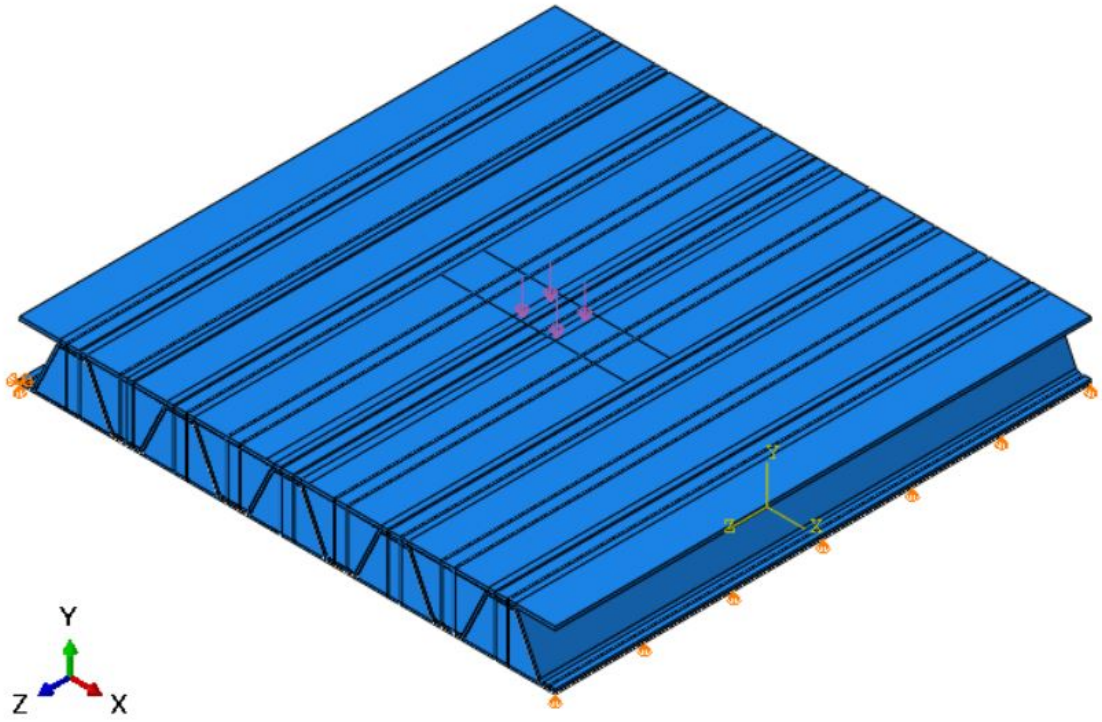

Figure 4.13: Global model of foam filled sandwich panel

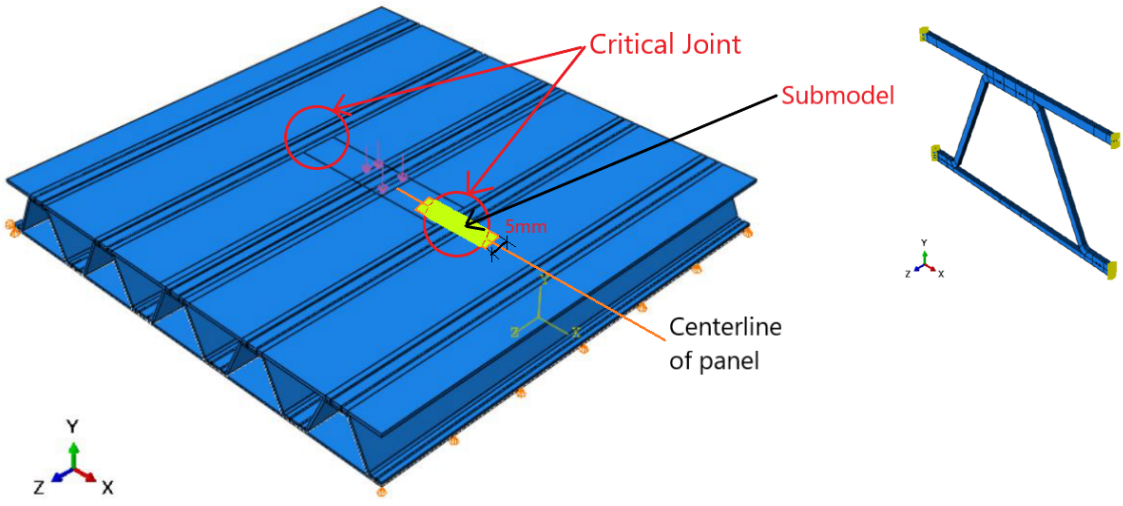

Figure 4.14: Location of 3D submodel in the 3D global model of sandwich panel

4.7.6. Element Type and Mesh Size

For meshing in global 3D Model 8-node linear brick (C3D8R - continuum solid element) element with reduced integration & hourglass control built-in was selected. For good results it is recommended that at least four element are present along the thickness of the plate. This was taken care of while assigning mesh seeds to the *Assembly*. An average element size of 10 mm was selected for analysis. The meshed model for both Global model without foam and with foam are shown in Fig. 4.15 and Fig. 4.16 respectively. C3D20R element was used for meshing in 3D submodel with an average element size of 1 mm. Empty and Foam Filled Submodel is shown in Figure 4.17 and Figure 4.18 respectively. Meshed submodels are shown in Figure 4.19 and Figure 4.20 respectively.

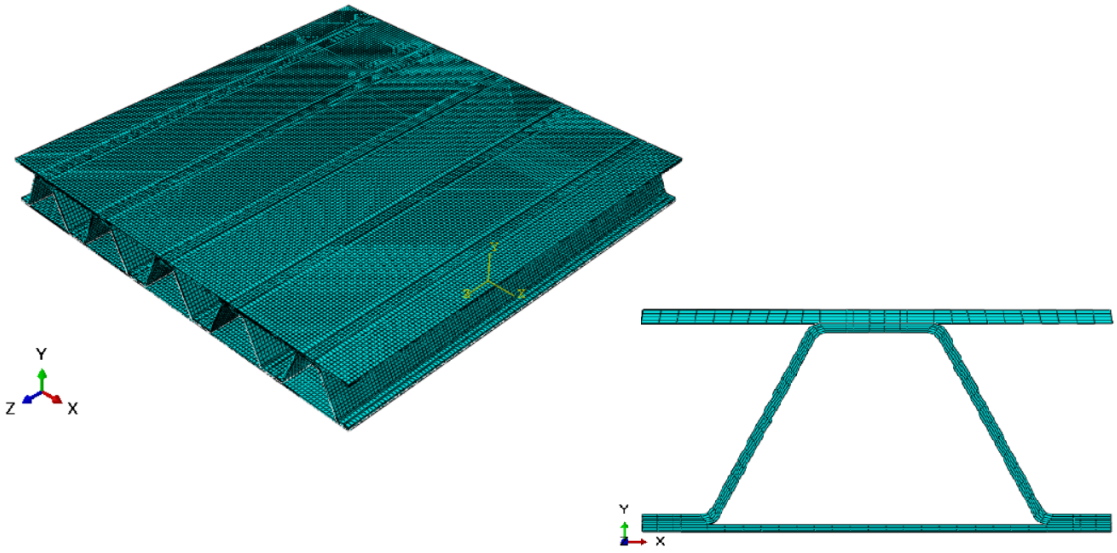

Figure 4.15: Meshed global model of empty sandwich panel

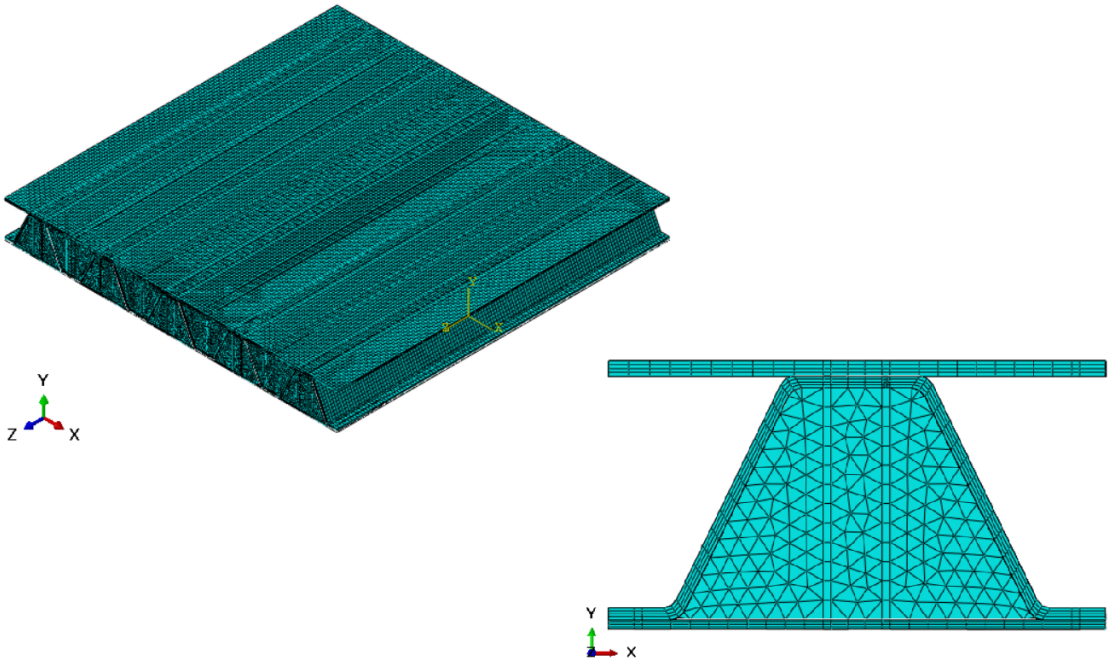

Figure 4.16: Meshed global model of foam filled sandwich panel

4.7.7. Notch Location

To calculate J-Integral value using submodel we created four notches on each side of two welds for one joint. Notch numbering for one representative submodel is shown in Fig. 4.21. In sandwich panel with dual stake laser welds location of critical notch can't be determined directly. The critical tensile from where we expect crack to originate could be seen by looking at the deformed shape of submodel. Based on this the location of two tensile notches for each joint was determined in this study. The notch where higher J-Integral value is observed should be taken as critical notch for that joint.

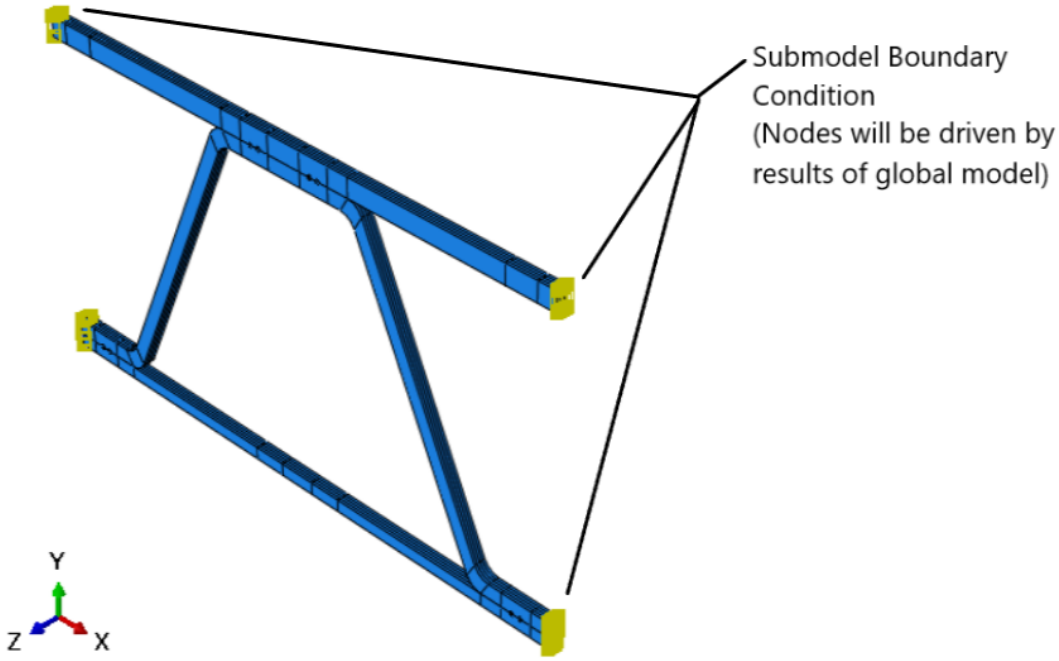

Figure 4.17: Submodel of empty sandwich panel

4.7.8. Tensile Notches

Unlike web core sandwich panels a joint in corrugated core panel has complex notch arrangement at critical dual stake laser welded joint. This makes deciding which notch is in tensile state difficult. A simple technique to differentiate tensile and compressive notches is outlined in Section 2.7 of [34]. The best way to determine fracture modes is by looking at displaced submodel. It's evident by looking at displaced submodel in Figure 4.22, Figure 4.23, Figure 4.24 and Figure 4.25 that two fracture modes, Mode - I and Mode - II, are present. The opening up of seams shows the location of tensile notches.

J-Integral in Submodel

A 3D submodel was used to estimate J-Integral value at all four notch locations of the critical joint. This section deals with interpreting results to arrive at J-Integral value for critical notch. Location of critical notch is obtained by looking at deformed shape of the submodel. As can be seen in Figure 4.23 and 4.25 a notch that opens is characterised as a tensile notch. An empty panel has two tensile notches while a foam filled panel only has one tensile notch. For empty panel we look at values of J-Integral at both tensile notches and the one with higher value will be characterised as a critical.

J-Integral estimate varies across the section. For the present case we have decided to use value obtained at center of the cross-section as J-Integral estimate. For an empty sandwich panel submodel the section numbering is shown in Figure 4.26. The corresponding J-Integral variation along the section is shown in Figure 4.27. The J-Integral value at each section (Sec 1 to Sec 42) is read at contour number 5. This is due to the fact that after contour 3 output values are quite stable as can be seen in Figure 4.29 and 4.30.

Relation between J and ΔJ

J Integral or J refers to the value of contour integral obtained at a certain loading while ΔJ refers to range of J-Integral value, $\Delta J = J_{max} - J_{min}$. In the present study we have considered $J_{min} = 0$ for the case of no loading. Therefore, $\Delta J = J_{max}$ or simply the calculated J-Int value for the the submodel.

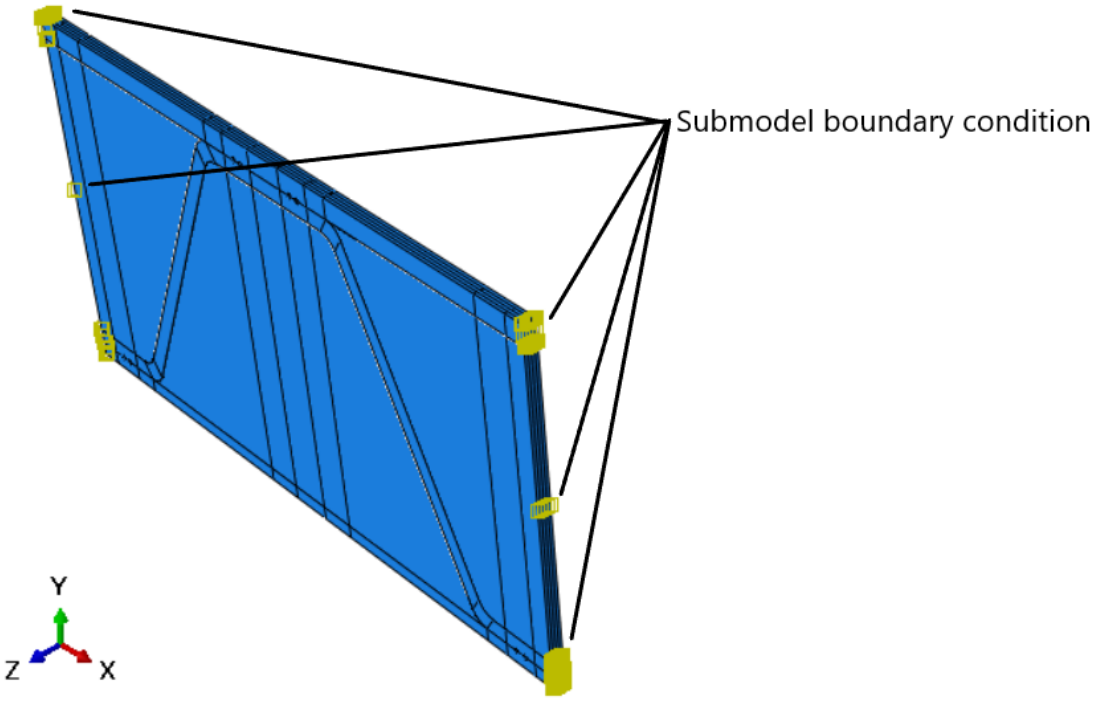

Figure 4.18: Submodel of foam filled sandwich panel

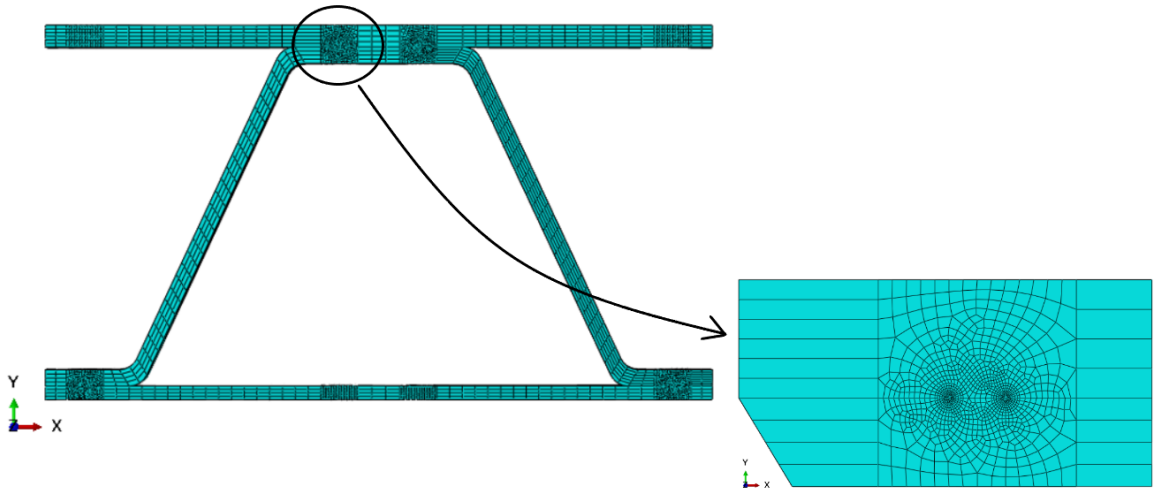

Figure 4.19: Meshed submodel of empty sandwich panel

4.7.9. Analysis and Results

For each 3D global model a 3D submodel was created. The J-Integral was calculated through these sub models using Abaqus *Contour Integral* option. Practice for good J-Integral estimate has already been discussed, refer Section 2.4.2 and 2.4.3 for details. Spider web meshing with Mid-Side node shifted by a quarter point (Quarter Point shift and square root singularity) was added in the model to get a more accurate assessment of J-Integral. J-Integral was requested for 5 contour around the crack tip. It is observed that J-Integral estimate from first two contour is not stable and estimate from third contour

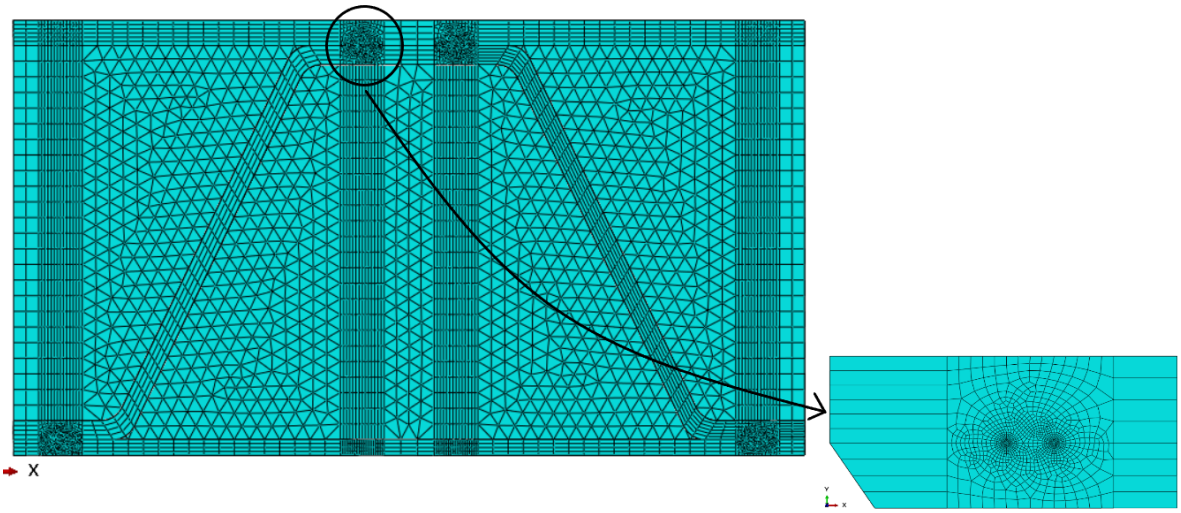

Figure 4.20: Meshed submodel of foam filled sandwich panel

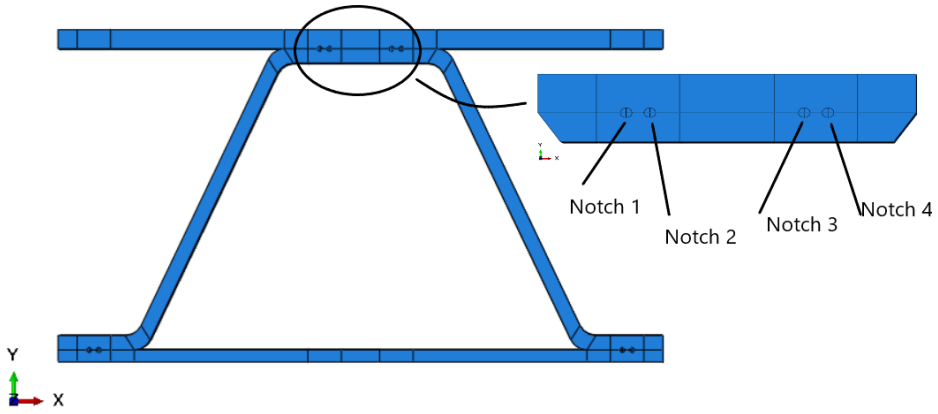

Figure 4.21: Notch numbering for critical joint in the submodel

onwards is more or less stable (or constant). Value of J-Integral at fifth contour was accepted as the J-Integral value. J-Integral value at contour number 5 at mid-section of the submodel was used for calculating cycles to failure.

The final results from two-stage FE analysis (Global Model and Submodel) are presented in Table. 4.3 and Figure 4.31. Relative fatigue life improvement is shown in Fig. 4.32 with respect to mass of filling material. Predicted fatigue life improvement is shown in Fig. 4.33 with respect to Young's Modulus of filling material.

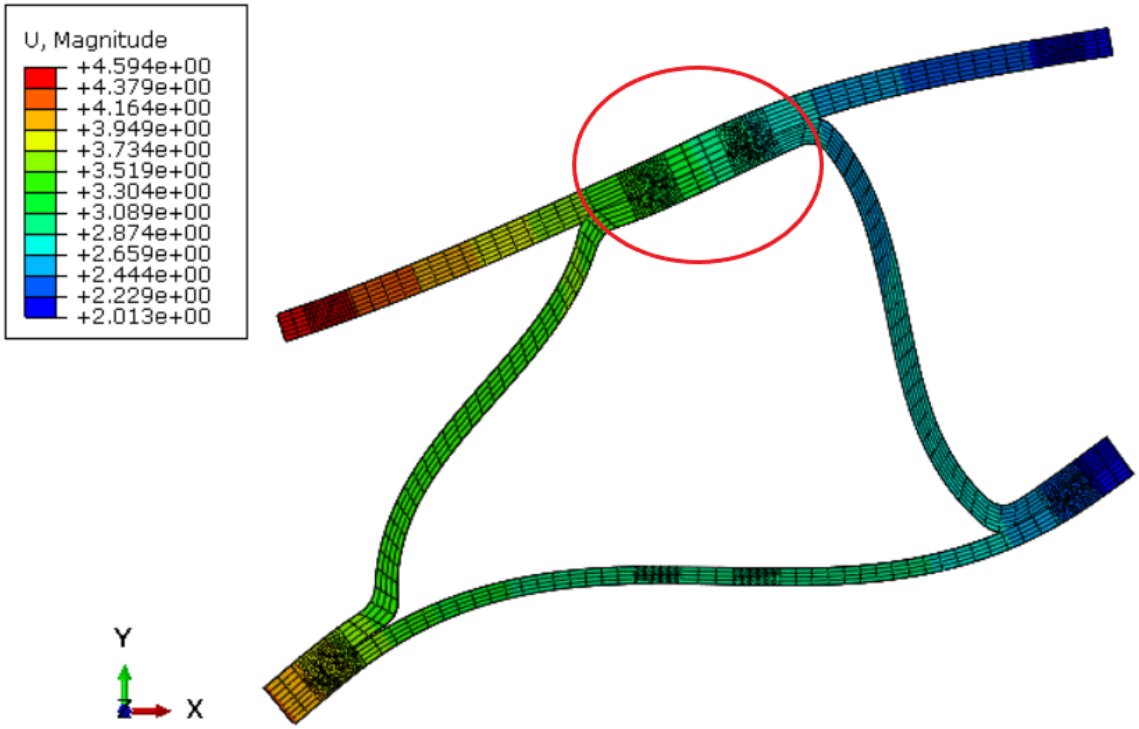

Figure 4.22: Displaced Submodel - Empty sandwich panel

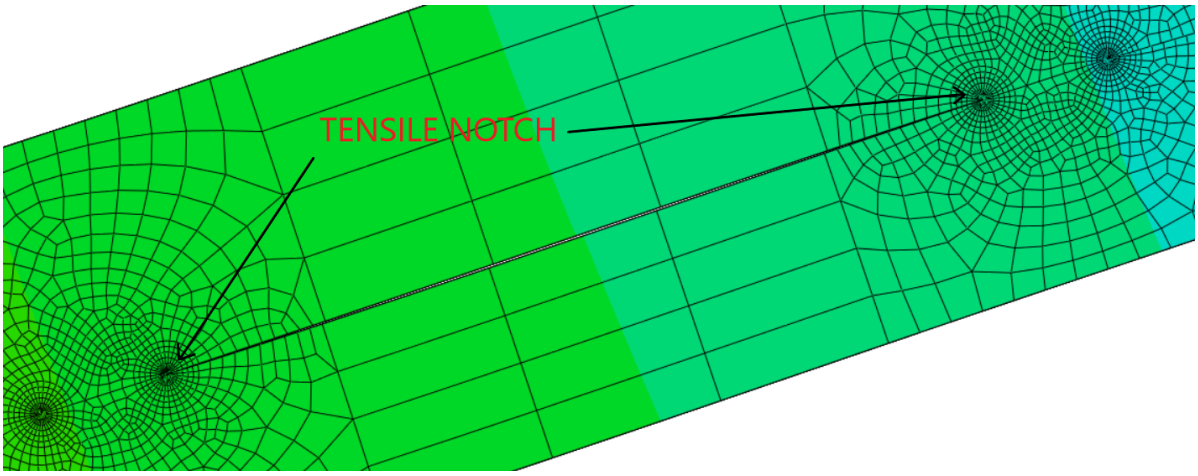

Figure 4.23: Enlarged view of seam opening in the marked zone of Figure 4.22

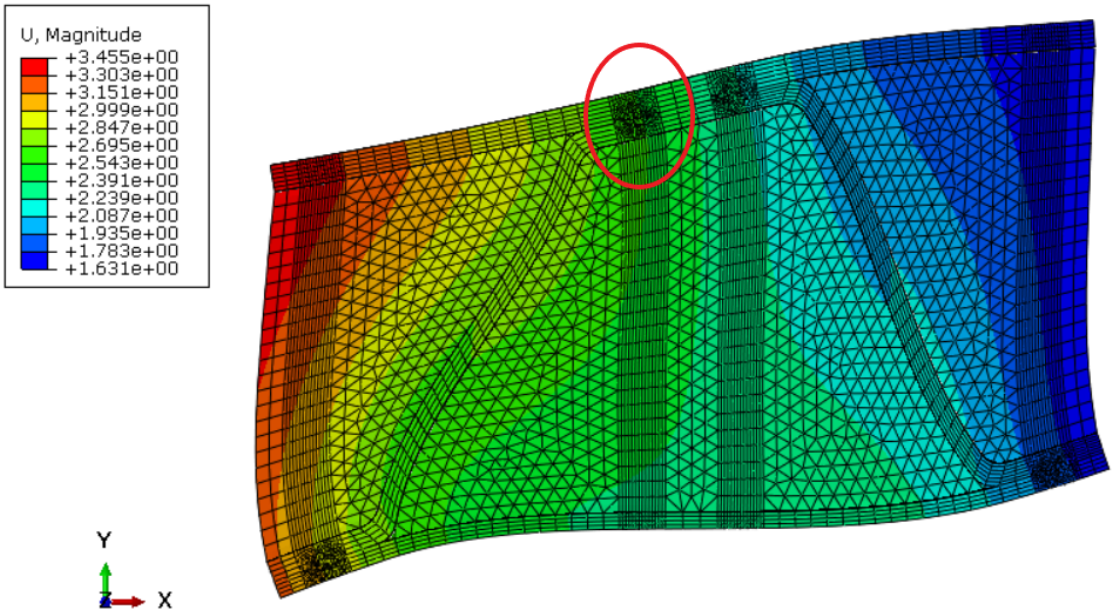

Figure 4.24: Displaced Submodel - Foam Filled sandwich panel

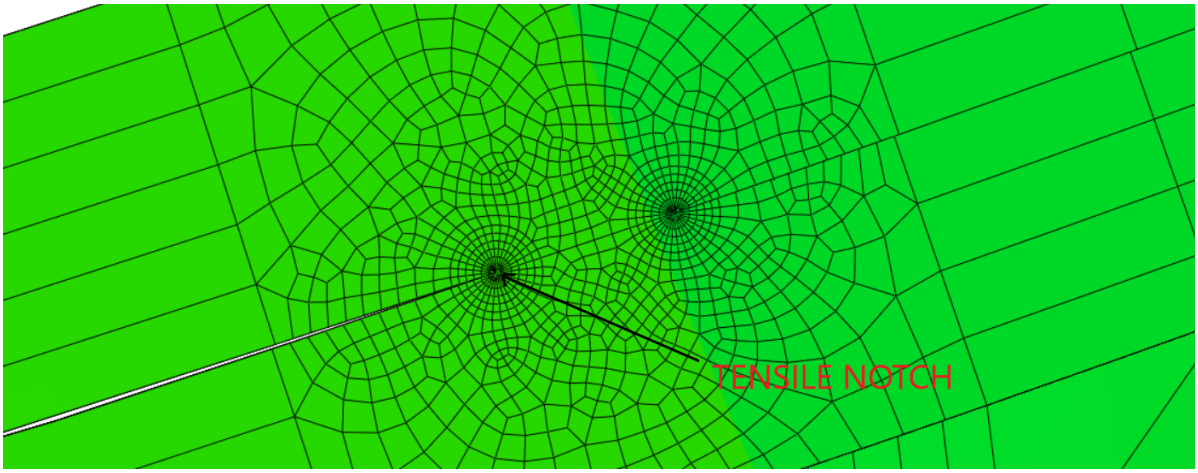

Figure 4.25: Enlarged view of seam opening in the marked zone of Figure 4.24

				Critical Joint	
Case	Density $[kg/m^3]$	Young's Modulus [MPa]	Mass [kg]	ΔJ [MPa mm]	Critical Notch Number
No Foam	0.0	0.0	0.0	0.099	Notch 2
H45	48.0	45.0	6.3	0.048	Notch 1
H60	60.0	58.5	8.4	0.041	Notch 1
H80	80.0	82.5	11.2	0.033	Notch 1
H100	100.0	110.0	14.0	0.032	Notch 1
H130	130.0	140.0	18.2	0.023	Notch 1
H200	200.0	205.0	28.0	0.022	Notch 1
H250	250.0	250.0	35.0	0.016	Notch 1

Table 4.3: Results of two stage FE Analysis on Empty and Foam Filled sandwich panel

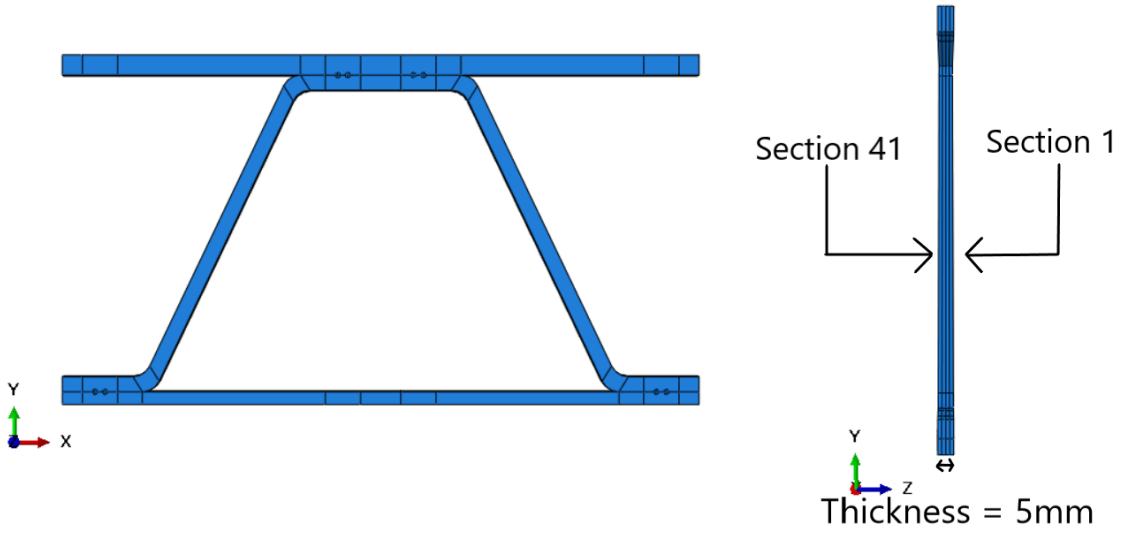

Figure 4.26: Front view of submodel and section numbering in cross section

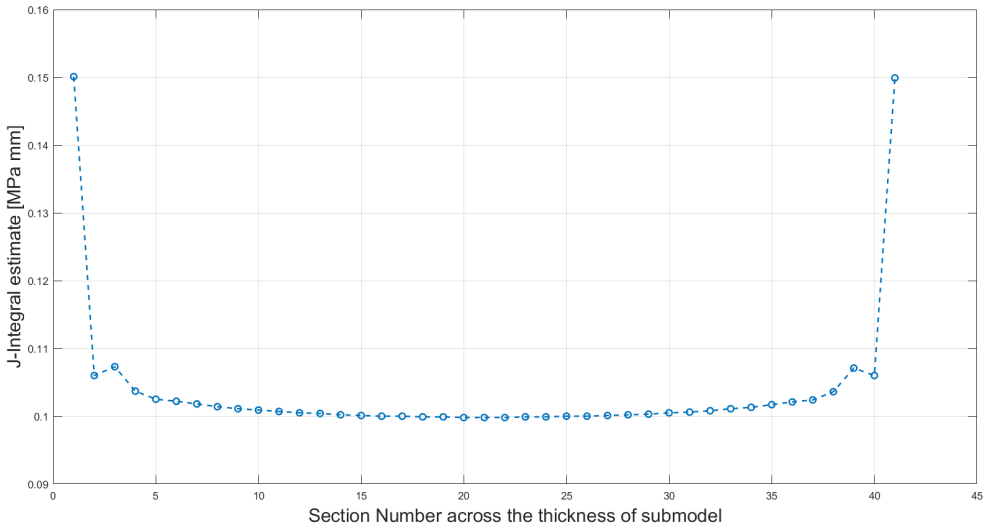

Figure 4.27: Typical variation of J-Integral value along the section thickness in submodel

SNo	ΔJ [MPa mm]	$\sqrt{\Delta J}$ $[MPa^{0.5}mm^{0.5}]$	N_f [cycles]
No Foam	0.099	0.3146	10,561,218
H45	0.048	0.2190	285,283,658
H60	0.041	0.2024	584,524,496
H80	0.033	0.1816	1,568,065,349
H100	0.032	0.1788	1,806,233,773
H130	0.023	0.1516	8,108,781,691
H200	0.022	0.1483	9,906,810,726
H250	0.016	0.1264	42,405,283,120

Table 4.4: Estimating N_f from $\sqrt{\Delta J}$ value for pressure load of ΔP = $24N/mm^2$

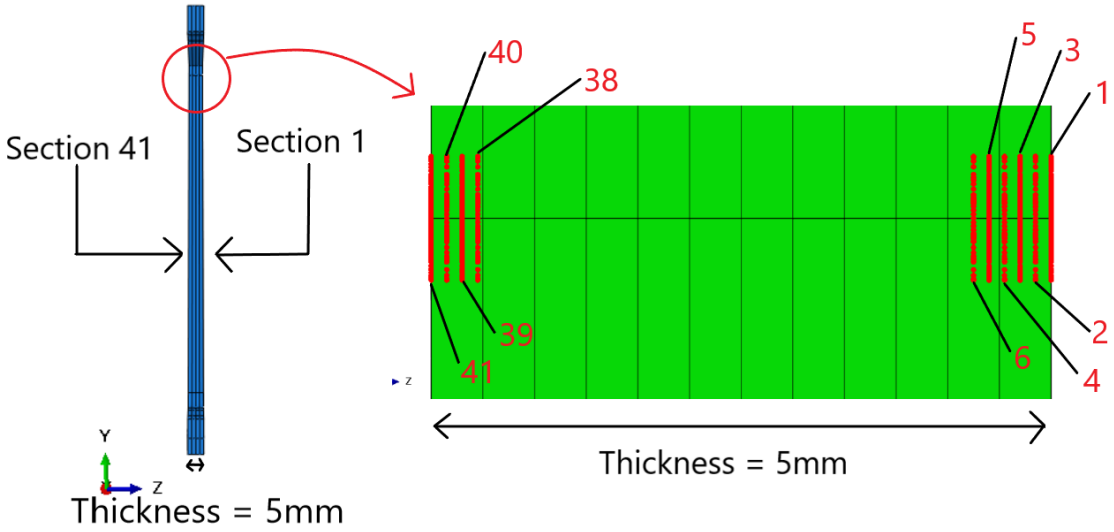

Figure 4.28: Section Numbering along thickness (=5 mm) of submodel. For 3D submodels Abaqus/CAE calculates J-Integral at finite number of sections along the thickness, 41 sections in this case.

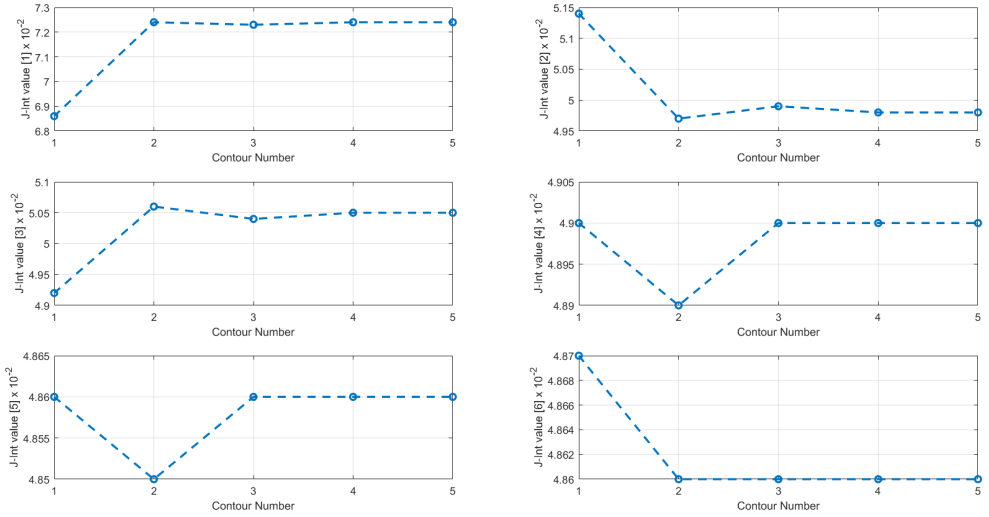

Figure 4.29: Typical J-Integral output for the marked section of Figure 4.28 (H45 Foam Submodel) - Section 1 to 6 (Note that after contour number 3 the J-Integral estimate is constant)

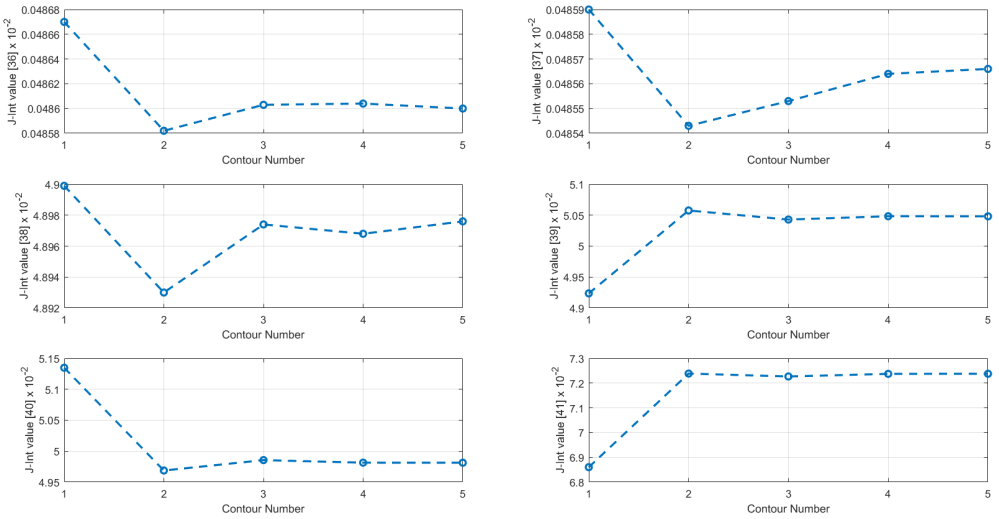

Figure 4.30: Typical J-Integral output for the marked section of Figure 4.28 (H45 Foam Submodel) - Section 36 to 41 (Note that after contour number 3 the J-Integral estimate is constant)

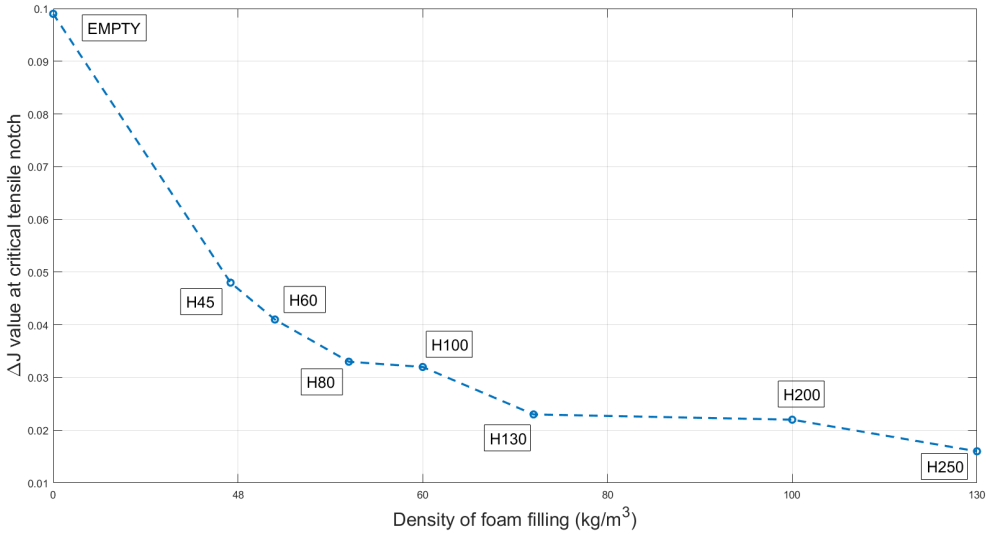

Figure 4.31: Variation in J-Integral value at critical tensile notch of sandwich panels for various submodels

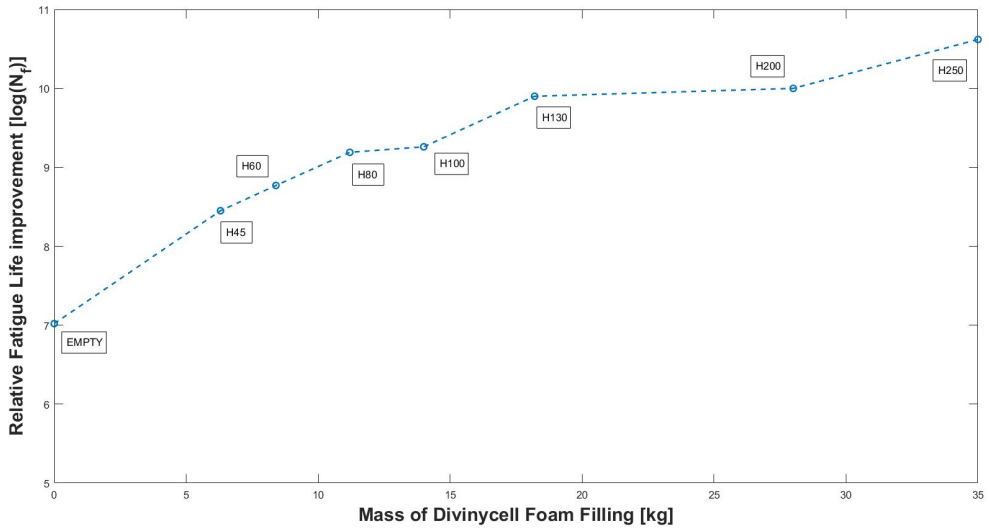

Figure 4.32: Relative fatigue life improvement w.r.t. mass of the filling material

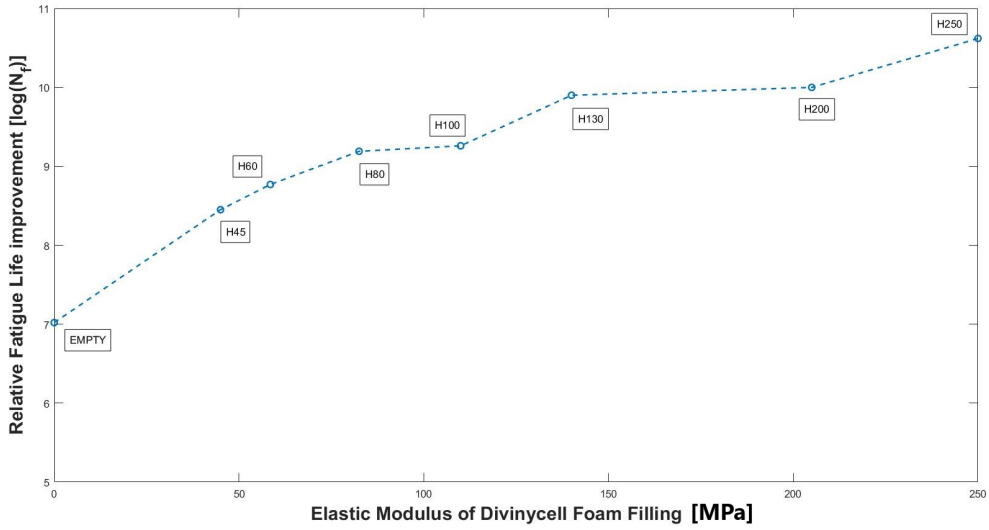

Figure 4.33: Relative fatigue life improvement w.r.t. Modulus of the filling material

5

Deck Sizing and Parametric Study

5.1. Introduction

This chapter deals with sizing of sandwich panel and geometrical parametric study to maximize critical elastic constants. The results from this study could be used to get optimum geometry for sandwich panel for use as bridge decks.

5.2. Deck Dimension - Preliminary Sizing

Preliminary estimates for sandwich panel are shown below along with the reason for selection -

- `Deck Plate Thickness` - The thickness of deck plate should be greater than 14 mm Refer EN 1993-2 Table C.1.
- `Pitch of Corrugation` - Pitch of corrugation or centre to center distance between cores should be between 600 mm to 900 mm. A larger pitch will reduce the number of corrugations required and number of welds too. But, since there is limitation on slenderness ratio (clear width to thickness ratio) of ≤ 25. This gives us an upper limit of $25x14 = 350mm$. Hence the clear distance between corrugations should be less than 350 mm and centre to centre distance should be between 600 mm - 900 mm.
- `Edge Distance of Corrugation` - Edge distance of first stiffener should be greater than the pitch of corrugation. Let's take it as 350 + 25 = 375 mm.
- `Core Plate Thickness` - Thickness of core plate should be greater than or equal to 6 mm but less than or equal to 10 mm. Let's take it as 10 mm.
- `Angle of Corrugation` - From Fig 3 of [23], we have plots showing the variation of transverse shear stiffness (D_{Qy}) with angle of corrugation (θ) for different h_c/t_c ratios. It is observed that an angle of 60° gives the highest value of D_{Qy} when other parameters are kept constant. As a preliminary dimension we take angle of corrugation $\theta = 60^\circ$. Impact of geometric parameters on D_{Qy} will be discussed in Section 5.4.3

The above items complete the assumptions needed for preliminary dimensioning of sandwich panel.

5.3. Deformation Mechanism - Bridge Superstructure

Before carrying out the parametric study, it is important to describe deformation mechanism of a deck - cross beam - Girder bridge system. Since, a sandwich panel bridge is quite similar to OSD in terms of load carrying behaviour, we expect similar deformation behaviour too. The following deformation mechanism are important in a bridge super structure (Table 5.1 describes them in brief) -

Out of the seven deformation mechanisms mentioned in Table. 5.1, a deck only supports three. These are - local deck plate deformation, panel deformation and global deformation. In *local deck plate deformation*, a deck withstands locally applied wheel load pressure. In *panel deformation*, a deck

Deformation Mechanism	Description
Local Deck plate deformation	Transfer of wheel loads from deck plate to rib walls
Panel deformation	Two-way load distribution for out-of-plane loading
Rib longitudinal flexure	Load Transfer by individual ribs (or core for sandwich panel) in the longitudinal direction
Floor beam in-plane flexure	Load transfer by ribs to floor beams
Floor beam distortion	In-plane and out-of-plane FB distortion due to loads from rib
Rib Distortion	Rib deformation when wheel is between two ribs
Global Deformation	Combined displacement of longitudinal girders and OSD

Table 5.1: Deformation Mechanism of a Bridge Superstructure

effectively distributes the load to underlying supporting structure. It is pertinent to add here that a sandwich panel performs better than traditional OSD in plate action. The inclination of core part of corrugated core panel enhances the transverse shear stiffness as compared to OSD. This leads to better plate action. For a bridge supported by transverse and longitudinal girders, improved plate action of sandwich panel is beneficial [24]. In *Global Deformation*, deck of bridge acts as a flange for main load carrying members (i.e. the longitudinal girders). These modes are shown in Figure 5.1.

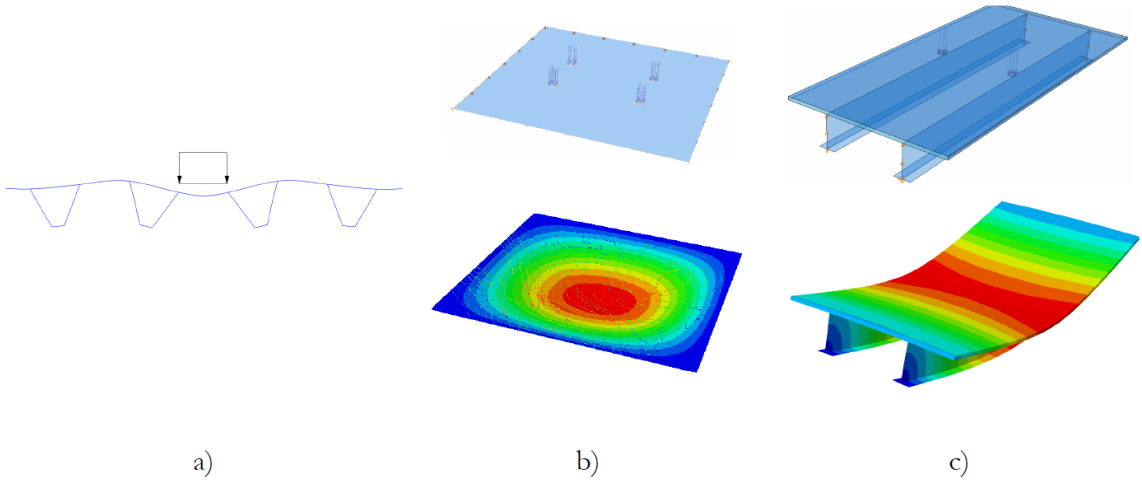

Figure 5.1: Deck Participation - (a) local deck plate deformation, (b) panel deformation and (c) global bending [24].

5.4. Parametric Study

5.4.1. Introduction

In Section 5.2 and 5.3, we discussed the preliminary sizing guidelines and deformation mechanism for an OSD bridge respectively. How different geometric parameters of a sandwich panel will affect the critical elastic constants will be discussed in this section. It is clear that increasing the thickness of face plate, core and height of the sandwich panel deck will lead to reduction in deflection. This could easily be explained by increase in bending stiffness of the panel. But, what is not known precisely is how much these individual parameters affect the panel response. This parametric study describes effect of individual geometric parameters on panel's elastic constants. These elastic constants directly affects the bending behaviour of panel.

In this parametric study we look at the response of sandwich panel with respect to changes in -

- Thickness of top and bottom face plates
- Thickness of core layer

- Height of core layer

Since, in this parametric study we are considering symmetric sandwich panel, thickness of both top and bottom face plates are referred to as a single parameter. Height of sandwich panel is an important geometric parameter. By changing it, stiffness and subsequently stiffness - to - weight ratio could either be increased or decreased. It is important to mention here how will we bring about increase in panel height. One way to do this is to increase or decrease the *Angle of Corrugation* while keeping the length of a unit cell of sandwich panel constant. Other option is to keep *Angle of Corrugation* unchanged but vary the length of *Crests* and *Troughs* of core layer. In this parametric study we only change angle of corrugation as we don't want to change the length of contact between core layer and face plates (top and bottom).

5.4.2. Parametric Study - Results

This section deals with effect of geometric parameters on five elastic constants of a sandwich panel. Knowing this variation is important for a proper dimensioning of a sandwich panel. The elastic constants considered are as follows -

- Bending Stiffness, D_x and D_y
- Transverse Shear Stiffness, D_{Qx}
- Twisting Stiffness, D_{xy}

Figure 5.2 shows the change is bending stiffness, D_x with respect to change in 3 input parameters, namely - thickness of top face plate, height of sandwich panel and thickness of core plate. Clearly in terms of stiffness, increase height of the sandwich panel will have maximum positive impact. This is due to the fact that increase in panel height directly increases the face plate contribution to moment of inertia. This is clearly visible in the said figure by the steep slope of the line corresponding to increase in height of the sandwich panel. Increasing the thickness of the core layer is the least effective way of increase bending stiffness, D_x. The curve corresponding to core thickness shows least increase in bending stiffness per unit increase in weight of a unit cell of sandwich panel. Impact from increasing the thickness of top and bottom face plates is in between these two cases.

Figure 5.3 shows the change is bending stiffness, D_y with respect to change in 3 input parameters, namely - thickness of top face plate, height of sandwich panel and thickness of core plate. By expression of D_y it was clear that there will be a negligible effect of increasing the core thickness, t_c and same can be observed in Figure 5.3. Similar to the case of Bending stiffness D_x, the effect of increasing the height of panel leads to steepest increase in D_y per unit increase in thickness. But, one key difference is that for same change in input parameter the increase in D_y is far less than increase in D_x. A unique aspect of bending stiffness, D_y is that it depends on both Young's modulus and Poisson's ratio. while D_x could be calculated solely from the geometric properties of the panel and Young's Modulus.

Figure 5.4 shows the change is transverse shear stiffness, D_{Qx} with respect to change in 3 input parameters, namely - thickness of top face plate, height of sandwich panel and thickness of core plate. It is clear from the expression for D_{Qx} that impact of increasing the face plate thickness will be negative. This is exactly what is observed in the figure. Impact from increasing h is also negligible. But, increasing core thickness is one way of increasing D_{Qx}.

The twisting stiffness, D_{xy} is independent of the properties of the core since symmetry requires that shear flow in the corrugated core sheet be zero [23]. Keeping this in mind, we only look at change in D_{xy} due to two geometric input parameters, i.e. Thickness of face plates and height of the panel. Figure 5.5 shows the effect on D_{xy} due to increase in these two geometric parameters. Increasing height of panel affects twisting stiffness steeply compared to increasing thickness of face plates.

5.4.3. Geometric parameters and D_{Qy}

Effect of geometric parameters on D_{Qy} is much more complex. To understand the effect of geometric parameters on D_{Qy}, we selected some parameters. These are - corrugation angle (α), ratio of height of core layer to thickness of steel plate in core ($\frac{h_c}{t_c}$) and ratio of pitch of corrugation to height of core

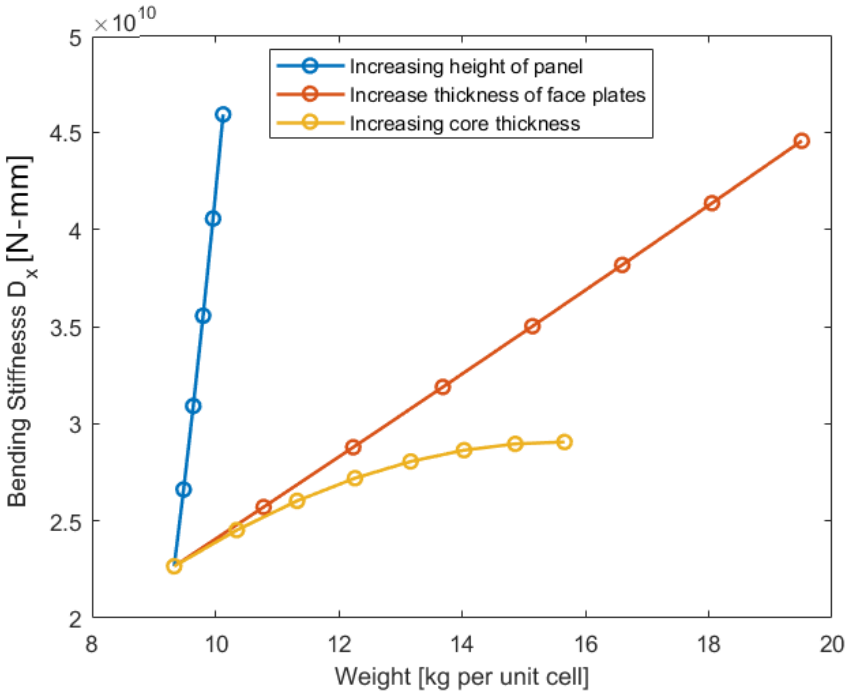

Figure 5.2: Influence of Input Parameters on Bending Stiffness, D_x

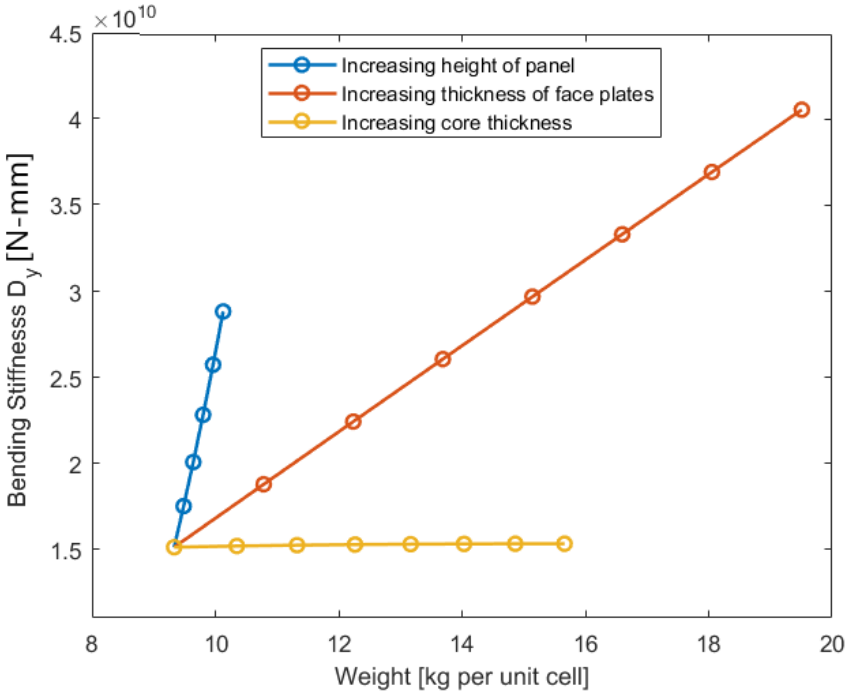

Figure 5.3: Influence of Input Parameters on Bending Stiffness, D_y

layer ($\frac{p}{h_c}$).

Initially we assumed h_c = 120 mm, h_c/t_c = 15. Ratio of p/h_c will be kept between 1 to 1.4. From Section 5.2, it is already known that a high angle of corrugation is preferred and therefore we take α = $60°$. Another important factor is thickness of face plates with respect to core thickness, t_c/t_f. This

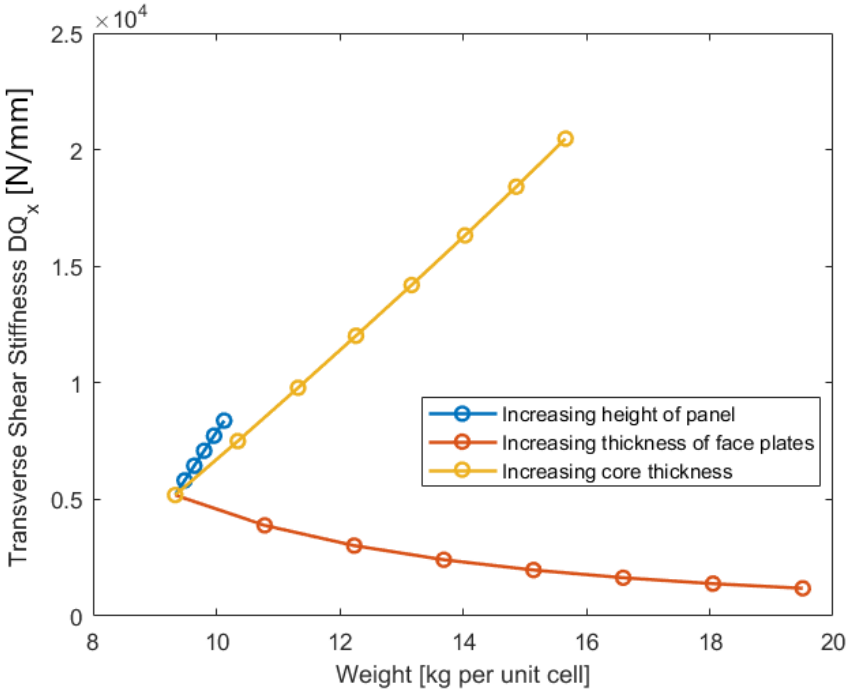

Figure 5.4: Influence of Input Parameters on Transverse Shear Stiffness, DQ_x

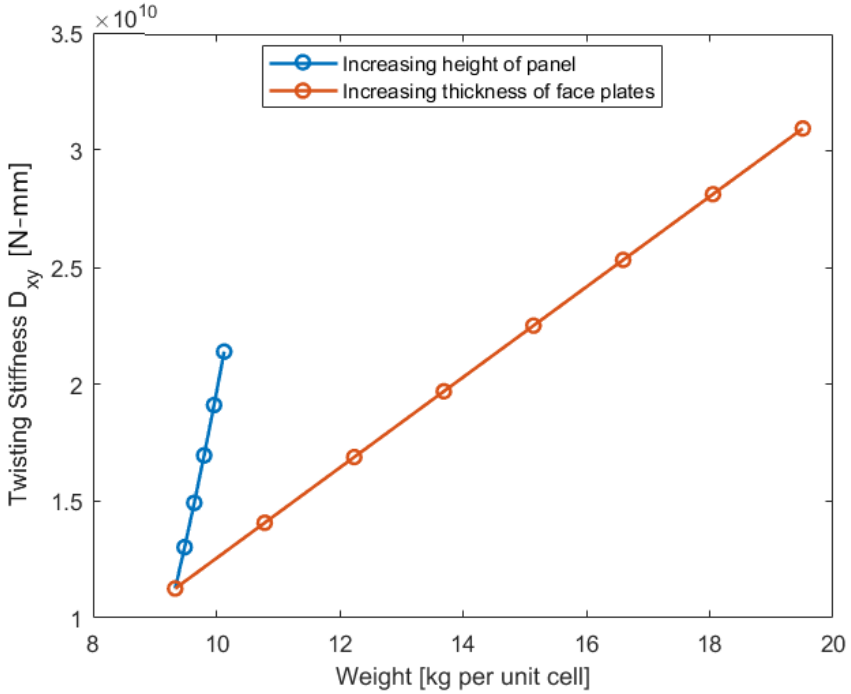

Figure 5.5: Influence of Input Parameters on Twisting Stiffness, D_{xy}

is kept between 0.6 and 1. The values obtained for the five elastic constants (D_x, D_y, D_{Qx}, D_{Qy} and D_{xy}) are shown in Table. 5.2. For h_c/t_c = 30 the results are shown in Table. 5.3.

Based on this analytical exercise, some recommendations are as follows. A higher angle of corrugation (α) above 60° is not recommended as it adversely affects the most critical elastic constant, D_{Qy}.

p/h_c ratio should be kept around 1 to 1.2 as higher ratio will lead to sharp decrease in D_{Qy}. As for t_c/t_f, it should be kept close to 0.6 to 1.0 with a value of 0.6 leading to more favourable D_{Qy} compared to D_{Qy} value for ratio of 1.0. h_c/t_c ratio should be around 15 to 25.

α	t_c/t_f -	p/h_c -	D_x [Nm]10^7	D_y [Nm]10^7	D_{xy} [Nm]10^7	D_{Qx} [N/m]10^7	D_{Qy} [N/m]10^7
60	0.6	1.0	3.23	2.54	1.91	50.60	9.58
		1.2	3.31	2.55	1.91	37.40	4.10
		1.4	3.37	2.55	1.91	28.80	2.05
	0.8	1.0	2.52	1.82	1.37	48.10	8.00
		1.2	2.60	1.83	1.37	35.60	3.20
		1.4	2.65	1.83	1.37	27.40	1.96
	1	1.0	2.12	1.42	1.06	46.60	7.00
		1.2	2.20	1.42	1.06	34.50	2.98
		1.4	2.25	1.43	1.06	26.60	1.66
70	0.6	1.0	3.47	2.55	1.91	46.90	3.01
		1.2	3.51	2.56	1.91	35.00	2.46
		1.4	3.54	2.56	1.91	27.10	2.19
	0.8	1.0	2.76	1.83	1.37	44.60	2.67
		1.2	2.80	1.83	1.37	33.30	1.47
		1.4	2.82	1.84	1.37	25.80	1.96
	1.0	1.0	2.36	1.43	1.06	43.20	2.36
		1.2	2.40	1.43	1.06	32.20	1.40
		1.4	2.43	1.43	1.06	25.00	0.96
80	0.6	1.0	3.69	2.56	1.91	43.40	1.46
		1.2	3.69	2.56	1.91	32.60	1.00
		1.4	3.69	2.56	1.91	25.40	0.70
	0.8	1.0	2.98	1.84	1.37	24.20	1.33
		1.2	2.98	1.84	1.37	31.00	0.89
		1.4	2.98	1.84	1.37	24.20	0.63
	1.0	1.0	2.58	1.44	1.06	40.00	1.23
		1.2	2.58	1.44	1.06	30.00	0.79
		1.4	2.58	1.44	1.06	23.50	0.60
90	0.6	1.0	3.90	2.57	1.91	39.90	0.84
		1.2	3.87	2.57	1.91	30.20	0.64
		1.4	3.84	2.57	1.91	23.70	0.46
	0.8	1.0	3.19	1.85	1.37	37.90	0.80
		1.2	3.15	1.85	1.37	28.70	0.58
		1.4	3.13	1.85	1.37	22.60	0.45
	1.0	1.0	2.79	1.44	1.06	36.80	0.78
		1.2	2.76	1.44	1.06	27.80	0.57
		1.4	2.73	1.44	1.06	21.90	0.42

Table 5.2: Effect of geometric parameters on elastic constants for h_c/t_c = 15.

5.4.4. Load vs Maximum Deflection

In this section effect of panel height on panel deflection response was studied. Linear elastic material properties were modified to Bilinear Stress Strain Curve with Kinematic Hardening. This is done to see how elastic-inelastic point of a load deflection curve changes with change in panel height. The response is shown in Figure 5.6. It is clear from the figure, the change from linear elastic to inelastic behaviour occurs at different load levels for panel of different heights. For panel of height 107.5 mm, 138.5 mm, 170.5 mm the change occurs at applied load level of approximately 40 kN, 50 kN and 60

α	t_c/t_f -	p/h_c -	D_x [Nm]10^7	D_y [Nm]10^7	D_{xy} [Nm]10^7	D_{Qx} [N/m]10^7	D_{Qy} [N/m]10^7
60	0.6	1.0	1.50	1.15	0.86	22.8	1.03
		1.2	1.53	1.15	0.86	16.90	0.43
		1.4	1.56	1.15	0.86	13.0	0.24
	0.8	1.0	1.19	0.84	0.63	22.20	0.86
		1.2	1.23	0.85	0.63	16.40	0.36
		1.4	1.26	0.85	0.63	12.70	0.19
	1	1.0	1.02	0.67	0.50	21.90	0.76
		1.2	1.06	0.67	0.50	16.20	0.32
		1.4	1.08	0.67	0.50	12.50	0.18
70	0.6	1.0	1.62	1.16	0.86	21.20	0.32
		1.2	1.63	1.16	0.86	15.80	0.19
		1.4	1.65	1.16	0.86	12.20	0.12
	0.8	1.0	1.13	0.85	0.63	20.6	0.27
		1.2	1.33	0.85	0.63	15.40	0.17
		1.4	1.34	0.85	0.63	11.90	0.11
	1.0	1.0	1.14	0.67	0.50	20.30	0.26
		1.2	1.16	0.67	0.50	15.10	0.14
		1.4	1.17	0.67	0.50	11.70	0.095
80	0.6	1.0	1.72	1.16	0.86	19.60	0.16
		1.2	1.73	1.16	0.86	14.70	0.11
		1.4	1.73	1.16	0.86	11.50	0.076
	0.8	1.0	1.42	0.85	0.63	19.10	0.14
		1.2	1.42	0.85	0.63	14.30	0.099
		1.4	1.42	0.85	0.63	11.20	0.069
	1.0	1.0	1.25	0.68	0.05	18.80	0.14
		1.2	1.25	0.67	0.50	14.10	0.095
		1.4	1.25	0.67	0.50	11.00	0.065
90	0.6	1.0	1.83	1.16	0.86	18.00	0.097
		1.2	1.81	1.16	0.86	13.60	0.073
		1.4	1.80	1.16	0.86	10.70	0.05
	0.8	1.0	1.53	0.86	0.63	17.50	0.088
		1.2	1.51	0.86	0.63	13.30	0.066
		1.4	1.50	0.85	0.63	10.40	0.049
	1.0	1.0	1.35	0.68	0.50	17.20	0.085
		1.2	1.33	0.68	0.50	13.10	0.064
		1.4	1.32	0.68	0.50	10.30	0.048

Table 5.3: Effect of geometric parameters on elastic constants for h_c/t_c = 30.

kN respectively.

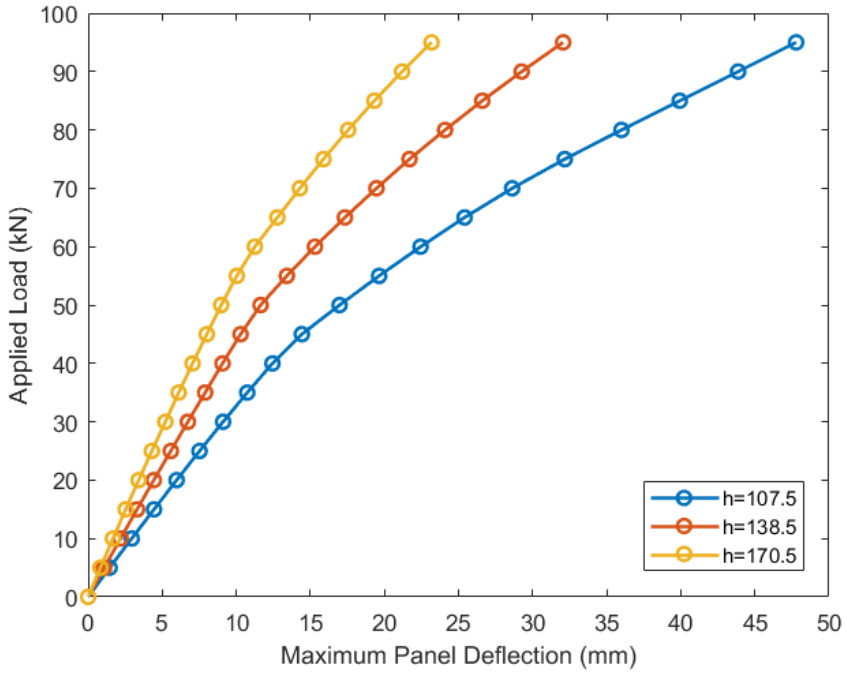

Figure 5.6: Load vs Maximum Deflection behaviour of a panel for kinematic hardening model

6

Conclusion & Recommendations

6.1. Conclusions

The aim of this thesis was to apply J-Integral based local approach for fatigue assessment of sandwich panels subjected to lateral loads. A second aim of this thesis was to justify the use of foam filling in sandwich panels by comparing fatigue performance of empty and foam filled sandwich panels. Existing research (refer [25], [6], [7]) pointed to the fact that CCSSP (Corrugated Core Sandwich Steel Panel) offers numerous advantages over OSD (Orthotropic Steel Deck). It was also observed (refer [13], [15], [14] and [12]) that the commonly used nominal stress approach is not suitable for laser welded joints due to large scatter in results. A local approach like J-Integral is preferred and has been used successfully on web-core sandwich panels and was therefore used in this study. J-Integral based local approach was utilised by taking $\sqrt{\Delta J}$ as a fatigue strength assessment parameter. Simplified FE models were developed to model dual stake laser welded sandwich panels so that output parameters (like panel deflection and stresses in plates) were estimated with good accuracy (i.e. 10% difference compared with experimental results).

The main findings of this research is summarised below -

***Objective 1* - Validation study to develop a FE model to accurately estimate bending response of a sandwich panel.**

A simplified FE model of sandwich panel was developed in this study for the purpose of validation. The results obtained from this model were compared with experimental and FE model results obtained by Tan et al. [33]. The FE models were developed for two different boundary conditions - (*SS ends only case* and *All Sides SS Case*). Output parameters like deflection and stresses were estimated with less than 10% difference with respect to experimental results obtained in Tan et al [33]. For *SS Ends only case* the maximum panel deflection differed by 2.1% from experimental observation. For *All Sides SS Case* the difference was 8.3%. It can be concluded that when panel is simply supported on two sides only, the results from FE model developed in this study matches well with experimental data. But when all four sides are supported, the accuracy of present FE model drops.

***Objective 2* - Selection of foam filling for a sandwich panel**

2D FEA was carried out on a beam extracted from a sandwich panel while 3D FE analysis was carried out on a small sandwich panel. The criteria used to decide optimum foam filling were - Decrease in surface stresses, increase in transverse shear stiffness and increase in self weight. Seven different foam fillings of Divinycell H type were investigated - H45, H60, H80, H100, H130, H200 and H250. *Ratio* of increase in DQy to increase in self-weight was chosen as deciding factor on suitability of various foams. Despite being the strongest, the analysis show that H250 is not the most optimum foam. From simple analytical estimate, H200 comes out as most optimum foam (*Ratio* - 0.048) followed by H250 (*Ratio* - 0.046) and H130 (*Ratio* - 0.038). This is due to the fact that a stronger foam like H250 will

cause more increase in self weight of the panel and thereby reducing it's efficiency.

***Objective 3* - J-Integral based local approach to estimate cycles to failure.**

A 3D FE model of size 1265 mm x 1265 mm was developed to quantify performance improvement in sandwich panel with foam filling. Four notches were observed at critical joint of a sandwich panel. For empty sandwich panel, out of these four notches - two were compressive notches and two were tensile notches. In foam filled sandwich panel, only one notch was in tension while other three were in compression. This difference could be due to the support provided by foam. Fatigue crack is expected to initiate from critical tensile notch only. Two stage FE modelling was used to calculate J-Integral value at this critical tensile notch. J-Integral value decreased as sandwich panels were filled with stronger foams (83.8% reduction in J-Integral value). Using $\sqrt{\Delta J}$ as fatigue strength assessment parameter, cycles to failure were estimated. Between empty and H250 foam filled panel cycles to failure increased by 4105 times. Using fatigue performance improvement as a judging criteria - H250 foam came out as best foam. One thing to note here is that post H130 the improvement was very small. Therefore, H130 could be characterised as the most optimum foam. Between empty and H130 foam filled panel cycles to failure increased by 768 times.

Apart from the above conclusions, the following sizing guidelines could also be drawn from the parametric study conducted in Section 5.4 -

Based on parametric study, sizing guidelines were developed with goal of maximising the value of critical elastic constant, D_{Qy}. It was found that a higher angle of corrugation (α) above 60° adversely affected the most critical elastic constant, D_{Qy}. It is recommended that p/h_c ratio should be kept around 1 to 1.2 as higher ratio will lead to sharp decrease in D_{Qy}. As for t_c/t_f, it should be kept close to 0.6 to 1.0 with a value of 0.6 leading to more favourable D_{Qy}. h_c/t_c ratio should be around 15 to 25. The guidelines of this short parametric study could be applied to obtain an optimal sizing of sandwich panel.

6.2. Recommendations

Some recommendations to further improve the FE model are as follows -

Rotational stiffness of welds were not incorporated in this study and the joint was assumed to be perfectly rigid. Refining the FE models by incorporating rotational stiffness of weld would make the local stresses around loaded area more accurate. Rotational stiffness could be incorporated in two ways - (a) by calculating rotational stiffness using DSM (Refer [25]), (b) for a panel of particular dimensions rotational stiffness could also be determined experimentally (Refer [30]). Based on experimental investigation, an equivalent weld thickness could be determined (which could then be used in FE modelling, refer [31]).

Improving the FE models - There were two primary FE models developed in this study. A) to assess bending behaviour of sandwich panel and B) to calculate J-Integral value at tensile notch. The results from second FE model is good but the output obtained from first model could be improved further. Focus should be on modifying the interaction properties and more realistic modelling of dual stake laser weld so that accuracy of FE model could be improved further.

Fatigue testing of a welded joint of a sandwich panel should be carried out. This is necessary to determine the parameters C and m of the regression equation. Once these parameters are known and verified, $\sqrt{\Delta J}$ could be used more accurately as a fatigue strength assessment parameter to calculate N_f.

Full 3D FE analysis should be carried out on a small trial bridge, preferably using moving loads. Once critical joints are located, a submodel could be used to estimate J-Integral value. If accurate C and m are available from experiments, better estimation of N_f would be possible.

Failure of panels should be studied. It was pointed out in [27] that empty sandwich beams were failing by plastic hinge formation at laser weld and foam filled sandwich beams were failing by shear failure of filling material followed by plastic hinge formation at laser weld.

Cost assessment should be carried out in order to determine the feasibility of laser welded sandwich (empty and foam filled) panels with respect to existing orthotropic decks.

Bibliography

[1] 8 Node Shell element. http://web.mit.edu/calculix_v2.7/CalculiX/ccx_2.7/doc/ccx/node39.html#2dexpansion. Accessed: 2019-04-23.

[2] Abaqus user's manual. https://abaqus-docs.mit.edu/2017/English/SIMACAEEXCRefMap/simaexc-c-docproc.htm. Accessed: 2018-06-18.

[3] Ted L Anderson. *Fracture mechanics: fundamentals and applications*. CRC press, 2017.

[4] Han Bin, Yu Bo, Xu Yu, Chen Chang-Qing, Zhang Qian-Cheng, and Lu Tian Jian. Foam filling radically enhances transverse shear response of corrugated sandwich plates. *Materials & Design*, 77:132–141, 2015.

[5] P D Boersma and FBP De Jong. Techniques and solutions for rehabilitation of orthotropic steel bridge decks in the netherlands. In *The 10th International Conference and Exhibition on Structural Faults and Repair*, 2003.

[6] SR Bright and JW Smith. Fatigue performance of laser-welded steel bridge decks. *Structural Engineer*, 82(21), 2004.

[7] SR Bright and JW Smith. A new design for steel bridge decks using laser fabrication. *Structural Engineer*, 85(21), 2007.

[8] Eurocode CEN. Eurocode 3: Design of steel structure - part 1-9: Fatigue. *EN 1993:1-9*, pages 1–37, 2005.

[9] Wan-Shu Chang, Edward Ventsel, Ted Krauthammer, and Joby John. Bending behavior of corrugated-core sandwich plates. *Composite structures*, 70(1):81–89, 2005.

[10] Robert Connor, John Fisher, Walter Gatti, Vellore Gopalaratnam, Brian Kozy, Brian Leshko, David L McQuaid, Ronald Medlock, Dennis Mertz, Thomas Murphy, et al. Manual for design, construction, and maintenance of orthotropic steel deck bridges. Technical report, 2012.

[11] H Divinycell. grade, technical manual. *Divinycell International AB*, 2010.

[12] D Frank, J Romanoff, and H Remes. Fatigue life improvement of laser-welded web-core steel sandwich panels using filling materials. *Analysis and Design of Marine Structures V*, page 261, 2015.

[13] Darko Frank, Heikki Remes, and Jani Romanoff. Fatigue assessment of laser stake-welded t-joints. *International Journal of Fatigue*, 33(2):102–114, 2011.

[14] Darko Frank, Heikki Remes, and Jani Romanoff. J-integral-based approach to fatigue assessment of laser stake-welded t-joints. *International Journal of Fatigue*, 47:340–350, 2013.

[15] Darko Frank, Jani Romanoff, and Heikki Remes. Fatigue strength assessment of laser stake-welded web-core steel sandwich panels. *Fatigue & Fracture of Engineering Materials & Structures*, 36(8): 724–737, 2013.

[16] A Hobbacher. Recommendations for fatigue design of welded joints and components, international institute of welding, doc. *XIII-2151r4-07/XV-1254r4-07, Paris, France*, pages 41–42, 2008.

[17] David Hutton. *Fundamentals of finite element analysis*. McGraw-Hill„ 2004.

[18] Y Izumi, T Sakagami, S Kubo, and T Tamakoshi. Detection of through-deck type fatigue cracks in steel bridges by self-reference lock-in thermography. In *EPJ Web of Conferences*, volume 6, page 38011. EDP Sciences, 2010.

[19] Anssi T Karttunen, Mikko Kanerva, Darko Frank, Jani Romanoff, Heikki Remes, Jasmin Jelovica, Sven Bossuyt, and Essi Sarlin. Fatigue strength of laser-welded foam-filled steel sandwich beams. *Materials & Design*, 115:64–72, 2017.

[20] DJL Kennedy, RA Dorton, and SDB Alexander. The sandwich plate system for bridge decks. In *International Bridge Conference*, pages 10–12. Citeseer, 2002.

[21] Menke Henderikus Kolstein. Fatigue classification of welded joints in orthotropic steel bridge decks. 2007.

[22] M.H. Kolstein. Fatigue classification of welded joints in orthotropic steel bridge decks. pages 1196–1207, 2009.

[23] Charles Libove and Ralph E Hubka. Elastic constants for corrugated-core sandwich plates. 1951.

[24] Peter Nilsson. Laser-welded corrugated core steel sandwich panels for bridge application. 2017.

[25] Peter Nilsson, Mohammad Al-Emrani, and Seyed Rasoul Atashipour. Transverse shear stiffness of corrugated core steel sandwich panels with dual weld lines. *Thin-Walled Structures*, 2017. ISSN 02638231. doi: 10.1016/j.tws.2017.04.008.

[26] James R Rice. A path independent integral and the approximate analysis of strain concentration by notches and cracks. *Journal of applied mechanics*, 35(2):379–386, 1968.

[27] J Romanoff, A Laakso, and P Varsta. Improving the shear properties of web-core sandwich structures using filling material. In *Proc. of 2nd Intl. Conference on Analysis and Design of Marine Structures, Editors Guedes Soares and Das, Taylor & Francis Group*, pages 133–138, 2009.

[28] Jani Romanoff and Alan Klanac. Design formulations for filled structural sandwich panels, report - m288. Technical report, Helsinki University of Technology - Ship Laboratory, 2004.

[29] Jani Romanoff and Petri Varsta. Bending response of web-core sandwich beams. *Composite Structures*, 73(4):478 – 487, 2006. ISSN 0263-8223. doi: https://doi.org/10.1016/j.compstruct.2005.02.018. URL http://www.sciencedirect.com/science/article/pii/S0263822305000668.

[30] Jani Romanoff, Heikki Remes, Grzegorz Socha, Mikko Jutila, and Petri Varsta. The stiffness of laser stake welded t-joints in web-core sandwich structures. *Thin-Walled Structures*, 45(4):453–462, 2007.

[31] Jani Romanoff, Petri Varsta, and Heikki Remes. Laser-welded web-core sandwich plates under patch loading. *Marine structures*, 20(1-2):25–48, 2007.

[32] Jaap Schijve. *Stress Intensity Factors of Cracks*, pages 105–140. Springer Netherlands, Dordrecht, 2009. doi: 10.1007/978-1-4020-6808-9_5. URL https://doi.org/10.1007/978-1-4020-6808-9_5.

[33] KH Tan, P Montague, and C Norris. Steel sandwich panels: finite element, closed solution, and experimental comparisons, on a 6 mx 2. 1 m panel. *Structural Engineer*, 67:159–66, 1989.

[34] A Zehnder. Fracture mechanics: Lecture notes in applied and computational mechanics vol. 62, 2012.

[35] Dan Zenkert. *An introduction to sandwich construction*. Engineering materials advisory services, 1995.

A

Appendix-A

A.1. Introduction

In this appendix, D_{Qy} for foam filled panel will be calculated. Contribution to D_{Qy} for a foam filled panel could be divided into two parts - 1. Contribution due to steel part (called D_{QSteel}) and, 2. Contribution due to foam (called D_{Qfill}). The derivation for all elastic constants for foam filled sandwich panels could be obtained from Romanoff et al. [28].

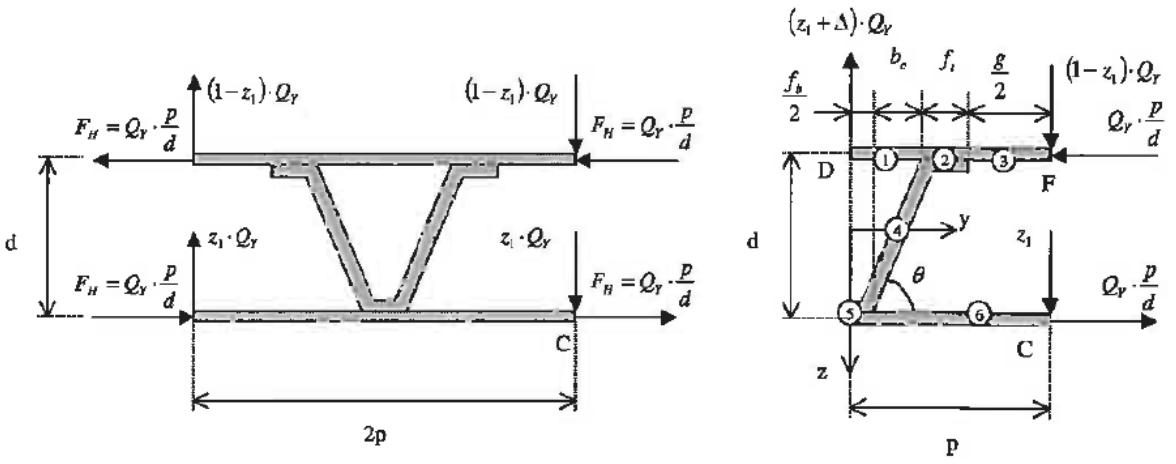

Figure A.1: Forces acting on segment and elements used in calculation [28] (Appendix A)

A.2. Calculating D_{Qy}

D_{Qy} can be calculated through a 5 step process, as follows -

- Calculate 1^{st} level parameters using equation (A4.43) to (A4.51)[1].
- Calculate 2^{nd} level parameters from equations (A4.52) to (A4.57)
- Calculate z_1 and Δ from equations (A4.58) to (A4.59).
- Calculated the needed deformations per shear force from equations (A4.60) to (A4.62).
- Calculate the shear stiffness $(A4.63)$

[1]All equation number refer to equations in Appendix A4 of [28]

Calculating DQy for foam - filled panels

Reference - Report No - M288 (Romanoff et al. [29]), University of Helsinki

```
% DQy = DQy,s (Steel Part) + DQy,fill (Fill Part)

% DQy,s (Contribution from steel part)
% DQy,fill (Contribution from foam filling)

% This is calculated using the equations given in Appendix A of
% report M-288
clc

%Geometric Parameters
% Refer Figure A.1 for description of geometric parameters
bc = 62.29; %Horizontal distance of one inclined part of sandwich panel
fb = 64.91; %Refer Figure A.1
tt = 8; %Thickness of top face plate
tw = 6; %thickness of core steel plate
mu = 0.3; % Poisson's ratio
s = 144.15; %Length of one inclined part of core of sandwich panel
theta = 64.4; %Angle of corrugation
dc = 125.5; %Vertical distance between trough and crest of core layer
d = 132; %Vertical distance between neutral axis of top and bottom face plate
E = 210000; %Young's modulus
p = 126.5; %{=253/2} = Half-pitch of corrugation
ft = 32.46; %Length of horizontal crest of core layer (Refer Figure A.1)
tb = 5; %Thickness of bottom face plate
g = 0; %Gap between core stiffner. Since core is continuous g=0.
hc = 130; %height of core
Gc = 12; %This refers to shear modulus of the filling material, taken as 12 for H-45 Divin
ycell Foam

% Shear Modulus
G = E/(2*(1+mu));
Gb=G;
Gt=G;
Gw=G;

% STEP I --> Level 1 Parameters --> Using Eq A4.43 to A4.51
a1 = -0.5 * (1-mu^2)*(2*bc+fb)^3/(E * tt^3);
b1 = (1-mu^2)/(E)*(bc^2*s/tw^3 + dc*sin(deg2rad(theta))/tw);
c1 = (1-mu^2)/(E)*p*dc/(d*tw)*(bc/s-s*bc/tw^2) - 0.5*(1-mu^2)/...
    (E)*p*fb*(3*fb+12*bc)*(1-dc/d)/(tw+tb)^3;
d1 = 0.25*(1-mu^2)/E*(fb^2*(2*fb+6*bc))/(tw+tb)^3;
e1 = (1-mu^2)/E*(ft*(4*ft^2+6*ft*g+3*g^2))/(tt+tw)^3+0.5*(1-mu^2)*g^3/(E*tt^3);
f1 = (1-mu^2)/E*(bc^2*s/tw^3+dc*sin(deg2rad(theta))/tw);
g1 = (1-mu^2)/(E)*p*dc/(d*tw)*(bc/s-s*bc/tw^2)+6*(1-mu^2)/E*p*fb*(dc-d)*bc/(d*(tw+tb)^3);
h1 = 1.5*(1-mu^2)/E*fb^2*bc/(tw+tb)^3;
i1 = -0.5*(1-mu^2)/E*(2*p-fb)^3/tb^3;

% STEP II --> Level 2 Paramters - Using Eq A4.52 to A4.57
j1 = a1 - d1 - b1;
k1 = d1 + c1 + b1;
l1 = d1 +2*b1 - a1;
m1 = -h1 - b1;
n1 = e1 + b1 + g1 + h1;
o1 = e1 + 2*b1 - i1 + h1;
```

```
% STEP III --> Calculate z1 and Delta using equations A4.58 and A4.59
%calculating delta
p1 = (k1/l1-n1/o1)/(m1/o1-j1/l1);
%Calculating z1
q1 = (j1*p1+k1)/(l1);

% STEP IV --> Calculating deformations per shear force using Eq A4.60 to
% A4.62
r1 = p/d*(1-mu^2)/E*(2*p-fb)/(2*tb);
s1 = (1-mu^2)*dc*fb*(1.5*(q1+p1-1)*fb+6*p*(1-dc/d))/(E*(tw+tb)^3) +...
     (p/d)*(-(1-mu^2)/E*(ft/(tt+tw)-g/(2*tt))+(1-mu^2)/(E)*(bc^2/(s*tw)...
     -sin(deg2rad(theta))*s^2*dc/tw^3))+(1-2*q1-p1)*...
     (1-mu^2)/(E)*(bc*s*dc/tw^3-sin(deg2rad(theta))*bc/tw);
t1 = (1-mu^2)/(E)*((1-q1-p1)*fb^2*(2*fb-6*p)+2*p*fb*(12*p-3*fb)*(1-dc/d))/(4*tw+tb)^3+...
     0.5*(1-mu^2)/(E)*q1*(2*p-fb)^3/(E*tb^3);

% STEP IV --> Calculating DQy,Steel Part{called DQy_1 here}
DQy1 = 1/((r1-s1)/d+t1/p);
DQy1

% DQy,fill (Filling Part) (called DQy_2 here)
% This is calculated using the equations given in Table 7
% of report M-288

%DQy2 = Gc*tw/p *(-ft+hc*p/tw - s - fb/2);
DQy2 = Gc*(1-tw/(2*p));
DQy2

%Calculate % increase due to foam filling below -
Inc = (DQy2)/DQy1*100;
Inc

%Calculating DQx {Just for comparing with DQy value}
DQx = (Gt*tt+Gw*tw/p*(ft+s+fb/2)+Gb*tb) + Gc*tw/p*(-ft+hc*p/tw-s-fb/2);
DQx
```

```
DQy1 =

   7.0971e+03


DQy2 =

   11.7154


Inc =

    0.1651


DQx =

   1.8524e+06
```

B

Appendix-B

B.1. Introduction

In this section, we describe how can we obtain elastic properties of a Corrugated Core Sandwich Steel Panel from it's geometrical and material properties. The formulae shown below were taken from NACA Report - Libove et al. [23]. For details on how these formulae were derived reference could be made to the aforementioned report.

B.1.1. Elastic Constants

There are 5 elastic constants that were used to completely describe the behaviour of a CCSSP. These are bending stiffness (D_x and D_y), transverse shear stiffness (D_{Qx} and D_{Qy}) and twisting stiffness (D_{xy}). Below we describe expressions to calculate all these constants.

Bending Stiffness, D_x

$$D_x = E_1 I_x \tag{B.1}$$

$$EI_x = E_c I_c + \frac{1}{2} E_1 t_1 h^2 \tag{B.2}$$

Bending Stiffness, D_y

$$D_y = \frac{EI_y}{1 - \mu_1^2 \left(1 - \frac{EI_y}{EI_x}\right)} \tag{B.3}$$

Transverse Shear Stiffness D_{Qx}

D_{Qx} refers to transverse shear stiffness in planes parallel to corrugation axis

$$D_{Qx} = \frac{G_c I t_c h}{p \int_0^l Q ds} \tag{B.4}$$

Transverse Shear Stiffness D_{Qy}

D_{Qy} refers to transverse shear stiffness in planes perpendicular to corrugation axis.

$$D_{Qy} = Sh\left(\frac{E_c}{1 - \mu_c^2}\right)\left(\frac{t_c}{h_c}\right) \tag{B.5}$$

Twisting Stiffness, D_{xy}

$$D_{xy} = 2GJ \tag{B.6}$$

$$GJ = \frac{1}{2} G_1 t_1 h^2 \tag{B.7}$$

Symbols

- E_1 and E_2 = Modulus of Elasticity for top and bottom face plates respectively, N/mm^2
- E_c = Modulus of Elasticity for corrugated-core sheet material, N/mm^2
- EI_x = Bending stiffness per unit width of a beam cut from CCSSP in x-direction, $N-mm$
- EI_y = Bending stiffness per unit width of a beam cut from CCSSP in y-direction, $N-mm$
- G_1, G_2 and G_c = Shear modulus of elasticity of lower-face, upper-face and corrugated-core sheet material respectively, N/mm^2
- GJ = Torsional stiffness per unit width of a beam cut from CCSSP in x-direction, $N-mm$
- h = distance between middle surfaces of top and bottom face plates, mm
- h_c = depth of corrugation, measured vertically from center line at crest to center line at trough, mm
- I_c = Moment of inertia per unit width of corrugation cross sectional area about middle plane, mm^3
- t_1, t_2 and t_c = thickness of bottom face plate, top face plate and corrugate-core layer respectively, mm
- μ_1, μ_2 and μ_c = Poisson's ratio of bottom face plate, top face plate and corrugated-core material respectively.
- S = Non dimensional coefficient in expression of D_{Qy}
- p = half of Corrugation Pitch
- Q = Static moment of cross hatched area about neutral axis
- s = distance measured along centerline of corrugation cross section, parallel to yz-plane. Refer Fig. B.1.

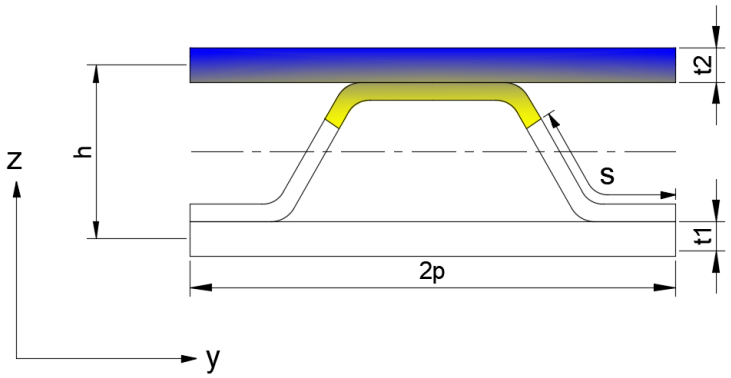

Figure B.1: Meaning of s in calculation of Integral $\int_0^l Q ds$